Some studies on Novel Phases of Neutron Stars and their Observational Consequences

by

Sajad Ahmad Bhat

Enrolment No.: PHYS05201504018

Saha Institute of Nuclear Physics, Kolkata

A thesis submitted to the
Board of Studies in Physical Sciences
In partial fulfillment of requirements
for the Degree of

DOCTOR OF PHILOSOPHY

of

HOMI BHABHA NATIONAL INSTITUTE

March, 2020

Homi Bhabha National Institute

Recommendations of the Viva Voce Committee

As members of the Viva Voce Committee, we certify that we have read the dissertation prepared by Sajad Ahmad Bhat entitled "Some studies on novel phases of neutron stars and their observational consequences" and recommend that it may be accepted as fulfilling the thesis requirement for the award of Degree of Doctor of Philosophy.

Munshi **Date : 26-05-2020**

Chairman - **Prof. Munshi Golam Mustafa**, SINP

Debades Bandyopadhyay **Date : 26-05-2020**

Guide / Convener - **Prof. Debades Bandyopadhyay**, SINP

Attended via Video Conferencing **Date : 26-05-2020**

Examiner - **Prof. Subrata Pal**, TIFR

Attended via Video Conferencing **Date : 26-05-2020**

Member - **Prof. Debasish Majumdar**, SINP

Attended via Video Conferencing **Date : 26-05-2020**

Member - **Prof. Ambar Ghosal**, SINP

Final approval and acceptance of this thesis is contingent upon the candidate's submission of the final copies of the thesis to HBNI.

I hereby certify that I have read this thesis prepared under my direction and recommend that it may be accepted as fulfilling the thesis requirement.

Date : 26-05-2020

Place : SINP, Kolkata

Debades Bandyopadhyay

Guide

STATEMENT BY AUTHOR

This dissertation has been submitted in partial fulfillment of requirements for an advanced degree at Homi Bhabha National Institute (HBNI) and is deposited in the Library to be made available to borrowers under rules of the HBNI.

Brief quotations from this dissertation are allowable without special permission, provided that accurate acknowledgement of source is made. Requests for permission for extended quotation from or reproduction of this manuscript in whole or in part may be granted by the Competent Authority of HBNI when in his or her judgment the proposed use of the material is in the interests of scholarship. In all other instances, however, permission must be obtained from the author.

Sajad Ahmad

SAJAD AHMAD BHAT

DECLARATION

I, hereby declare that the investigation presented in the thesis has been carried out by me. The work is original and has not been submitted earlier as a whole or in part for a degree / diploma at this or any other Institution / University.

Sajad Ahmad

SAJAD AHMAD BHAT

List of Publications arising from the thesis

1. **“Dense matter in strong gravitational field of neutron star,”**
   Sajad A. Bhat and Debades Bandyopadhyay
   J. Astrophys. Astr., **2018**, 39, no. 1, 18 .

2. **“Moment of inertia, quadrupole moment, Love number of neutron star and their relations with strange matter equations of state,”**
   Debades Bandyopadhyay, Sajad A. Bhat, Prasanta Char and Debarati Chatterjee
   Eur. Phys. J., **2018**, A54, no. 2, 26.

3. **“Neutron star equation of state and GW170817.”**
   Sajad A. Bhat and Debades Bandyopadhyay,
   J. Phys., **2019**, G46, no. 1, 014003.

4. **“Cooling of Dark-Matter Admixed Neutron Stars with density-dependent Equation of State,”**
   Sajad A. Bhat and Avik Paul
   Accepted in “The European Physical Journal C.”
   arXiv:**1905.12483**

Sajad Ahmad

SAJAD AHMAD BHAT

DEDICATED TO

Mohammad Altaf and Hajrah

ACKNOWLEDGEMENTS

First of all, I am extremely grateful to Almighty Allah for providing me courage and patience to pursue my passion. Secondly, I sincerely thank my parents for the unwavering support and sacrifices in the tough times of my academic career. For paying gratitude to all the teachers who taught me in my lifetime, I remind myself of Hazrat Ali (R.A) who said, “I am slave to the person who has taught me even a single word, he may sell me or set me free”. I would also like to thank my PhD supervisor Prof. Debades Bandyopadhyay for the consistent guidance and invaluable discussions and suggestions during my PhD tenure. I must also thank all my Post M.Sc. teachers particularly, Prof. Palash Baran Pal who is undoubtedly one of the best teachers I have learnt from during my academic career. My PhD journey in the company of wonderful friends, colleagues and faculties at my home institute was one of the most cherishing experience of life. Next, I am very thankful to my siblings and relatives for the good wishes and encouragement throughout my life. My special thanks to Dr. Muzaffar and Dr. Niyaz who were a motivating force behind me to move from Kashmir University to Saha Institute. I sincerely thank my senior Dr. Prasanta Char for his help and guidance in the early stage of my PhD and other friends namely, Anshu, Kamakshya, Susnata, Amit, Biswajit, Rome, Roopam, Madhurima, Avik, Satyabrata, Suraj, Upala, Sunita for making interactive and joyful atmosphere in the APC division. I also thank my friends ouside SINP namely Asif and Shabir for weekly fun for easing the PhD pressure. Lastly, I am also grateful to the whole canteen staff of MSA 1 hostel particularly, Shaktida and Suresda for their motherly service.

SAJAD AHMAD BHAT

Contents

List of Figures

List of Tables

SUMMARY

Neutron stars (NSs) are excellent laboratories for superdense and cold nuclear matter. The density in the interior of NSs can be as high as several times the saturation density, hence exotic matter like hyperons [1, 2], kaon or pion condensate [3, 4], quarks [5] are supposed to be populated inside the core of NSs. Dark matter (DM) [6–8] may also be captured inside NSs. The presence of exotic matter including the DM softens the EoS and hence, reduces the maximum mass of NSs [9]. Since the environment of NS interior cannot be reproduced in terrestrial laboratories, we rely exclusively on NS observations. Masses and radii of NSs are the two most important probes in this regard. This is because the mass-radius relationship and the maximum allowed mass of a NS are the characteristics of a particular EoS. Moreover, moment of inertia measurements of relativistic binary systems can be very crucial for constraining the NS EoS. PSR J0737-3039A of the double pulsar system is the most suitable candidate in this regard. Since $I \propto MR^2$ and mass of this pulsar has been measured with high accuracy, the measurement of I by the Square Kilometer Array (SKA) in future will allow a precise determination of its radius. The tidal deformability also plays an important role in constraining the NS EoS. This is because the tidal deformability depends on the mass and radius of NSs as $\Lambda \propto (R/M)^5$ [10] and both mass and radius sensitively depend on the EoS. Knowing the upper limit of the effective tidal deformability of the binary neutron star (BNS) merger components from gravitational wave (GW) observations and a complementary lower bound possibly provided by the electromagnetic analyses of these events, one can constrain the NS EoS. We adopt a density dependent relativistic hadron (DDRH) field theory for the description of strongly interacting dense baryonic matter [11]. We also consider EoSs involving antikaon condensate and undergoing a first-order hadron-quark (HQ) phase transition [9]. Next, we explore the impact of strange matter EoSs involving Λ hyperons, Bose-Einstein condensate of K^- mesons and first-

order HQ phase transition on the moment of inertia (I), quadrupole moment (Q) and tidal deformability parameter of slowly rotating NSs. It is noted that the relation between moment of inertia and compactness shows almost universal behaviour except for the EoSs with a first-order HQ phase transition. The important findings of this investigation are the universal relations involving the I-Q and I-Love number relations, which are preserved by the EoSs including Λ hyperons and antikaon condensate [12], but violated in presence of a strong first-order hadron-quark phase transition [9]. This violation of the universal relations can have observable consequences in the gravitational wave (GW) analysis of binary neutron star (BNS) inspirals. Next, properties of NSs in GW170817 are studied using different EoSs involving nucleons, Λ hyperons and quarks resulting in $2M_\odot$ NSs. The computations of tidal deformability parameters predict that soft to moderately stiff EoSs are allowed by the 50% and 90% credible regions obtained from the GW observation of BNS merger GW170817, whereas the stiffest hadron-quark EoS is ruled out. Moments of inertia, quadrupole moments and radii of merger components of GW170817 are also computed. It is noted that the value of I is similar to the text book value of 10^{45} g cm^2 [13].

Apart from the effect of strange exotic matter on the NS EoS, the presence of DM inside NSs can also modify the EoS and structure of NS [6]. We propose a DM admixed density-dependent EoS where the fermionic DM interacts with nucleons via the Higgs portal. The presence of DM can hardly influence the distribution of particles inside NS. Considering APR and DM modified DD2 EoS, we investigated the cooling of NSs and compared our results with the observed astronomical cooling data of three pulsars namely PSR B0656+14, Geminga and PSR B1055-52. It is found that for DM admixed DD2 EoS, the results with all chosen DM masses and Fermi momenta agree well with the observational data except for lighter NSs and the cooling becomes slightly faster as compared to normal NSs with increasing DM mass and Fermi momenta [14].

Homi Bhabha National Institute

SYNOPSIS OF Ph.D. THESIS

1. **Name of the Student:** **Sajad Ahmad Bhat**
2. **Name of the Constituent Institution:** **Saha Institute of Nuclear Physics**
3. **Enrollment No.:** **PHYS05201504018**
4. **Title of the Thesis:** **Some studies on novel phases of neutron stars and their observational consequences**
5. **Board of Studies:** **Physical Sciences**

SYNOPSIS

Neutron stars are born in the aftermath of supernova explosions of gaint stars with mass greater than 8 solar masses. Neutron stars have a mass of about $2M_\odot$ and a radius of about 12 Km[1]. These are the most compact objects after black holes. They are the excellent laboratories for superdense and cold nuclear matter. The density in the interior of neutron stars can be as high as 10 times the saturation density, hence exotic matter like hyperons[2, 3] , kaon or pion condensate[4, 5], quarks[6] and possibly dark matter[7] are supposed to be populated inside the core of neutron stars. The presence of exotic matter softens the equation of state and hence, reduces the maximum mass of neutron stars[8]. The equation of state (EoS) of the superdense matter is yet to be known and a challenging task. Any model of EoS suggested should not only describe the matter at high densities but also reproduce the properties of the matter observed at saturation density. There exist a wide variety of theoretical models in the literature to describe the dense matter inside neutron stars but only one model which satisfies all the observational constraints will survive in the future.

Since the environment of neutron star interior cannot be reproduced in terrestrial laboratories, we rely exclusively on neutron star observations. Masses and radii of neutron stars are the two most important probes in this regard. This is because the mass-radius relationship and the maximum allowed mass of a neutron star are the characteristics of a particular equation of state. High precision measurements of masses and radii of neutron stars can disqualify a particular theoretical equation of state model if the mass-radius relationship doesn't satisfy the observed values of mass and radius. Usually theoretical models including exotic particles at high densities inside the core give softer EoS which leads to a smaller maximum mass, as compared to the models which do not take exotic particles into consideration. The observed maximum mass for neutron stars can, therefore, limit the number of equation of state models by disqualifying those which predict smaller maximum mass than that of the observed. In the recent times, the maximum mass of a neutron star kept on changing with the accurate mass measurements of $1.97^{+0.04}_{-0.04}\ M_{\odot}$[9] for PSR J1614-2230 in 2010, $2.01^{+0.04}_{-0.04}\ M_{\odot}$[10] for PSR J0348+0432 subsequently in 2013 and $2.14^{+0.10}_{-0.09}\ M_{\odot}$[11] for PSR J0740+6620 in 2019. PSR J0740+6620 is discovered using shapiro delay measurements of this binary pulsar system. It is the most massive neutron star observed to date and it places stringent constraint on the neutron star equation of state. But $2.01^{+0.04}_{-0.04}\ M_{\odot}$ for PSR J0348+0432 is still the most accurately measured mass of a $2M_{\odot}$ neutron star.

Moment of inertia measurements of relativistic binary systems can be very crucial for constraining the neutron star EoS. PSR J0737-3039A of the double pulsar system is the most suitable candidate in this regard . Since $I \propto MR^2$ and mass of this pulsar has been measured with high accuracy, measurement of I will allow a precise determination of its radius. Moment of inertia of such an object is determined usually by measuring the spin-orbit coupling[12, 13], which contributes to the motion of the pulsar system in two ways. On one hand it causes an extra advancement in the periastron angle(ω) and on the other hand it induces a precession of the orbital plane around the direction of the total angular momentum of the system. Since the total angular momentum is conserved and orbital angular momentum dominates the spin angular momenta of the two pulsars, orbital angular momentum practically represents a fixed direction in space and spin precession amplitudes remain substantial. According to Lattimer et al. (2005)[13] , moment of inertia of PSR J0737-3039A could be measured within 10% accuracy with few years of future observations and that could put stringent constraint on the neutron star EOS. In near future, the Square Kilometer Array (SKA) is expected to determine the moment of inertia of J0737-3039A and in relativistic neutron star binaries with even higher precision. Consequently, the moment of inertia measurement along with accurately measured mass of pulsar A would determine the radius of pulsar A accurately and hence put strong constraint on equation of sate.

Neutron stars are characterized not only by mass and radius but also by rotational speed through their moment of inertia and, how much deformation they can undergo through their tidal deformability and quadrupole moment. Tidal deformability plays an important role in constraining the neutron star equation of state. This is because tidal deformability depends on the mass and radius of neutron stars as $\Lambda \propto (R/M)^5$ [14] and both mass and radius sensitively depend on equation of state. Tidal deformability appears in the gravitational wave phase of binary neutron star (BNS) inspirals at the 5PN order[15]. Knowing the upper limit of effective tidal deformability of the binary components from gravitational wave observations, one can constrain the neutron star equation of state. Furthermore, it was shown by Yagi and Yunes that moment of inertia, Love number and quadrupole moment individually depend sensitively on neutron star's internal structure and hence on the unknown equation of state. But the relations between moment of inertia, Love number and quadrupole moment are independent of the neutron star's internal structure and hence independent of the equation of state[16]. These relations are called universal relations. If one observable is known, the other two can be estimated from universal relations. Moreover, Love-Q relation can be used to remove degeneracy between spin and quadrupole moment both of which occur at the 2 PN order[17, 18] in the gravitational wave (GW) phase of the BNS inspiral. However, we found lack of evidences in the literature regarding whether these universal relations will hold good in presence of a strong first-order phase transition or not. That motivates us to investigate the impact of first-order phase transition inside neutron star on the universal relations.

Recently, the unprecedented joint detection of gravitational waves from a BNS merger event GW170817 by LIGO and VIRGO detectors followed by the detection of its transient counterparts across the electromagnetic spectrum opened the door of multimessenger astrophysics[19, 20]. The detection of short gamma ray burst designated as GRB 170817A by Fermi and INTEGRAL at 1.7 seconds after GW signal provided the first clinching evidence of the direct association of short gamma ray bursts (GRBs) to neutron star mergers. The fate of the merger event can be closely associated with the ejected material estimated from the analysis of electromagnetic signal[21]. The existence of blue ejecta with modest electron fraction rules out the prompt collapse to black hole and can be explained only if the collapse to black hole is delayed by the formation of short lived hypermassive neutron stars (HMNS) supported by differential rotation. The compact remnant spins down by the gravitational wave emission and redistribution of angular momentum takes place and finally might have collapsed to a black hole near the mass shedding limit of a uniformly rotating neutron star. This conclusion about the fate of the merger remnant leads to the upper bound on the maximum mass of non-rotating stars[22] and might put further stringent constraint on the equation of state. Moreover, GW170817 event is very important in constraining the neutron star equation of state as the GW analysis of this event provided the upper bound on effective tidal deformability and a complementary lower bound is provided by the electromagnetic analysis of this event.

We adopt a density dependent relativistic hadron (DDRH) field theory for the description of strongly interacting dense baryonic matter[23]. Baryon-baryon interaction in the DDRH model is mediated by exchanges of scalar σ meson, responsible for strong attractive force, vector ω meson, responsible for strong repulsive force and ρ mesons, responsible for neutron-proton asymmetry in the system. The EoSs for the charge-neutral and beta-equilibrated matter made of nucleons, hyperons, antikaon condensate and leptons is constructed in the DDRH field theory. Also we consider two more equations of state undergoing first-order hadron-quark phase transition. In one case, DDRH model is employed for hadronic matter above saturation density and this hadronic phase includes all hyperons plus Δ resonance. A non-local extension of Nambu-Jona-Lasinio model is adopted to describe the quark phase made of u,d and s quarks[24]. The hadron-quark mixed phase is governed by the Gibbs rules. This hadron-quark (HQ) EoS is denoted by HQ1 in our work. In the other case, hadronic phase is composed of only nucleons and is described by NL3 model where as the effective bag model including quark interaction is adopted for the quark phase[25]. This hadron-quark EoS is called HQ2 hereafter.

We investigate the impact of strange matter equations of state involving Λ hyperons, Bose-Einstein condensate of K^- mesons and first-order hadron-quark phase transition on moment of inertia, quadrupole moment and tidal deformability parameter of slowly rotating neutron stars. All these equations of state are compatible with the $2M_{solar}$ constraint. The presence of strange exotic matter reduces the pressure and makes equation of state softer as compared to nuclear matter equation of state. Moreover, it is found that moments of inertia corresponding to strange matter equations of state are lower as compared to nuclear matter equation of state for higher neutron star masses. Also it is noted that the relation between moment of inertia and compactness shows almost universal behaviour except for the equation of state with a first-order hadron-quark phase transition. Furthermore, it is also noted that the quadrupole moment decreases with mass and approaches the Kerr value of a black hole for maximum mass neutron stars. The main findings of this investigation are the universality of the I-Q and I-Love number relations, which are preserved by the EoSs including Λ hyperons and antikaon condensates, but broken in presence of a strong first-order hadron-quark phase transition[26]. This violation of the universal relation can have observable consequences in the gravitational wave analysis of BNS inspirals because in case of neutron stars with a strong first-order hadron-quark phase transition, these relations can no longer be used to remove degeneracy between spin and quadrupole moment both of which occur at the 2PN order in the gravitational wave phase of the binary inspiral[17, 18]. Using Love-Q relation, the averaged spin parameter χ_s of BNS inspiral can be measured with high accuracy[16]. Hence the violation of universality will reduce the measurement accuracy of spin parameter.

Next, properties of neutron stars in GW170817 are investigated using different equations of state (EoSs) involving nucleons, Λ hyperons, quarks resulting in $2M_\odot$ neutron stars as described above. This calculation is performed using the same EoS for merger components and for low spin prior case. It is found from the computations of tidal deformability parameters that soft to moderately stiff equations of state are allowed by the 50% and 90% credible regions obtained from the gravitational wave observation of BNS merger GW170817, whereas the stiffest hadron-quark EoS which lies above the upper 90% limit, is ruled out. A correlation among the tidal deformabilities and masses is found to exist as already predicted. Furthermore, moments of inertia and quadrupole moments of merger components of GW170817 are estimated. It is noted that the value of moment of inertia is similar to the text book value of 10^{45} g cm^2[27].

Apart from the effect of strange exotic matter on the equation of state of neutron stars, the presence of dark matter (DM) inside neutron stars can also modify the equation of state and structure of neutron star[7]. The presence of self-annihilating dark matter inside neutron star can heat the neutron star and affects its cooling properties[28]. Non self-annihilating dark matter will only accumulate inside the star and affect its stellar structure[29]. Motivated by some of the recent works on dark matter admixed neutron stars (DMANSs), we propose a DM admixed density-dependent equation of state where the fermionic DM interacts with the nucleons via Higgs portal. Presence of DM can hardly influence the particle distribution inside neutron star (NS) but can significantly affect the structure as well as the EoS of neutron stars. Introduction of DM inside neutron stars softens the equation of state and hence mimics the effect of other exotica e.g., quark matter[29]. We explored the effect of variation of DM mass and DM fermi momentum on the neutron star EOS. Moreover, DM-Higgs coupling is constrained using dark matter direct detection experiments. Next, we studied cooling of normal neutron stars using the APR and DD2 EoSs and DMANSs using the dark-matter modified DD2 with varying DM mass and fermi momentum. We have done our analysis by considering different neutron stars masses. Also DM mass and DM fermi momentum are varied for fixed neutron star mass and DM-Higgs coupling. We calculated the variations of luminosity and temperature of neutron star with time for all EoSs considered in our work and then compared our calculations with the observed astronomical cooling data of three pulsars namely PSR B0656+14, Geminga and PSR B1055-52. It is found that the APR EoS agrees well with the pulsar data for lighter and medium mass neutron stars but cooling is very fast for heavier neutron star. For DM admixed DD2 EoS, we found that in case of medium and heavier mass neutron stars, all chosen DM masses and fermi momenta agree well with the observational data but for lower mass neutron stars, all DM fermi momenta and high DM masses barely agree with the observations. Furthermore, only lower DM mass agrees with observations in case of lighter neutron stars. Cooling becomes faster as compared to normal neutron stars in case of increasing DM mass and fermi momenta. It is infered from the calculations that if low mass super cold neutron stars are observed in future that may support the fact that heavier WIMP can be present inside neutron stars[30].

In this thesis work, the effect of exotic matter involving hyperons, antikaon condensate and hadron-quark phase transitions on moment of inertia, tidal deformability and quadrupole moment of slowly rotating neutron stars is studied. It is found that these three quantities individually are sensitive to the equation of state but the relations between them are insensitive to the equation of state and hence show universal behaviour except in case of a strong first-order hadron-quark phase transition where the universality is violated. Next we studied a set of different EoSs, including exotic matter equations of state, in the light of first BNS merger event GW170817. It is found that soft to moderately stiff equations of state are allowed. Moreover, moments of inertia and quadrupole moments of BNS components are estimated. Finally, we studied effect of one more exotic form of matter namely dark matter on the equation of state of neutron stars and the consequential effect on the cooling of neutron stars. Cooling curves are fairly in agreement with observational cooling data of pulsars and it is found that cooling becomes faster as compared to normal neutron stars when the dark matter mass and fermi momentum increases.

References

[1] B. P. Abbott *et al.* [LIGO Scientific and Virgo Collaborations], Phys. Rev. Lett. **121**, no. 16, 161101 (2018)

[2] N. K. Glendenning, Astrophys. J. **293**, 470 (1985).

[3] N.K. Glendenning, Compact Stars, Nuclear Physics, Particle Physics and General Relativity(New York, Springer, 1997).

[4] See Mesons in Nuclei, vol. 3, M. Rho, D. Wilkinson, Eds. (North-Holland, Amsterdam, 1979).

[5] D. B. Kaplan and A. E. Nelson, Phys. Lett. B **175**, 57 (1986)

[6] J. C. Collins and M. J. Perry, Phys. Rev. Lett. **34**, 1353 (1975)

[7] G. Panotopoulos and I. Lopes, Phys. Rev. D **96**, no. 8, 083004 (2017) A. Das, T. Malik and A. C. Nayak, Phys. Rev. D **99**, no. 4, 043016 (2019) A. Quddus, G. Panotopoulos, B. Kumar, S. Ahmad and S. K. Patra, arXiv:1902.00929 [nucl-th].

[8] D. Bandyopadhyay, S. A. Bhat, P. Char and D. Chatterjee, Eur. Phys. J. A **54**, no. 2, 26 (2018)

[9] P. Demorest, T. Pennucci, S. Ransom, M. Roberts and J. Hessels, Nature **467**, 1081 (2010)

[10] J. Antoniadis, P. C. C. Freire, N. Wex, T. M. Tauris, R. S.Lynch, et al., Science **340**, 448(2013)

[11] H. T. Cromartie *et al.*, doi:10.1038/s41550-019-0880-2 arXiv:1904.06759 [astro-ph.HE].

[12] A. G. Lyne *et al.*, Science **303** 1153 (2004)

[13] J. M. Lattimer and B. F. Schutz, Astrophys. J. **629**, 979 (2005)

[14] T. Hinderer, Astrophys. J. **677**, 1216 (2008)

[15] B. D. Lackey and L. Wade, Phys. Rev. D **91**, no. 4, 043002 (2015)

[16] K. Yagi and N. Yunes, Science **341**, 365 (2013)

[17] E. Poisson, Phys. Rev. D **57**, 5287 (1998)

[18] L. Santamaria *et al.*, Phys. Rev. D **82**, 064016 (2010)

[19] B. P. Abbott *et al.* [LIGO Scientific and Virgo Collaborations], Phys. Rev. Lett. **119**, no. 16, 161101 (2017)

[20] B. P. Abbott *et al.* [LIGO Scientific and Virgo Collaborations], Astrophys. J. Lett. **848**, L13 (2017)

[21] B. Margalit and B. D. Metzger, Astrophys. J. **850**, no. 2, L19 (2017)

[22] L. Rezzolla, E. R. Most and L. R. Weih, Astrophys. J. **852**, no. 2, L25 (2018)

[23] S. Banik, M. Hempel and D. Bandyopadhyay, Astrophys. J. Suppl. **214**, no. 2, 22 (2014)

[24] M. Orsaria, H. Rodrigues, F. Weber and G. A. Contrera, Phys. Rev. D **87**, no. 2, 023001 (2013)

[25] I. Mishustin, R. Mallick, R. Nandi and L. Satarov, Phys. Rev. C **91**, 055806 (2015)

[26] D. Bandyopadhyay, S. A. Bhat, P. Char and D. Chatterjee, Eur. Phys. J. A **54**, no. 2, 26 (2018)

[27] S. A. Bhat and D. Bandyopadhyay, J. Phys. G **46**, no. 1, 014003 (2019)

[28] C. S. Chen and Y. H. Lin, JHEP **1808**, 069 (2018)

[29] F. Sandin and P. Ciarcelluti, Astropart. Phys. **32**, 278 (2009)

[30] S. A. Bhat and A. Paul, arXiv:1905.12483 [hep-ph].

Publications in Refereed Journal:

a. Published

1. "Dense matter in strong gravitational field of neutron star," Sajad A. Bhat and Debades Bandyopadhyay, **J. Astrophys. Astr. 39, 18 (2018)**.

2. "Moment of inertia, quadrupole moment, Love number of neutron star," Debades Bandyopadhyay, Sajad A. Bhat, Prasanta Char and Debarati Chatterjee, **Eur. Phys. J. A 54, no. 2, 26 (2018)**.

3. "Neutron star equation of state and GW170817," Sajad A. Bhat and Debades Bandyopadhyay, **J. Phys. G 46, no. 1, 014003 (2019)**.

b. Accepted

NIL

c. Communicated

"Cooling of Dark-Matter Admixed Neutron Stars with density-dependent Equation of State," Sajad A. Bhat and Avik Paul, arXiv:**1905.12483**.

d. Conference paper

NIL

Other ongoing works

a. **Book/Book Chapter**

NIL

b. **Manuscript in preparation**

NIL

b. **Talk/Poster presentation**

1. Oral presentation on “Violation of universal relations in rotating neutron stars” in UGC sponsored national seminar on “Growth Points in Physics (GPP-2017)” organised from 21 st to 23 rd of October 2017 in university of Kashmir

2. Poster presentation on “Role of strong first-order hadron-quark phase transition on universality relation” in ASI-2018 held at Osmania University, Hyderabad during 05-09 Feberuary 2018

3. Oral presentation on “Constraining Neutron Star Equation of State with GW170817” in workshop on “The first Compact Star Merger Event - Implications for nuclear and particle physics” organised during 14-18 October 2019 in ECT* Villazzano Italy

Signature of Student: Sajad Ahmad

Date : 19-12-2019

Doctoral Committee:

To

Dean, HBNI

Mr. Sajad Ahmad Bhat has been working as a research fellow in Saha Institute of Nuclear Physics since 2015 and is registered (Enrolment No. PHYS05201504018) with Homi Bhabha National Institute, Mumbai for the Ph.D. programme in physical sciences. He has made significant progress in his thesis work titled "Some studies on novel phases of neutron stars and their observational consequences". He published three papers in international journals of repute and one paper has been communicated for publication. These papers will be part of his thesis.

Based on the satisfactory progress of the thesis work of Mr. Sajad Ahmad Bhat, his seminars over past three years and pre-synopsis seminar, the doctoral committee recommends that Mr. Sajad Ahmad Bhat be allowed to submit his Ph.D. thesis to HBNI, Mumbai.

S. No.	Name	Designation	Signature	Date
1.	Prof. Munshi Golam Mustafa	Chairman	Munshi	19/12/19
2.	Prof. Debades Bandyopadhyay	Guide	Debades Bandyopadhyay	19.12.2019
3.	Prof. Debasish Majumdar	Member	Debasish Majumdar	19/12/2019
4.	Prof. Ambar Ghosal	Member	Ambar Ghosal	19/12/2019

Chapter 1

Introduction

Neutron stars are the best known astrophysical laboratories for superdense cold matter. These stars are born as a result of gravitational collapse of massive stars during type II supernova explosions. They are very compact with masses of the order of $2M_{\odot}$ and radii about 10-15 Km. The matter density at the surface of neutron stars is $\rho \lesssim 10^4 g/cm^3$, but the density at the core could be several times the saturated nuclear matter density. At such high densities, different exotic froms of matter like hyperons [1, 2, 15], meson condensates [3, 4], deconfined quarks [5], color superconducting strange quark matter [16, 17] are supposed to be present. Moreover, dark matter can also be captured and accumulated inside neutron stars [6–8]. Despite many proposed theoretical models, the exact nature and behaviour of the matter present in the core is still unknown and is an open challenge. These compact stars are rotating fast in order to conserve the angular momentum retained from the supernova explosions. Because of rapid rotation and presence of charged particles, neutrons stars have very strong magnetic fields ($\sim 10^{12} G$). Any successful model of the matter at such extreme conditions should not only describe the superdense matter but also reproduce the properties of matter observed at the saturation density.

1.1 History of Neutron Stars

Compact stars were first theoretically predicted as gigantic nuclei by Landau in Zurich in February 1931 but the work was not published until February 1932 [18]. This work was coincidently published on 29th of February 1932 just a few days after the publication of discovery of neutron in Nature on 27 February 1932 [19] which led to the wrong association of Landau's paper with the discovery of the neutron. Landau wrote in that paper that protons and electrons constituted atomic nuclei and did not annihilate [20]. This statement supports the fact that his work was done even before the discovery of neutron. The explicit prediction of neutron stars was done, nearly two years after the discovery of the neutron, by Walter Baade and Fritz Zwicky [21] at Caltech in December 1933 while trying to explain the tremendous amount of energy released in supernova explosions. They explained supernovae explosion as a transition from ordinary stars to the stars which contain closely packed neutrons in their final stage and hence are given the name neutron stars. In the later works, they proposed that such stars may have very small radius and can be extremely dense. Moreover, it was proposed that the gravitational packing energy could be very large and can exceed the ordinary nuclear matter packing fractions because neutrons can be packed more efficiently as compared to nuclei and electrons. Consequently, neutron stars could reperesent the most stable matter configuration [22]. Neutron stars were finally discovered as radio pulsars on 28 November 1967 by Jocelyn Bell [23].

1.2 Type II Supernova and birth of Neutron Star

Neutron stars are born in the aftermath of supernova explosion of massive stars. Stars with masses greater than eight solar masses evolve more rapidly than main sequence stars. The evolution of a massive star is a steady process which accelerates towards higher temperature and density in the core. When the temperature in the core of the star reaches to around 10^7 K , four hydrogen nuclei are fused into a helium nucleus, releasing thermal energy that heats the stars's core and provides the outward thermal pressure that supports the star against the gravitational collapse in a process known as stellar or hydrostatic equilibrium. The star spends most of it's lifetime nearly 10^7 years in the hydrogen burning phase. The helium produced gets accumulated in the core because the temperature in the core is not yet sufficient enough for the helium to fuse. When the hydrogen in the core gets exhausted the core contracts and gets heated to a temperature high enough for the helium to fuse to carbon. The star spends nearly 10^6 years in the helium burning phase. This cycle is repeated at a steadily increasing pace through the stages burning carbon, oxygen and silicon. The final stage of silicon burning produces a core of iron from which no further energy can be extracted through nuclear burning and the fusion stops in the core. At this stage, the star has an onionlike structure with the iron core embedded in a mantle of silicon, sulphur, oxygen, neon, carbon and helium and finally surrounded by attenuated envelope of hydrogen. In the surrounding shells of Si, O, C, He and H overlaying the central core, the nuclear burning continues and it adds to the mass of the iron core as shown in Fig.(1.1). The gravitational pull compresses the star to a very high density so that the electrons become relativistic. The kinetic energy of relativistic electrons increases to the extent that the capture of electrons by protons and nuclei i.e. the inverse beta decay takes place and hence the supporting electron pressure is reduced and falls below the point at which any further increase in mass of the core is supported against the gravity. At this stage, the core has attained its maximum mass (between $1.2M_{\odot}$ and $1.5\ M_{\odot}$) [24] called the Chandrasekhar limit. The core rapidly undergoes an implosion in less than a second. Large number of energetic neutrinos are produced in the core due to neutronization of the core through the inverse beta decay during the collapse. The interaction cross-section of highly energetic neutrinos and nuclei becomes dominant at very high density $\sim 10^{12}$ g/cm^3 so that the neutrinos are trapped in the imploding core. As the density increases to a very high value due to further compression, the Fermi energy of the thermalised neutrinos and electrons increases and any further gravitational contraction of the core is resisted by their pressure along with the short-range repulsion of nucleon-nucleon interaction because the iron core is converted into nuclear matter. At this stage, the infalling material is rebounded from the highly stiffened core and as a result a shock wave originates within the core interior travelling outwards and dissipating energy due to the photodisintegration of the nuclei coming in its path. The shock wave stalls after traveling a few hundred kilometers [25]. The energy released in the process is of the order of 10^{53} ergs [21]. A small fraction less than one percent of the huge gravitational binding energy is transported to the stalled shock through a complicated interplay of neutrino heating and convection which is yet to be understood [25]. This explosion energy is responsible for the ejection of all materials except the core of the progenitor star in a type II supernova explosion [21]. The sufficiently hot compact object called protoneutron star having a temperature of a few tens of MeV is cooled to an MeV or so in an interval of a few seconds by the loss of traped neutrinos [26] and the core acquires an equilibrium composition of neutrons, protons, leptons and possibly hyperons and quraks. Thus a neutron star is born with a radius of about 10 kilometers and the average density is nearly 10^{14} times greater than that of the earth. The newly born neutron star continuously cools for millions of years by the diffusion of photons to the star surface and their subsequent radiation into space.

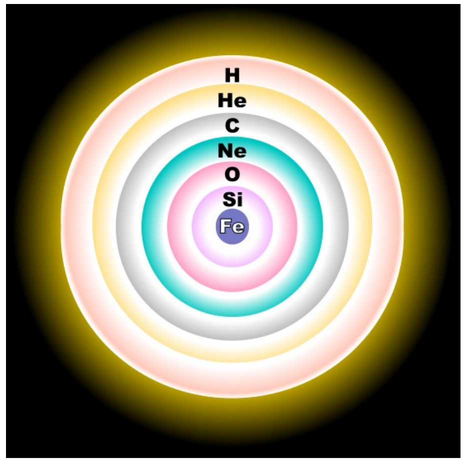

Figure 1.1: Onion-like structure of a massive star prior to core collapse supernova [27]

1.3 Neutron Star Cooling

The cooling of neutron stars sensitively depends on the state of superdense matter in the interior which mainly controls the neutrino emission and also on the structure of the outer layers where photon emission is controlled. The cooling simulations can provide important information about the various physical processes taking place in the interior of neutron stars when confronted with observations in different regions of electromagnetic spectrum like soft X-ray, extreme UV, UV and optical observations of the thermal photon flux emitted from the surface. For newly born hot neutron stars, neutrino emission is the predominant mechanism of cooling with an initial time-scale of few seconds. The neutrino cooling continues to dominate for at least initial thousand years or even longer for the slow cooling scenarios. Neutrino emission is overtaken by the photon emission after the internal temperature has dropped sufficiently. Theoretical cooling calculations can serve as one of the principal windows for unveiling the properties of superdense nuclear matter and the structure of neutron star because of the sensitive dependence of cooling on the adopted nuclear equation of state (EoS), the neutron star mass, magnetic field strength, superfluidity, meson condensates, and the possible presence of color-superconducting quark matter [28, 29]. Moreover, the information about the temperature-sensitive properties such as transport coefficients, crust solidification, and internal pulsar heating mechanisms can be obtained from the thermal evolution of neutron stars [30].

Neutron star in Cassiopi A supernova remnant is very important in understanding the cooling mechanism of neutron stars. It is the youngest known thermally emitting isolated neutron star in our galaxy. Also, it is the first neutron star for which cooling has been observed directly. It is among very few isolated neutron stars whose age and surface temperatures are very well determined and hence is important in understanding the thermal evolution and interior properties of neutron stars. Nearly 20 years of monitoring of this neutron star, since it was discovered by Chandra X-ray Observatory in 1999, has shown that there is a decrease in it's temperature by 2-3% per decade. This cooling rate is significantly faster than that can be explained by standard neutron star cooling theories. This provides a strong evidence for the existence of superfluidity in neutron star cores [31–33]. Once the temperature is below the critical temperature of superfluid transition, neutron superfluidity and proton superconductivity opens a new channel for neutrino emission by continuous breaking and formation of cooper pairs. Hence the cooling of the neutron star is enhanced. This rapid cooling is expected to continue for several more decades. In future, Chandra observations will be more reliable and temperature measurements of this neutron star will be more accurate. Hence, the results will put stringent constraints on the neutron star equation of state [33].

1.4 Structure and Composition of Neutron Stars

It has been observed in November 2009 by Chandra X-ray Observatory, that the atmosphere of neutron stars contains a thin veil of carbon. Also, it has been calculated that the carbon atmosphere is only 4 inches thick [34]. This is because of compression due to extremely large surface gravity of neutron stars which is 100 billion times stronger than on earth. This carbon is formed here from a combination of material that falls back after the supernova explosion and from nuclear reactions taking place on the hot neutron star surface converting hydrogen and Helium into Carbon.

Internal structure of a neutron star can be described as consisting of outer crust, inner crust, outer core and inner core as shown in Fig.(1.2). Each of the regions will be briefly described here:

Outer Crust: The outer crust consists of a lattice of neutron-rich nuclei immersed in a uniform gas of electrons. As we move towards the center of neutron star, the increasing pressure due to increase in overlaying matter favors the neutronization (which happened during supernova stage) and consequently increasing the neutron density in the nuclei. Thus the outer crust contains nuclei of different neutron-to-proton ratio.

Inner Crust: As we continue to move inwards, the density continues to increase until it reaches the neutron drip density ($\sim 4.3 \times 10^{11} g/cm^3$) at which neutrons drip out of nuclei and we have a region of free neutrons and electrons and nuclei. The nuclei are in equilibrium with free neutrons. The density of free neutrons increases as we move towards the boundary of outer core where density is nearly $0.5\rho_0$ ($\rho_0 \sim 2.7 \times 10^{14} g/cm^3$) and mostly free neutrons exist here. The inner crust contains hierarchy of phases of nuclei called the nuclear pasta phases. Also, since the interior temperatures of neutron stars are very small compared to Fermi energy of neutrons, neutrons may form cooper pairs and hence superfluid at critical temperature of about $10^9 - 10^{10}$ K. The necessary ingredient for the formation of cooper pairs is a long range attractive interaction between neutrons. At the densities relevant for inner crust, neutrons are supposed to form S_0^1 bound states. Since the neutrons are superfluid, any angular momentum will be carried by the array of quantised vortices. These vortices can pin to the nuclear lattice because of the coherence length being comparable to the size of nuclei. This prevents the neutron superfluid from spinning down and hence it stores angular momentum which can be released catastrophically giving rise to a pulsar glitch [35].

Outer Core: The outer core which occupies the density range $0.5\rho_0 \lesssim \rho \lesssim 2\rho_0$ is supposed to contain proton and neutron superfluids, electrons and muons. Here ρ_0 is the saturated nuclear matter density. At these densities, neutrons pair in P_2^3 bound states and low density protons are supposed to pair in S_0^1 bound states. Protons being charged particles form a proton superconductor. Neutron superfluid vortices in the core may get pinned to the proton flux tubes. This pinning is strongest in the region where vortex lines are perpendicular to the flux tubes [36] .

Inner Core: The composition of inner core where density $\rho > 2\rho_0$ is unknown. Heavy exotic particles may be present at such high density like hyperons, meson condensates, deconfined quarks and possibly superconducting strange quark matter. The density at the center may be several times the saturation density. There can be highly variable crystalline structure of hadron-quark mixed phase at such high densities and pulsar glitches may have some connection to this crystalline structure in the inner core of neutron stars [37, 38]. The interior crystalline structure of the mixed phase separated from the crustal solid by a nuclear liquid offers interesting possibilities for interaction when a glitch originates in one of them and also in the postglitch recovery [2]. These matters are yet to be investigated .

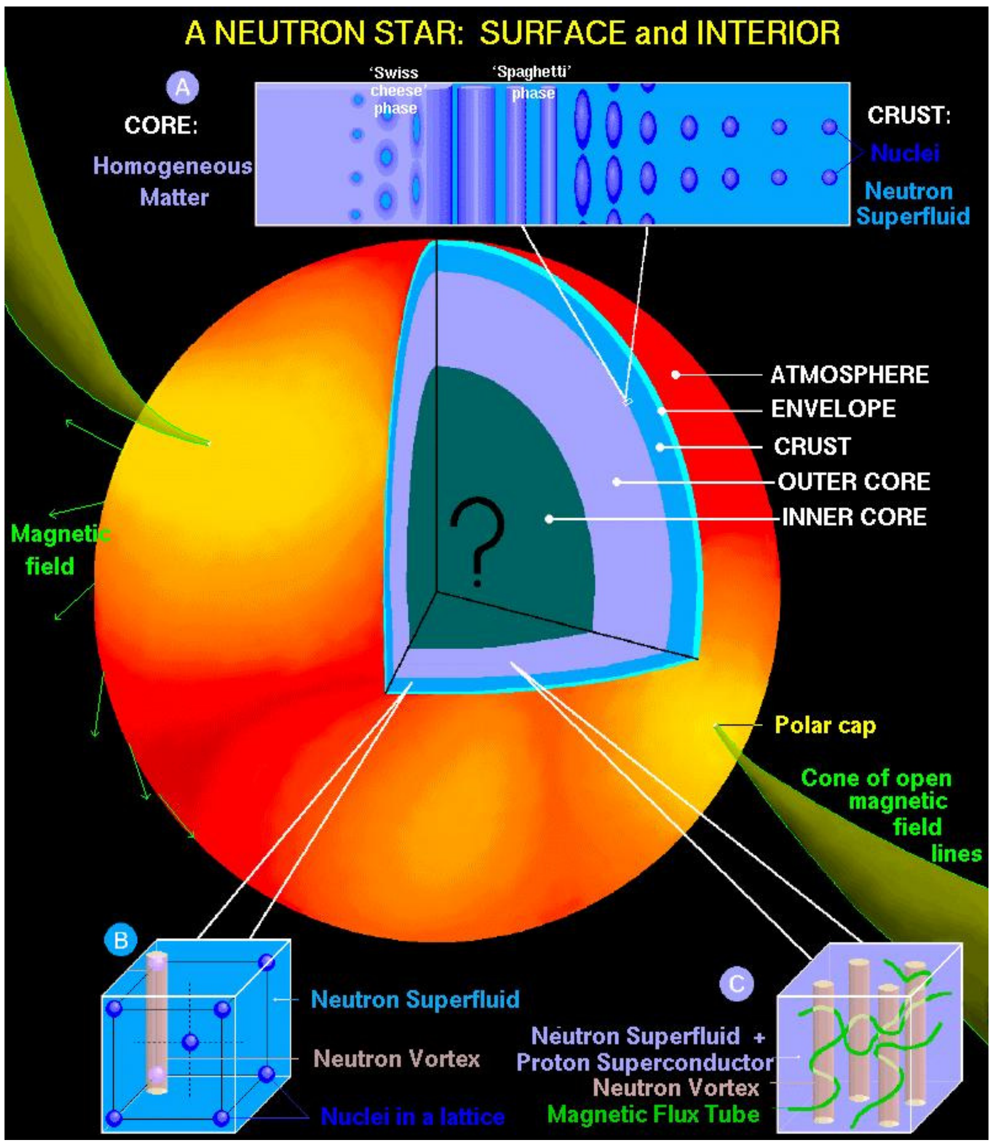

Figure 1.2: Cross section showing expected structure and composition of a neutron star [39]

1.5 Observational Constraints on Neutron Stars

Pulsar, a stellar pulsating source of electromagnetic radiation mainly radio waves, is a strongly magnetised rotating neutron star. Neutron stars are extremely dense and have short regular rotational periods born as a result of collapse of a massive star during supernova explosion. Neutron stars being extremely reduced in size and hence highly compact objects have highly reduced moment of inertia. Rotational period of these stars become very small (from milliseconds to few seconds) in order to conserve the angular momentum retained after the supernova explosion. There is a misalignment between the rotational axis and the magnetic axis of this rapidly rotating star. Two radiation cones are emitted from polar caps along the magentic axis. The beam can be seen once every rotation when it hits the line of sight and pulsed nature of radiation is observed. In case of rotation-powered pulsars where rotational energy is responsible for radiation, an electric field is produced due to rotational movement of highly strong magnetic field which accelerates the protons and electrons on the surface resulting in the creation of radiation beam emitted along the poles of magnetic axis. Due to the emission of electromagnetic radiation, the rotational speed of pulsar slows down with time until the the rotation becomes slow enough to turn off the radiation mechanism. However, it is worth mentioning that the theoretical explanation of radiation mechnaism of pulsars is still in its infancy. Radio observation of pulsars are crucial for constraining the neutron star equation of state which will be discussed in detail hereafter.

Since it is not possible to reproduce the environment of neutron star interior in terrestrial laboratories, we are exclusively dependent on neutron star observations. In this regard, the two most important probes are the masses and radii of neutron stars. This is because the mass-radius relationship and the maximum allowed mass of a neutron star are the characteristics of a particular equation of state. A particular theoretical equation of state model can be disqualified by high precision measurements of masses of neutron stars if the maximum allowed mass is inconsistent with the observed masses. Usually theoretical models including exotic particles at high densities inside the core result in softer EoS which leads to a smaller maximum mass, as compared to the models which do not take exotic particles into consideration. The observed maximum mass for neutron stars can, therefore, limit the number of equation of state models by disqualifying those which predict smaller maximum mass than that of the observed. In the recent times, the maximum mass of a neutron star kept on changing with the accurate mass measurements of $1.97^{+0.04}_{-0.04}\ M_{\odot}$ [40] for PSR J1614-2230 in 2010, $2.01^{+0.04}_{-0.04}\ M_{\odot}$ [41] for PSR J0348+0432 subsequently in 2013 and $2.14^{+0.10}_{-0.09}\ M_{\odot}$ [42] for PSR J0740+6620 in 2019. PSR J0740+6620 is discovered using Shapiro delay measurements of this binary pulsar system. It is the most massive neutron star observed to date and it places stringent constraint on the neutron star equation of state. But $2.01^{+0.04}_{-0.04}\ M_{\odot}$ for PSR J0348+0432 is still the most accurately measured mass of a $2M_{\odot}$ neutron star.

Moment of inertia (I) measurements of relativistic binary systems are very crucial for constraining the neutron star EoS. The most suitable candidate in this regard is PSR J0737-3039A in this double pulsar system. Since $I \propto MR^2$ and mass of this pulsar has been measured with high accuracy, measurement of I will allow a precise determination of its radius. Moment of inertia of such an object can be determined usually by measuring the spin-orbit coupling [43, 44], which contributes to the motion of the pulsar system in two ways. On one hand, it causes an extra advancement in the periastron angle(ω) and on the other hand, it induces a precession of the orbital plane around the direction of the total angular momentum of the system. Since the total angular momentum is conserved and orbital angular momentum dominates the spin angular momenta of the two pulsars, orbital angular momentum practically represents a fixed direction in space and spin precession amplitudes remain substantial. According to Lattimer et al. (2005) [44] , moment of inertia of PSR J0737-3039A could be measured within 10% accuracy with few years of future observations and that could put stringent constraint on the neutron star EoS. In near future, the Square Kilometer Array (SKA) is expected to determine the moment of inertia of J0737-3039A and in relativistic neutron star binaries with even higher precision. Consequently, the moment of inertia measurement along with accurately measured mass of pulsar A would determine the radius of pulsar A accurately and hence put strong constraint on equation of sate.

Radius estimation of neutron stars have been done using several models of the X-ray emission from quiescent neutron stars [45], from accretion-powered millisecond pulsars [46] and from neutron stars during thermonuclear X-ray bursts [47]. The inferred radii typically range from $10km$ to $14km$ and is consistent with most theoretical predictions. However, there can be significant systematic errors in these estimates, because a model providing a formally good fit to the data can still yield a credible interval for the radius that can strongly exclude the true value [48].

In contrast, observation and subsequent analyses of the soft X-ray pulse waveforms using the Neutron Star Interior Composition Explorer (NICER) are expected to be less susceptible to systematic errors. Analyses of synthetic waveforms was carried out before the launch of NICER. It was shown that despite using model assumptions which are different from the true situation (e.g., different emission or beaming patterns, different spectra, or different surface temperature distributions) there is no significant bias in the parameter estimates, provided the fit was formally good [49]. Also, simple pulse waveform models have been fit previously to the soft X-ray waveforms of rotation-powered pulsars observed using ROSAT, Extreme Ultraviolet Explorer (EUVE) [50] and XMM-Newton [51]. These fits provide estimates for the radii of these pulsars that were consistent with the expected range of neutron-star radii, but the number of counts available was too small to obtain tight constraints.

Recently, NICER provided the estimates of the mass and radius of the isolated 205.53 Hz millisecond pulsar obtained using a Bayesian inference approach to analyze it's energy-dependent thermal X-ray waveform. This approach is thought to be less subject to systematic errors than other approaches for estimating neutron star radii. A variety of emission patterns on the stellar surface are explored. The best-fit model has three oval, uniform-temperature emitting spots and provides an excellent description of the pulse waveform observed using NICER. The radius and mass estimates given by this model are $R = 13.02^{+1.24}_{1.06}\ km$ and $M = 1.44^{+0.15}_{0.14}\ M_{\odot}(68\%)$ [52]. These measurements of R and M for PSR J0030+0451 will improve the astrophysical constraints on the EoS of cold, catalyzed nuclear matter above saturation density.

Another group also reported the mass and radius of PSR J0030+0451 using Bayesian parameter estimation which is conditional on pulse-profile modeling of NICER X-ray spectral-timing event data. The inferred mass and radius are $1.34^{+0.15}_{-0.16}\ M_{\odot}(68\%)$ and $12.71^{+1.14}_{-1.19}\ km$ [53], respectively. In this work, relativistic ray-tracing of thermal hot spots of pulsar's surface is performed and two distinct hot regions are assumed based on noticing two clear pulsed components in the phase-folded pulse-profile data. From the set of different models considered, the evidence strongly favors a configuration wherein both hot spots are in the same rotational hemisphere with one hot spot being small whileas the other an azimuthally extended narrow crescent. This implies offset dipolar and multipolar magnetic field structure. It can have major implications on pulsar emission mechanism and can completely change the way pulsar works. The mass and radius estimates of PSR J0030+0451 provided by both groups are consistent with previous neutron star mass measurements, with tidal deformability of neutron stars in GW170817 and with nuclear physics considerations.

1.6 Gravitational Waves and Neutron Star Binaries

Gravitational waves are the disturbances created in the spacetime curvature by the accelerated masses that propagate outwards from the source of disturbance at nearly the speed of light. These are like ripples in the spacetime which are constantly passing through earth. These waves emitted from the sources at extremely large distances have a miniscule effect on earth and hence extremely sophisticated and sensitive detectors are required to detect them. In 1893 , Oliver Heaviside discussed for the first time the possibility of gravitational waves by considering the analogy between the inverse-square law in gravitation and electromagnetism [54]. Later Henri Poincaré suggested in 1905 an analogy between the electromagnetic radiation radiated by an accelerated charge and the gravitational radiation radiated by accelerated masses in a relativistic field theory of gravity [55]. Albert Einstein subsequently predicted the gravitational waves in 1916 based on his general theory of relativity. The discovery of Hulse-Taylor binary pulsar in 1974 offered the first indirect evdence of gravitational wave existence which fetched the Nobel Prize to the duo [56]. Gravitational waves were first directly observed on 14 September 2015 by the Advanced LIGO detectors and the waves originated from merging of a pair of binary black holes [57]. The detection was announced by the LIGO and Virgo Scientific Collaboration On 11 February 2016. Two more detections were confirmed after the first detection was announced. Moreover a fourth gravitational wave event of binary black hole merger was observed on August 2017 and also an unprecedented joint detection of binary neutron star merger named as GW170817 in gravitational waves and electromagnetic signal was done on 08 August 2017 [58] (see Fig.1.3) which opened the era of multimessenger astronomy.

From the observations of first observed neutron star binary discovered by Hulse and Taylor, it was found that the orbit was losing energy due to the gravitational wave emission and the first indirect evidence of gravitational waves was achieved [59]. The orbit of a binary neutron star system shrinks with time and gravitational wave emission is enhanced which leads to acceleration of the inspiral. The gravitational waves thus emitted were predicted to be detected by the ground based detectors in the late stages of the inspiral [60]. For such systems, the form of the gravitational wave signal is an accurately calculated chirp signal. The frequency of the signal sweeps the detectors' sensitive bandwith which lies in the range 10-1000Hz typically. The rate of occurance of such inspiral events is estimated to be in the range 3 to 100 per year in case of signals detectable at about 100 Mpc by the Advanced LIGO. It is worth mentioning that apart from determining the parameters such as masses and spins of the binary inspiralling system from the analyses of these waves, several other cosmological and astrophysical parameters can be possibly determined. Measuring cosmological distances, probing the nonlinear regime of general relativity and testing alternative theories of gravity are some achievable milestones worth mentioning here.

Gravitational wave signals from late stages of the binary neutron star inspiral are more important for probing the superdense matter in the interior of neutron star. When the orbital separation of the binary becomes comparable to the size of the binary components, each of the components starts tidally disrupting the companion. Each of the components develops mass-quadrupole moment due to the tidal field of the companion and the coalescence is accelerated. How much a neutron star is deformed by the tidal field of companion is determined by a parameter known as tidal deformability or tidal polarizability which is only dependent on the equation of state of superdense matter inside neutron star. Tidal effects in binary neutron star inspiral become increasingly important as the frequency increases over time and can affect the phase of the gravitational wave. Analysis of the gravitational wave signal using some standard binary neutron star waveform models can be used to constrain the tidal deformability of neutron stars. Since the tidal deformability is sensitive to equation of state of neutron star, upper limit on tidal deformability constrains the neutron star equation of state [58, 61].

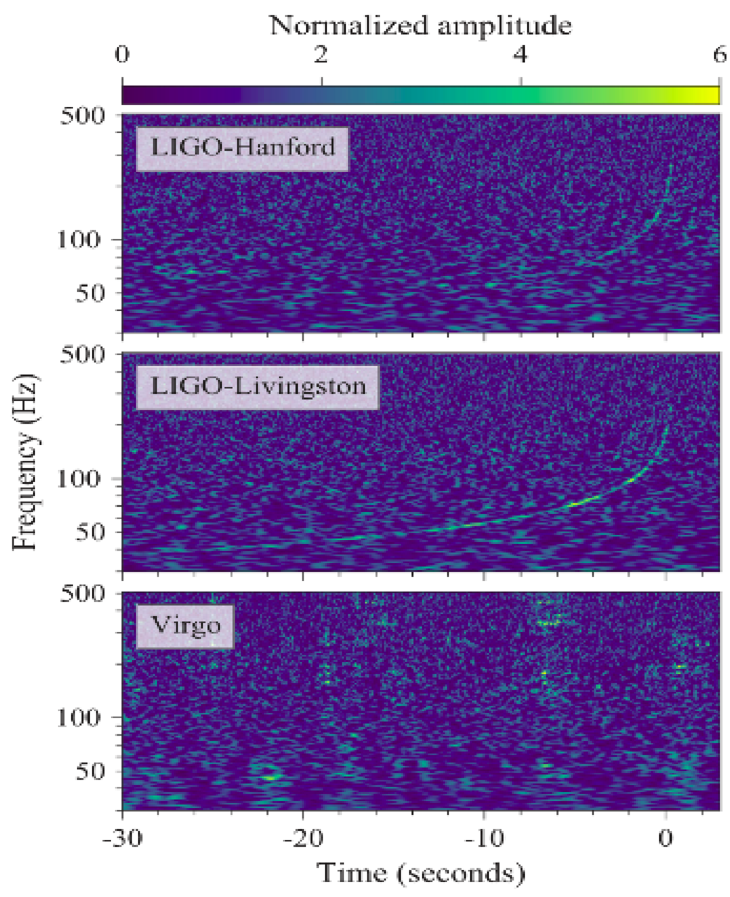

Figure 1.3: Frequency-time detection plot of GW170817 [58]

1.7 Universality in Neutron Stars

Apart from the mass, radius and moment of inertia, neutron stars are also characterised by the macroscopic parameters like tidal deformability and quadrupole moment. Each of these quantities is sensitive to the neutron star's internal structure. Yagi and Yunes were the first to find the universal relations between the moment of inertia, Love number and quadrupole moment that are independent of neutron star's internal structure [62]. B. Haskell et al. later showed that these relations remain nearly universal in case of purely poloidal and purely toroidal magnetic field configurations and different field configurations lead to different I-Q relations. Furthermore, they showed that in case of twisted torus magnetic field, I-Q relation depends sensitively on the equation of state and I-Love-Q universality is lost in case of long spin periods i.e. $P \gtrsim 10$ sec and strong magnetic fields i.e. $B \gtrsim 10^{12}$ G [63]. Another group later showed that I-Love-Q relations lose universality for rotating speeds faster than few hundreds Hz [64]. It was claimed by George Pappas et al. that this type of universal behaviour can promote neutron stars to most promising candidates (next to black holes) for testing theories of gravity [65]. Y. H. Sham et al. found that these universal relations in Eddington-inspired Born-Infeld (EiBI) gravity were essentially the same as in GR and hence showed that there exists at least one modified gravity theory that is indistinguishable from GR in view of these universal relations [66]. P. Pani and Berti proved that I-Love-Q relations in scalar-tensor theories coincide with generalised relativistic ones, so these parameters can not be used to discriminate between scalar-tensor theories and general relativity [67]. I-Love-Q relations were shown to be satisfied for hybrid stars [68] and in case of protoneutron stars also after the smoothening out of the entropy gradients [69]. Moreover, Yagi and Yunes studied the effect of pressure anisotropy on universal relations and showed that anisotropy affects the universal relations only weakly [70]. Furthermore, P. Pani showed that I-Love-Q relations for gravastars are dramatically different from those of ordinary compact stars but the approach to black hole limit is continuous and non-polynomial and as a result such relations can be used to discern a gravastar from an ordinary compact star [71, 72].

To explain universality, Yagi and Yunes have given two possible reasons: (i) these relations depend mostly on internal structure far from core where all realistic equations of state approach each other.; (ii) as the compactness increases I-Love-Q relations approach that of black hole which doesn't have internal structure dependence [73]. Later they, phenomenologically, suggest that universality arises as an emergent approximate symmetry stating that as one flows in stellar structure phase space from noncompact star region to relativistic star region (see Fig.1.4), the eccentricity variation inside stars decreases , leading to self-similarity in their isodensity contours which finally lead to universal behaviour in exterior multipole moments [74]. Later it was shown that I-Love-Q relations of incompressible stars can well approximate those of relativistic compact stars and universality can be attributed to incompressible limit of I-Love-Q relations [75]. They also showed that I-Love-Q relation of incompressible stars was stationary with respect to changes in EoS about the incompressible limit and hence universality can be attributed to proximity of compact stars to incompressible stars [76].

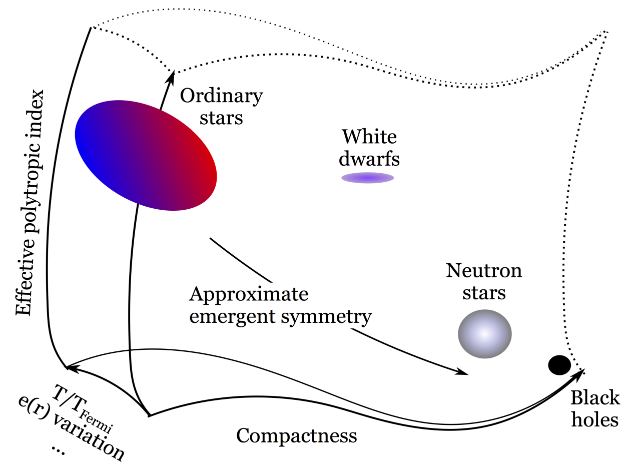

Figure 1.4: Schematic diagram of the stellar phase space wherein compact stars live in bottom-right corner of this space whileas non-compact stars live in top-left corner [74].

1.8 Applications of I-Love-Q Universal Relations

These relations can immediately be applied to observational astrophysics, Gravitational Waves and fundamental physics. In the observational case, the measurement of any one member of the I-Love-Q trio will provide information about the other two members even if the later two are not easily accessible from an observational point of view.

In case of GW physics, I-Love-Q relation can break degeneracy between NS spins and quadrupole moment for a given sufficiently large SNR detection of NS binary inspiral. The first spin-orbit coupling contribution enters in the phase of waveform at 1.5 PN . One can extract this phase term for a large SNR detection and measure a certain combination of individual spins. However, in order to extract both spins one needs to measure also the spin-spin correction to the waveform which enters at 2 PN order [77]. At 2 PN order quadrupole moment also modifies the waveform phase which leads to 100% degeneracy between Q(rotational) and individual spins [78].

Q-Love relation can be used to break this degeneracy as Q can be written as a function of Love number which enters at 5 PN order in the waveform phase [79]. To extract Love number, second generation ground based detectors could be used. Such a measurement of Love number along with Q-Love relation can determine NS quadrupole moment. This allows for the measurement of the averaged spin $\chi_s = \frac{\chi_1+\chi_2}{2}$.

In case of fundamental physics, the independent measurement of any two members of the I-Love-Q trio would allow for model independent and EoS independent tests of GR. One can also constrain modified gravity theories by requiring that I-Love-Q curves in these theories pass through measurement error box of these quantities.

1.9 My Thesis

This thesis is organised in the following way. In chapter 2, unified and non-unified EoS models are discussed in details and different equations of state are obtained including the ones containing exotic matter like hyperons, kaon condensate within the framework of RMF models with and without density dependent couplings. Deconfined quarks are described by the effective bag model and the non-local extension of Nambu-Jona-Lasinio model. Universal relations between moment of inertia, love number (or tidal deformability) and quadrupole moment and their violation under a strong first-order hadron-quark phase transition are discussed in chapter 3. In chapter 4, properties like radius, moment of inertia and quadrupole moment of the merger components of the binary neutron star merger event GW170817 are estimated and also the equation of state of neutron star is constrained using the upper limit of effective tidal deformability obtained from the GW analysis of GW170817. Chapter 5, discusses the effect of non self-annihilating fermionic dark matter on the equation of state of neutron star and its consequence on cooling of neutron stars is discussed. Finally, we conclude in Chapter 6.

Chapter 2

Equation of State Models

2.1 Introduction

Interior structure of a neutron star can be divided into outer crust, inner crust, outer core and inner core. As the density ranges of these regions are different, several models relevant for each of the regions have been proposed. Different regions have different degrees of freedom as described in Chapter 1. We consider two types of EoS models namely, unified and non-unified. In the unified case, the same nucleon-nucleon interaction of RMF models is adopted both in low- and high-density matter. In the case of non-unified model, the RMF models that are employed to describe the EoS of matter in the core, are matched with the EoS of the outer and inner crust. A model developed by Baym, Pethick and Sutherland (BPS) [80] is adopted for low density part ($\rho \lesssim 1.7 \times 10^{12} g/cm^3$) of the crust whereas for the high density part ($1.7 \times 10^{12} g/cm^3 \lesssim \rho \lesssim 1.35 \times 10^{14} g/cm^3$) of the crust, Negele and Vautherin EoS model [81] is used.

For unified EoS model, an extended version of nuclear statistical equilibrium (NSE) model [82] is utilised for the matter composed of light and heavy nuclei, and unbound nucleons at low temperatures and sub-saturation density. Nucleon-nucleon interaction for unbound nucleons is described by RMF models which also describe the matter at higher densities. Several different parameterizations of RMF models like DD2 [83], DDME2 [84], NL3 [85], SFHo [86], SFHx [87], TM1 [88], TMA [89] are exploited for nuclear matter EoS. We also employ an extended version of DD2 RMF model developed by Banik, Hempel, Bandyopadhyay (BHB) which includes Λ hyperons and this model is known as BHB$\Lambda\phi$ [11]. We describe above mentioned models in the following sections.

2.2 Equation of State of Crust for Non-unified Models

The outer crust is composed of nuclei and electrons and extends from density $\sim 10^4$ g/cm^3 to neutron drip density $\sim 4.3 \times 10^{11}$ g/cm^3. Baym, Pethick and Sutherland extensively studied and calculated the EoS for the above mentioned density range [80]. The BPS model will be discussed here for determining the sequence of equilibrium nuclei and calculating the equation of state. In the ground state of matter, nuclei are arranged in a lattice in order to minimize the coulomb interaction energy. In this model Wigner-Seitz approximation is adopted. Every lattice volume is represented by a spherical cell containing one nucleus at its center. Each cell is charge neutral containing Z number of electrons where Z is the nuclear charge. The Coulomb interaction is neglected between cells. In order to find the equilibrium nucleus (A, Z) for a given pressure P , one should minimize the Gibbs free energy per nucleon with respect to A and Z. The total energy density can be expressed as

$$E_{tot} = n_N(W_N + W_L) + \epsilon_e(n_e). \tag{2.1}$$

where W_N is the energy of the nucleus including the rest mass energy of the nucleons and is explicitly given as

$$W_N = m_n(A - Z) + m_p Z - bA, \tag{2.2}$$

with b as the binding energy per nucleon. From the atomic mass table compiled by Audi, Wapstra and Thibault (2003), one can obtain the experimental nuclear masses [90]. Also the theoretical extrapolation of Moller et al (1995) can be used for the rest of the nuclei [91]. The lattice energy of the cell is given by

$$W_L = -\frac{9}{10}\frac{Z^2 e^2}{r_C}\left(1 - \frac{5}{9}\left(\frac{r_N}{r_c}\right)^2\right) \tag{2.3}$$

Here r_C repesents the cell radius and $r_N \simeq r_0 A^{1/3}$ (where $r_0 \simeq 1.16$ fm) represents the nuclear radius. The first term in W_L denotes the lattice energy for point nuclei and the second term denotes the correction due to the finite size of the nucleus (uniform proton charge distribution is assumed in the nucleus). Furthermore ϵ_e denotes the electron energy density and P is the total pressure given by

$$P = P_e + \frac{1}{3}W_L n_L \tag{2.4}$$

The baryon number density n_b and nuclei number density n_N are related as

$$n_b = A n_N. \tag{2.5}$$

and the charge neutrality condition requires

$$n_e = Zn_N. \tag{2.6}$$

Gibbs free energy per nucleon is minimized by varying A and Z at fixed pressure P and is given as

$$g = \frac{E_{tot} + P}{n_b} = \frac{W_N + 4/3W_L + Z\mu_e}{A} \tag{2.7}$$

A sequence of equilibrium nuclei is obtained by minimizing the Gibbs free energy per nucleon. It is found that as the density increases, ^{56}Fe nucleus is no longer energetically favourable. The nuclei become neutron rich with increasing density because of the electron capture process. When the Gibbs free energy of ^{118}Kr becomes equal to the neutron mass, neutrons drip out of nuclei and this marks the end of outer crust.

The inner crust ($4.3 \times 10^{11} g/cm^3 \lesssim \rho \lesssim 2.7 \times 10^{14} g/cm^3$) of neutron star contains neutron rich nuclei immersed in a gas of neutrons along with a uniform background of electrons. A consistent and unified description was established by several groups for the nuclear matter inside neutron rich nuclei and neutron gas outside them using a single expression for the energy density as a function of neutron and proton densities and of their gradients [92, 93]. To calculate the ground state of inner crust, Neggele and Vautherin [81] made the most ambitious early attempt using Hatree-Fock calculations with effective nucleon-nucleon interaction. In order to minimize the Coulomb interaction, nuclei in the inner crust form a body centered cubic lattice approximated by Wigner-Seitz cell. Interaction between the cells is neglected and electrical neutrality is maintained in each cell. Each unit cell contains

N neutrons and Z protons and the nuclear effective Hamiltonian is given by

$$H_N^{eff} = \sum_{j=i}^{A} t_j + \frac{1}{2} \sum_{j,k=1, j\neq k}^{A} v_{jk}^{eff} \tag{2.8}$$

where t_j is the kinetic energy operator of j-th nucleon and v_{jk}^{eff} is an operator for the effective two-body interaction between the jk nucleon pair. Usually, v_{jk}^{eff} contains a component which represents an effective two-body interaction of the three-body forces and is important in dense nucleon medium. Effective nuclear Hamiltonian H_N^{eff} has to reproduce the relevant properties of the ground state of the many-nucleon system, particularly the ground state energy E_0. The complete Hamiltonian of a unit cell is $H_{cell}^{eff} = H_N^{eff} + V_{Coul} + H_e$, where V_{coul} and H_e correspond to Coulomb interaction between charged constituents of matter (protons and electrons), and that of a uniform electron gas, respectively. The absolute ground state configuration is found by minimizing $E_{cell}(N, Z)$ at fixed $A = N + Z$. The neutron drip point corresponds to the threshold density, at which neutron Fermi level becomes unbound. Protons do not drip out of nuclei even at highest densities considered. As the matter density increases, the neutron gas density outside nuclei increases, and the density of protons within nuclei decreases. The prediction of strong shell effects for proton was one of the most interesting results of Negele and Vautherin [94]. This can be visualised by persistence of $Z = 40$ (closed proton subshell) from neutron drip to about $3 \times 10^{12} g/cm^3$, and $Z = 50$ (closed major proton shell) for $3 \times 10^{12} g/cm^3 \lesssim \rho \lesssim 3 \times 10^{13} g/cm^3$. It is important to note that when nuclei are immersed in a neutron gas, the co-existing high density phase inside nucleus and low density phase outside it should be treated in a thermodynamically consistent manner. Also, the surface energy of the interface between the two phases should be determined with good accuracy. It was later shown by Bonche, Levit and Vautherin [95–97] that this problem can be solved by using the subtraction procedure wherein the nuclei are realised after subtraction of neutron gas from the cell.

2.3 Equation of State of Crust for Unified Models

We adopt the extended NSE model [82] developed by Hempel and Schaffner-Bielich (HS) to describe the matter containing light and heavy nuclei along with unbound nucleons at low temperatures and sub-saturation densities. Heavy nuclear clusters co-existing with nucleons in this low density region is known as non-uniform or inhomogeneous nuclear matter. In the HS model, nuclei are treated as non-relativistic particles applying Maxwell-Boltzmann statistics along with medium corrections such as internal excitations or Coulomb screening. The masses of nuclei are taken from experimental data and from nuclear structure calculations. In order to ensure the dissolution of heavy nuclei to uniform matter at high densities, excluded volume effects are taken into account. Nucleon-nucleon interaction for unbound nucleons are described by the RMF model with the same parameterization as used for the high density core.

We calculate the pressure and energy density from the total canonical partition function given by

$$Z(T, V, \{N_i\}) = Z_{nuc} \prod_{A,Z} Z_{A,Z} Z_{Coul}, \tag{2.9}$$

where V denotes the volume of the system.

Helmholtz free energy can be written using the partition function as

$$F(T, V, \{N_i\}) = -TlnZ = F_{nuc} + \sum_{A,Z} F_{A,Z} + F_{Coul}, \tag{2.10}$$

where F_{nuc}, F_{Coul}, and $F_{A,Z}$ denote the free energies of nucleons, the Coulomb free energy, and the free energy of the nucleus represented by the Maxwell-Boltzmann distribution [82].

Once the excluded volume effects are implemented in a thermodynamically consistent manner [82], the number density of the nuclei will be given by

$$\begin{aligned} n_{A,Z} &= \kappa g_{A,Z}(T)\left(\frac{M_{A,Z}T}{2\pi}\right)^{3/2} \\ &\times \exp\left(\frac{(A-Z)\mu_n^0 + Z\mu_p^0 - M_{A,Z} - E_{A,Z}^{Coul} - P_{nuc}^0 V_{A,Z}}{T}\right), \end{aligned} \tag{2.11}$$

where κ represents the nuclear volume fraction, defined in terms of local number densities and takes values between 0 and 1.

Next, the free energy density can be written as [82]

$$\begin{aligned} f &= \sum_{A,Z} f_{A,Z}^0(T, n_{A,Z}) + f_{Coul}(n_e, n_{A,Z}) + \xi f_{nuc}^0(T, n_n', n_p') \\ &-T\sum_{A,Z} n_{A,Z} ln(\kappa), \end{aligned} \tag{2.12}$$

where the first term comes from the contribution of the non-interacting gas of nuclei. Here the Coulomb free energy is denoted by f_{Coul}. We multiply the free energy density of the interacting nucleons, f_{nuc}^0, by the available volume fraction of nucleons ξ. n_n' and n_p' represent the local number densities of neutrons and protons, respectively. The last term corresponding to a hard-core repulsion of nuclei goes to infinity as κ approaches zero near the saturation density. At this stage, the uniform matter is formed.

The energy density can be expressed by the following expression [82]

$$\epsilon = \xi\epsilon^0_{nuc}(T, n'_n, n'_p) + \sum_{A,Z} \epsilon^0_{A,Z}(T, n_{A,Z}) + f_{Coul}(n_e, n_{A,Z}), \tag{2.13}$$

$$\epsilon^0_{A,Z}(T, n_{A,Z}) = n_{A,Z}(M_{A,Z} + \frac{3}{2}T + \frac{\partial g}{\partial T}\frac{T^2}{g}). \tag{2.14}$$

The pressure is given by

$$P = P^0_{nuc}(T, n'_n, n'_p) + \frac{1}{\kappa}\sum_{A,Z} P^0_{A,Z}(T, n_{A,Z}) + P_{Coul}(n_e, n_{A,Z}), \tag{2.15}$$

$$P^0_{A,Z}(T, n_{A,Z}) = Tn_{A,Z}. \tag{2.16}$$

It is important to mention here all the quantities relevant for nucleonic contributions are calculated using the same RMF model parameterization as employed for the core and taking into account general Fermi-Dirac statistics. In the internal partition function of nuclei, $g_{A,Z}(T)$ in Eq. 2.11, only excited states up to the binding energy of the corresponding nucleus are taken into account in order to keep the nucleus bound [98]. If no cutoff is applied in the integral for the excited states, arbitrarily large excitation energies would contribute to the energy density. It is found in different applications of the EoS that the cutoff leads to a well behavior of the energy density.

To match the crust with the core, a standard thermodynamic criterion is followed wherein the free energy per baryon at fixed temperature T, baryon number density n_B and proton fraction Y_p is to be minimized.

2.4 Equation of State of Core

The central density of core is several times the saturation nuclear matter density ($\sim 2.7 \times 10^{14} g/cm^3$) and the exact nature of matter at such extreme density is yet to be understood. Various theoretical models have been attempted to explain the structure and nature of such matter. Walecka model, a Lorentz covariant theory of dense matter involving baryons and mesons, is widely applied to neutron star matter [99]. Non-linear scalar meson terms are included to reproduce the saturation properties of nuclear matter. Extrapolating the properties of nuclear matter beyond saturation density lead to uncertainties. The high density behaviour in the Relativistic Mean Field (RMF) calculations is usually taken into account by introducing the non-linear self interaction terms for scalar and vector meson fields [100]. But because of the instabilities and higher order field dependencies appearing probably at high densities this may not be a reliable approach. More suitable approach will be to make meson-baryon couplings density dependent [83, 101, 102]. In this density dependent model (DD2), a rearrangement term appears in the baryon chemical potential and changes the pressure and hence equation of state significantly. Existence of the novel phases of matter such as hyperons, condensate of pions and kaons and also deconfined quarks is still an open issue. Pauli's exclusion principle makes the appearance of strangeness inevitable in the high density baryonic matter.

2.4.1 Density Dependent Relativistic Hadron Field Theory

In our work, we have considered a phase transition (could be first order or second order) from hadronic to antikaon condensed matter. Hadronic phase contains different species of baryon octet while as electron and muons form a uniform background. The

Lagrangian density for baryons is given as

$$\begin{aligned}
\mathcal{L}_B \;\; = \;\; & \sum_B \bar{\psi}_B \left(i\gamma_\mu \partial^\mu - m_B + g_{\sigma B}\sigma - g_{\omega B}\gamma_\mu \omega^\mu - g_{\phi B}\gamma_\mu \phi^\mu \right. \\
& \left. - g_{\rho B}\gamma_\mu \boldsymbol{\tau}_B \cdot \boldsymbol{\rho}^\mu \right) \psi_B \\
& + \frac{1}{2}\left(\partial_\mu \sigma \partial^\mu \sigma - m_\sigma^2 \sigma^2 \right) - \frac{1}{4}\omega_{\mu\nu}\omega^{\mu\nu} \\
& + \frac{1}{2} m_\omega^2 \omega_\mu \omega^\mu - \frac{1}{4}\phi_{\mu\nu}\phi^{\mu\nu} + \frac{1}{2} m_\phi^2 \phi_\mu \phi^\mu \\
& - \frac{1}{4}\boldsymbol{\rho}_{\mu\nu} \cdot \boldsymbol{\rho}^{\mu\nu} + \frac{1}{2} m_\rho^2 \boldsymbol{\rho}_\mu \cdot \boldsymbol{\rho}^\mu .
\end{aligned} \tag{2.17}$$

Here ψ_B represents the baryon octet and baryon-baryon interaction is mediated by the exchange of scalar σ, vector ω and isovector ρ mesons. τ_B is the isospin operator and $g_{\alpha B}$ denote the meson-baryon couplings. An additional vector meson ϕ is included for hyperon-hyperon interaction only [100, 103].

Muons and electrons in the background are treated as non-interacting particles and are described by the Lagrangian $\mathcal{L}_l$ as

$$\mathcal{L}_l = \sum_{l=e^-,\mu^-} \bar{\psi}_l \left(i\gamma_\mu \partial^\mu - m_l \right) \psi_l . \tag{2.18}$$

In the rest frame of static, isotropic matter in the ground state, meson field equations are self-consistently solved maintaining the charge neutrality and baryon number conservation. The meson field equations take the following form in the mean field approximation (MFA),

$$\begin{aligned}
m_\sigma^2\sigma &= \sum_B g_{\sigma B} n_B^s, \\
m_\omega^2\omega_0 &= \sum_B g_{\omega B} n_B, \\
m_\rho^2\rho_{03} &= \sum_B g_{\rho B}\tau_{3B} n_B, \\
m_\phi^2\phi_0 &= \sum_B g_{\phi B} n_B. \qquad (2.19)
\end{aligned}$$

The number density and scalar density of baryons are given as

$$n_B = \langle\psi_B^\dagger\psi_B\rangle = \frac{\gamma}{(2\pi)^3}\int_0^{k_{F_B}} d^3k = \frac{k_{F_B}^3}{3\pi^2}, \qquad (2.20)$$

$$\begin{aligned}
n_B^s = \langle\bar{\psi}_B\psi_B\rangle &= \frac{\gamma}{(2\pi)^3}\int_0^{k_{F_B}} \frac{m_B^*}{\sqrt{k_{F_B}^2 + m_B^{*2}}} d^3k \\
&= \frac{m_B^*}{2\pi^2}[k_{F_B}\sqrt{k_{F_B}^2 + m_B^{*2}} - m_B^{*2} ln\frac{k_{F_B} + \sqrt{k_{F_B}^2 + m_B^{*2}}}{m_B^*}] \qquad (2.21)
\end{aligned}$$

Dirac equation for the spin 1/2 particles is given as

$$[\gamma_\mu(i\partial^\mu - \Sigma_B) - m_B^*]\psi_B = 0. \qquad (2.22)$$

Here $m_B^* = m_B - g_{\sigma B}\sigma$ is the effective baryon mass and $\Sigma_B = \Sigma_B^{(0)} + \Sigma_B^{(r)}$ is the vector self energy where first term $\Sigma_B^0 = g_{\omega B}\omega_0 + g_{\rho B}\tau_{3B}\boldsymbol{\rho_{03}} + g_{\phi B}\phi_0$ contains non-vanishing components of vector mesons and the second term, rearrangement term $\Sigma_B^r = \sum_B[-\frac{\partial g_{\sigma B}}{\partial n_B}\sigma n_B^s + \frac{\partial g_{\omega B}}{\partial n_B}\omega_0 n_B + \frac{\partial g_{\rho B}}{\partial n_B}\tau_{3B}\boldsymbol{\rho_{03}} n_B + \frac{\partial g_{\phi B}}{\partial n_B}\phi_0 n_B]$ arises due to density dependence of meson-baryon couplings [101]. It is important to mention here that ϕ meson doesn't couple with nucleons i.e. $g_{\phi B} = 0$ for $B = n, p$. Due to density dependence of couplings baryon chemical potential takes the form

$$\mu_B = \sqrt{k_B^2 + M_n^{*2}} + \Sigma_B^0 + \Sigma_B^r.$$

Next the β-equilibrium is imposed on the neutron star matter. Chemical equilibrium in the neutron star matter is maintained by the equilibrium condition $\mu_i = b_i\mu_n - q_i\mu_e$ where μ_i is the chemical potential of ith baryon, b_i is it's baryon number and q_i is the charge. μ_e and μ_n are the chemical potentials of electron and neutron, respectively.

The energy density due to baryons and leptons is given by

$$\begin{aligned}\epsilon_B &= \frac{1}{2}m_\sigma^2\sigma^2 + \frac{1}{2}m_\omega^2\omega_0^2 + \frac{1}{2}m_\rho^2\rho_{03}^2 + \frac{1}{2}m_\phi^2\phi_0^2 \\ &+ \sum_B \frac{2J_B+1}{2\pi^2}\int_0^{k_{F_B}} \sqrt{k^2+m_B^{*2}}k^2dk \\ &+ \sum_l \frac{1}{\pi^2}\int_0^{k_{F_l}} \sqrt{k^2+m_l^2}k^2dk \qquad (2.23)\end{aligned}$$

Unlike the energy density, the pressure contains the rearrangement term as well and can be expressed as

$$\begin{aligned}P_B &= -\frac{1}{2}m_\sigma^2\sigma^2 + \frac{1}{2}m_\omega^2\omega_0^2 + \frac{1}{2}m_\rho^2\rho_{03}^2 + \frac{1}{2}m_\phi^2\phi_0^2 \\ &+ \Sigma_B^{(r)}\sum_B n_B + \frac{1}{3}\sum_B \frac{2J_B+1}{2\pi^2}\int_0^{k_{F_B}} \frac{k^4dk}{\sqrt{k^2+m_B^{*2}}} \\ &+ \frac{1}{3}\sum_l \frac{1}{\pi^2}\int_0^{k_{F_l}} \frac{k^4dk}{\sqrt{k^2+m_l^2}} \qquad (2.24)\end{aligned}$$

Rearrangement term does not appear in the energy density expression but contributes to the pressure through baryon chemical potentials. The rearrangement term takes care of the energy momentum conservation and thermodynamic consistency of the system [101].

To determine the density-dependent meson-nucleon couplings, the prescription of Typel et. al [83, 102] is adopted and couplings can be described as [104]

$$g_{\alpha B}(n_b) = g_{\alpha B}(n_0) f_\alpha(x), \tag{2.25}$$

where $n_b = \sum_B n_B$ and $x = \frac{n_b}{n_0}$. The function $f_\alpha(x)$ is explicitly given by

$$\begin{aligned} f_\alpha(x) &= a_\alpha \frac{1 + b_\alpha (x + d_\alpha)^2}{1 + c_\alpha (x + d_\alpha)^2}; \alpha = \sigma, \omega \\ &= exp[-a_\alpha (x - 1)]; \alpha = \rho \end{aligned} \tag{2.26}$$

The number of parameters gets reduced by constraining these functions as $f_\sigma(1) = f_\omega(1) = 1$, $f'_\sigma(0) = f'_\omega(0) = 0$ and $f_\sigma(1) = f_\omega(1) = 1$, $f''_\sigma(1) = f''_\omega(1)$ [83]. Exponential density dependence is considered for isovector mesons ρ becuase ρ meson-nucleon coupling decreases at higher densities [104]. Finite nuclei properties like binding energies, charge and diffraction radii, surface thicknesses, spin-orbit splittings, and the neutron skin thickness of $^{208}\mathrm{P}b$ are fitted to determine the saturation density n_0, mass of σ meson m_σ, couplings $g_{\alpha B}(n_0)$ and coefficients a_α,b_α,c_α,d_α [83, 102] as tabulated in table 2.1. The fit provides the saturation density $n_0 = 0.149065 fm^{-3}$, binding energy per nucleon $B = -16.02$MeV and incompressibility $K = 242.7$MeV. Masses of neutron, proton, ω and ρ mesons are 939.56536, 938.2703, 783 and 763 MeV, respectively.

meson α	$g_{\alpha B}(\rho_0)$ in MeV	a_α	b_α	c_α	d_α
ω	13.342362	1.369718	0.496475	0.817753	0.638452
σ	10.686681	1.357630	0.634442	1.005358	0.575810
ρ	3.626940	0.518903			

Table 2.1: Parameters of meson-nucleon couplings in DD2 EOS.

Apart from DD2 parameterization, we have used one more DD parameterization known as DDME2 [84]. This is obtained by fitting finite nuclei properties like total binding energies BE, charge radii r_c and the differences between the radii of neutron and proton density distributions $r_{np} = (r_n - r_p)$. The fit provides the saturation density $n_0 = 0.152 fm^{-3}$, binding energy per nucleon $B = -16.14$MeV and incompressibility $K = 250.89$MeV. Masses of σ, ω and ρ mesons are 550.1238, 783 and 763 MeV, respectively. The parameterization of this model is given below in table 2.2

meson α	$g_{\alpha B}(\rho_0)$ in MeV	a_α	b_α	c_α	d_α
ω	13.0189	1.3892	0.9240	1.4620	0.4775
σ	10.5396	1.3881	1.0943	1.7057	0.4421
ρ	3.6836	0.5647			

Table 2.2: Parameters of meson-nucleon couplings in DDME2 EOS.

To determine hyperon-meson couplings, SU(6) symmetry relations are used for determining vector coupligs [100] as follows,

$$\begin{aligned} \frac{1}{2}g_{\omega\Lambda} = g_{\omega\Sigma} = g_{\omega\Xi} = \frac{1}{3}g_{\omega N}, \\ \frac{1}{2}g_{\rho\Sigma} = g_{\rho\Xi} = g_{\rho N}; g_{\rho\Lambda} = 0, \\ 2g_{\phi\Lambda} = 2g_{\phi\Sigma} = g_{\phi\Xi} = -\frac{2\sqrt{2}}{3}g_{\omega N}. \end{aligned} \tag{2.27}$$

Scalar meson (σ) coupling to hyperons is determined using potential depth of hyperon (Y) in the saturated nuclear matter

$$U_Y^N(n_0) = -g_{\sigma Y}\sigma + g_{\omega Y}\omega_0 + \Sigma_N^{(r)}, \tag{2.28}$$

where $\Sigma_N^{(r)}$ contains only nucleonic contribution. Λ-hypernuclei data suggests the Λ-potential depth, $U_\Lambda^N(n_0) = -30$ MeV [105, 106]. Because of the repulsive Σ-potential depth in nuclear matter ,Σ hyperons are not considered here. We neglect Ξ hyperons because Ξ hypernuclei data are scarce. Maximum mass of neutron stars is not changed significantly due to a particular choice of hypernuclear potential depths [107]. Using the value of $U_\Lambda^N(n_0) = -30$, we get the scaling factor as $R_{\sigma\Lambda} = \frac{g_{\sigma\Lambda}}{g_{\sigma N}} = 0.62008$.

2.4.2 Equation of State in nonlinear Walecka Model

We introduce here unified EoSs developed by Steiner, Fischer, and Hempel, based on NSE model for matter below the saturation density and nonlinear Walecka model with additional meson couplings. The Lagrangian for nonlinear Walecka model with cross meson terms is given by

$$\begin{aligned}
\mathcal{L}_B \;=\; & \sum_{B=n,p} \bar{\psi}_B \left(i\gamma_\mu \partial^\mu - m_B + g_{\sigma B}\sigma - g_{\omega B}\gamma_\mu \omega^\mu - \frac{1}{2} g_{\rho B}\gamma_\mu \boldsymbol{\tau}_B \cdot \boldsymbol{\rho}^\mu \right) \psi_B \\
& + \frac{1}{2}\left(\partial_\mu \sigma \partial^\mu \sigma - m_\sigma^2 \sigma^2 \right) \\
& - \frac{1}{4}\omega_{\mu\nu}\omega^{\mu\nu} + \frac{1}{2} m_\omega^2 \omega_\mu \omega^\mu \\
& - \frac{1}{4}\boldsymbol{\rho}_{\mu\nu} \cdot \boldsymbol{\rho}^{\mu\nu} + \frac{1}{2} m_\rho^2 \boldsymbol{\rho}_\mu \cdot \boldsymbol{\rho}^\mu - U(\sigma) \\
& + \frac{\kappa}{24} g_{\omega B}^4 (\omega^\mu \omega_\mu)^2 + \frac{\lambda}{24} g_{\rho B}^4 (\boldsymbol{\rho}_\mu \cdot \boldsymbol{\rho}^\mu)^2 \\
& + g_{\rho B}^2 f(\sigma, \omega^\mu \omega_\mu) \cdot \boldsymbol{\rho}^\mu \cdot \boldsymbol{\rho}_\mu,
\end{aligned} \tag{2.29}$$

where τ_B is the isospin operator and $U(\sigma)$ represents the self-interactions terms for scalar σ meson and is given as

$$U(\sigma) = \frac{\zeta}{6}(g_{\sigma B}\sigma)^3 + \frac{\xi}{24}(g_{\sigma B}\sigma)^4 \tag{2.30}$$

and

$$f(\sigma, \omega^\mu\omega_\mu) = \sum_{i=1}^{6} a_i\sigma^i + \sum_{j=1}^{3} b_j(\omega^\mu\omega_\mu)^j \tag{2.31}$$

This model contains 17 parameters which provide sufficient enough freedom to fine tune both the low- and high-density part of the isospin sector independently [87]. These two EoSs are represented as SFHo and SFHx where "o" denotes optimal and "x" stands for extremal. The most probable mass-radius curve of Steiner et al. [86] was fitted in SFHo and the radius of low-mass neutron stars was minimized in SFHx model leading to a low value (23.18 MeV) for the density slope of the symmetry energy at the saturation density [87]. If the last two terms are neglected in the Lagrangian density given by Equation (2.29), it reduces to the same Lagrangian density as that of TM1 and TMA EoS models with different parameter sets [88, 89]. TMA [89] parameterization is based on an interpolation of the two parameter sets TM1 and TM2 [88], which were fitted to binding energies and charge radii of light (TM2) and heavy nuclei(TM1). In these cases also, a unified EoS was constructed based on the NSE model for the low-density matter and the Lagrangian density without last two terms in Equation (2.29) for nucleon-nucleon interaction for low as well as high-density matter [109].

2.4.3 Antikaon Condensation

Now we discuss the Bose-Einstein condensation of antikaons. The antikaon condensed phase is made of species of the baryon octet, isospin doublet of antikaons with electrons and muons forming a uniform background. The baryon-baryon interaction Lagrangian density is already discussed in section 2.4.1. We treat the antikaon-baryon interaction on the same footing as the baryon-baryon interaction.

Antikaons are described in the minimal coupling scheme by the Lagrangian density [110–113] given by

$$\mathcal{L}_K = D_\mu^* \bar{K} D^\mu K - m_K^{*2} \bar{K} K, \tag{2.32}$$

where $D_\mu = \partial_\mu + ig_{\omega K}\omega_\mu + ig_{\rho K}\tau_K.\rho_\mu + ig_{\phi K}\phi_\mu$ is the covariant derivative and $m_K^* = m_K - g_{\sigma K}\sigma$ is the effective mass of (anti)kaons with m_K as the bare kaon mass. $K \equiv (K^+, K^0)$ and $\bar{K} \equiv (K^-, \bar{K}^0)$ denote the isospin doublets for kaons and antikaons, respectively.

The in-medium energies of antikaons for the s-wave condensation are given by

$$\omega_{K^-,\bar{K}^0} = m_K^* - g_{\omega K}\omega_0 - g_{\phi K}\phi_0 \mp g_{\rho K}\rho_{03}. \tag{2.33}$$

Scalar and vector densities of antikaons for s-wave condensation at T=0, are the same and are given as

$$n_{K^-,\bar{K}^0} = 2(\omega_{K^-,\bar{K}^0} + g_{\omega K}\omega_0 + g_{\phi K}\phi_0 \pm g_{\rho K}\rho_{03})K\bar{K}. \tag{2.34}$$

The onset of antikaon condensation is fixed by the requirement of chemical equilibrium in neutron star matter. The chemical equilibrium is attained through

$$N \rightleftharpoons N + \bar{K}, \quad e^- \rightleftharpoons K^- + \nu_e, \tag{2.35}$$

where $\bar{K} \equiv (K^-, \bar{K}^0)$ and $N \equiv (n, p)$. Hence, the equilibrium conditions are given as

$$\mu_n - \mu_p = \mu_{K^-} = \mu_e, \quad \mu_{\bar{K}^0} = 0, \tag{2.36}$$

where μ_{K^-} and $\mu_{\bar{K}^0}$ represent the chemical potentials of K^- and $\bar{K}^0$, respectively.

In the presence of antikaon condensates, the meson field equations in the mean field approximation will take the form given by

$$\begin{aligned} m_\sigma^2\sigma &= \sum_B g_{\sigma B} n_B^s + g_{\sigma K}\sum_{\bar{K}} n_{\bar{K}}, \\ m_\omega^2\omega_0 &= \sum_B g_{\omega B} n_B - g_{\omega K}\sum_{\bar{K}} n_{\bar{K}}, \\ m_\rho^2\rho_{03} &= \sum_B g_{\rho B}\tau_{3B} n_B + g_{\rho K}\sum_{\bar{K}} \tau_{3\bar{K}} n_{\bar{K}}, \\ m_\phi^2\phi_0 &= \sum_B g_{\phi B} n_B - g_{\phi K}\sum_{\bar{K}} n_{\bar{K}}. \end{aligned} \tag{2.37}$$

Only baryons and leptons contribute to the pressure and antikaon condensate ($\mathbf{p}=0$) does not have any pressure contribution. However, the meson fields are altered because of the presence of additional term due to (anti)kaons in the field equations. Charge neutrality condition is also modified by the presence of K^- mesons. Energy density of antikaons can be expressed as

$$\epsilon_{\bar{K}} = m_K^*(n_{K^-} + n_{\bar{K}^0}). \tag{2.38}$$

Hence total energy density having contributions from baryons , antikaons and leptons can be expressed as $\epsilon = \epsilon_B + \epsilon_{\bar{K}}$.

Meson-anti(kaon) couplings are calculated on the same footing as that of meson-hyperon couplings but without considering any density-dependence. From the quark model and isospin counting rule, coupling constants of ω and ρ mesons with kaons are obtained. Coupling constant of ϕ mesons with kaons is obtained from SU(3) symmetry relations and the value of $g_{\pi\pi\rho}$ [100] i.e.

$$g_{\omega K} = \frac{1}{3} g_{\omega N}; \qquad g_{\rho K} = g_{\rho N} \qquad and \qquad \sqrt{2} g_{\phi K} = 6.04. \tag{2.39}$$

The real part of the K^- optical potential depth at the saturation density is utilised to calculate the scalar coupling constant ($g_{\sigma K}$) [100, 101, 110, 111]

$$U_{\bar{K}}(n_0) = -g_{\sigma K}\sigma - g_{\omega K}\omega_0 + \Sigma_N^{(r)}. \tag{2.40}$$

It is inferred from the study of kaon atoms that (anti)kaon nucleon optical potential is attractive. However, there is a controversy about the depth of the potential. The phenomenological fits to kaonic atom data prefer the potential to be extremely deep whileas unitary chiral model calculations suggest the potential to be shallow. There is a lack of consensus regarding the range of values of $U_{\bar{K}}$ and different experiments suggest values from -50 to -200 MeV [108]. We consider a set of values for $U_{\bar{K}}$ and the corresponding coupling constants $g_{\sigma K}$ are mentioned in the table 2.3.

$U_{\bar{K}(MeV)}$	-60	-80	-100	-120	-140
$g_{\sigma\bar{K}}$	-1.24609	-0.72583	-0.20557	0.31469	0.83495

Table 2.3: Parameters of σ meson-(anti)kaon couplings in DD2 EOS.

2.4.4 Hadron-quark Phase Transition

In our work, we consider two equations of state that undergo a first order phase transition from hadronic to quark matter [114–116]. In the first case, for the hadronic matter above the saturation density, the DDRH model as described in section 2.4.1 is employed here. The hadronic phase includes all hyperons plus Δ resonance [114]. For quark matter made of u, d, s quarks, a non-local extension of the Nambu-Jona-Lasinio model [117] is adopted. The hadron-quark mixed phase is ruled by the Gibbs rules. The Gibbs conditions for phase equilibrium is that the temperature (here $T = 0$), the pressure and chemical potentials μ_b and μ_q corresponding to baryon and electric charge, are equal in two phases and is given by

$$P_H(\mu_b, \mu_q, T) = P_Q(\mu_b, \mu_q, T). \tag{2.41}$$

For a volume V comprising of a bulk quantity of matter, the above condition must be supplemented by conditions of global baryon number conservation and global electric charge conservation which are given by

$$\begin{aligned} q &= (1-\chi)q_H(\mu_b, \mu_q, T) + \chi q_Q(\mu_b, \mu_q, T), \\ \rho &= (1-\chi)\rho_H(\mu_b, \mu_q, T) + \chi \rho_Q(\mu_b, \mu_q, T), \end{aligned} \tag{2.42}$$

where $\chi = V_Q/(V_H + V_Q)$ and it takes values in the range $0 < \chi < 1$. The solution of Eq. 2.41 and Eqs. 2.42 is different for each proportion of the phases χ so that all the properties including the pressure will vary through the mixed phase. We denote this hadron-quark (HQ) EoS by HQ1 hereafter. In another case, the hadronic phase is composed of only nucleons and described by the NL3 model [85] whereas the effective bag model including quark interaction is adopted for the quark phase [116]. The HQ mixed phase in this case is based on the Maxwell construction. This HQ EoS is denoted by HQ2 hereafter.

Chapter 3

I-Love-Q Universal Relations

3.1 Introduction

The equation of state (EoS) of dense matter is a key ingredient in understanding the physics of core-collapse supernovae, neutron stars and neutron star mergers. It is a highly challenging task for the scientific community to determine the dense matter EoS. The matter below the saturation density might be constrained by the inputs from the laboratory nuclear physics experiments. On the other hand, the EoS of supradense matter with density several times normal nuclear matter density is explored by astrophysical observations.

Multi-wavelength observations are performed for investigating neutron stars. These observations resulted in macroscopic properties of neutron stars, for example, masses, surface magnetic fields and temperatures. Mass measurement has reached a high precision level in case of neutron star binaries particularly relativistic binaries involving pulsars. The highest neutron star mass accurately measured so far is

2.01±0.04 M_{solar} [41]. This constrains the dense matter EoS severely. Radius measurement is still a debatable issue. Efforts to extract information about radius due to surface emission in X-ray thermonuclear bursts and from accreting neutron stars in quiescence are going on, but complicated by uncertainties in the composition of atmosphere and distance to sources. Recently, NICER provided the estimates of the mass and radius of the isolated 205.53 Hz millisecond pulsar. The data was analysed independently by two groups using different methods. One of the groups used Bayesian inference approach to analyze it's energy-dependent thermal X-ray waveform and reported the mass and radius as $R = 13.02^{+1.24}_{-1.06}\ km$ and $M = 1.44^{+0.15}_{-0.14}\ M_{\odot}(68\%)$ [52], repectively. Whileas the other group adopted Bayesian parameter estimation which is conditional on pulse-profile modeling of NICER X-ray spectral-timing event data and obtained the mass and radius as $1.34^{+0.15}_{-0.16}\ M_{\odot}(68\%)$ and $12.71^{+1.14}_{-1.19}\ km$ [53], respectively. An alternative to this is the measurement of moment of inertia (I), for example that of pulsar A in double pulsar system PSR J0737-3039 [44, 118]. There will be many fold increase in the number of newly discovered pulsars in relativistic binaries with the advent of highly sensitive Square Kilometre Array (SKA). This will facilitate faster estimation of moment of inertia in the SKA era. Consequently, simultaneous knowledge of mass and radius of the same neutron star will be available. Furthermore, this might lead to the better understanding of the EoS in neutron star interior.

After the discoveries of black hole (GW150914 [57]) and neutron star merger events (GW170817 [58] and GW190425 [119]), gravitational waves open up a new landscape into astrophysical observations. It is expected that gravitational wave detectors such as Advanced LIGO, VIRGO, KAGRA or LIGO-India [120] might record gravitational waves from more neutron star merger events in future. Gravitational waves from merging neutron stars provide an interesting opportunity to probe dense matter in neutron star interior and its EoS [58, 121]. In the late stage inspiral of binary neutron stars, tidal deformations could be estimated. This tidal deformation depends on the EoS. The tidal deformation is described by a set of parameters known as Love numbers. The quadrupole Love number (k_2) is an important quantity which is given by the ratio of quadrupole and tidal tensors. It might be possible to extract the Love number from the detection of gravitational wave signal [10, 122, 123]. The recent investigation on this issue found that the Love number was related to moment of inertia and spin induced quadrupole moment (Q) through universal relations [62].

A universal relation might describe the exterior spacetime of a compact object independently of its internal structure. These relations are valid under certain physical conditions. For example, the universal relations are broken at high rotational frequencies $\sim 1kHz$ [64] and high magnetic field $\sim 10^{13}G$ [63]. The details about the so called I-Love-Q relations can be found in the recent review by Yagi and Yunes [124] and references therein. However, it is to be investigated whether these relations will also hold strong in presence of a first order phase transition inside the neutron star or not.

It is known that observed masses, radii and moments of inertia might be direct probes of compositions and EoS of dense matter in neutron stars. The appearance of novel phases of hyperons, Bose-Einstein condensate of antikaons and quarks could be highly plausible above 2-3 times normal nuclear matter density in neutron star interior. Strange matter such as hyperon matter [100, 107, 125, 126], kaon condensed matter [4, 127] or quark matter [128], makes the EoS softer and results in smaller maximum mass compared with that of neutron stars made of neutrons and protons only. Latest observations demand that EoS models have to explain two solar mass or more massive neutron stars. Hyperon matter EoS models encounter a precarious situation. This is known as the hyperon puzzle. This puzzle was solved by introducing an extra repulsion into the EoS [107].

Recent advances in multi-wavelength observations of neutron stars and the detection of gravitational waves in neutron star merger motivate us to investigate dense matter EoSs involving strangeness degrees of freedom and their impact on the moment of inertia, quadrupole moment and love number. Furthermore, we are interested to explore whether universal relations among those observables hold good even in presence of exotic matter involving first order phase transition or not.

3.2 Equations of State

We compute the moment of inertia, quadrupole moment and love number in slowly rotating neutron stars. Each of these quantities is dependent on the EoS. The EoS for charge-neutral and beta-equilibrated matter made of baryons, antikaon condensate and leptons is constructed. We adopt a density dependent relativistic hadron (DDRH) field theory for the description of strongly interacting dense baryonic matter. Baryon-baryon interaction in the DDRH model is mediated by exchanges of scalar σ, vector ω, ϕ and ρ mesons and is given by the Lagrangian density [11,102,129] in section 2.4.1. The exchange of ϕ mesons accounts for the repulsive hyperon-hyperon interaction and could be a plausible solution to the hyperon puzzle. Nucleon-nucleon interaction is not mediated by ϕ mesons.

Meson field equations are solved in the mean field approximation (MFA). Finally we obtain the pressure versus energy density known as the EoS as given by Ref. [11, 129]. We note that, for density dependent couplings, the pressure includes the rearrangement term which takes care of many body effects and thermodynamic consistency.

It is found that the effective mass and in-medium energy of antikaons decrease with baryon density. The s-wave Bose-Einstein condensate of antikaons ($\mathbf{p} = 0$) appears when the electron chemical potential is equal to the in-medium energy of antikaons. The hadronic to antikaon condensate phase transition could be either a first or second order phase transition. Baryons are embedded in the antikaon condensate. The kaon-baryon interaction is treated on the same footing as the baryon-baryon interaction in Eq. (2.17) of section 2.4.1. The Lagrangian density for (anti)kaons in the minimal coupling scheme [110, 113, 129] in section 2.4.3. We obtain the EoS in the antikaon condensed phase by solving the equations of motion in the MFA. Here kaon-meson couplings are not density dependent.

Next we consider two more equations of state (HQ1 and HQ2) wherein hadronic matter undergoes a first order phase transition to quark matter [114–116] as described in section 2.4.4 of Chapter 2.

3.3 Model of Rotating Neutron Stars

Majority of observed galactic neutron stars rotate slowly. The fastest rotating neutron star has a spin frequency of 716 Hz. A neutron star is deformed due to rotation or tidal field. Here rigidly rotating neutron stars are studied assuming a stationary, axisymmetric spacetime and the line element as given by [130, 131]

$$ds^2 = -N^2 dt^2 + A^2(dr^2 + r^2 d\theta^2) + B^2 r^2 \sin^2\theta (d\phi - N^\phi dt)^2 \ , \tag{3.1}$$

where metric functions N, N^ϕ, A, B depend on coordinates r and θ.

The energy-momentum tensor for a perfect fluid describing the matter, is

$$T^{\mu\nu} = (\varepsilon + P)u^\mu u^\nu + P g^{\mu\nu} , \tag{3.2}$$

where ε is the energy density, P is the pressure and u^μ is the fluid four velocity.

The equilibrium configurations for rotating neutron stars are obtained by solving the Einstein field equations. In case of rigid rotation, this is equivalent to solving a first integral of the equation of fluid stationary motion [130]

$$H(r,\theta) + lnN - \ln\Gamma(r,\theta) = const , \tag{3.3}$$

where Γ represents the Lorentz factor of the fluid with respect to the Eulerian observer and the fluid log-enthalpy is

$$H = ln\left(\frac{\varepsilon + P}{nm_B}\right) , \tag{3.4}$$

where n and m_B are baryon density and rest mass, respectively.
The first-integral (Eq. 3.3) is integrable within the 3+1 formalism, where those reduce to Poisson-like partial differential equations that are then solved numerically using spectral scheme within the numerical library LORENE [132, 133]. The input parameters for the model are an EoS, the rotation frequency Ω and the central log-enthalpy H_c. Global properties of rotating neutron stars such as gravitational mass, circumferential equatorial radius, angular momentum, moment of inertia and quadrupole moment are estimated within this formalism using the asymptotic behaviour of lapse function (N) and the component of the shift vector (N^ϕ), in terms of metric potential and the source [130, 131]. The gravitational mass, angular

momentum and quadrupole moment are given respectively as [131, 134, 135],

$$M = \frac{1}{4\pi} \int \sigma_{lnN} \; r^2 \sin^2\theta dr d\theta d\phi \ , \tag{3.5}$$

$$J = \int A^2 B^2 (E+p) U r^3 \sin^2\theta dr d\theta d\phi \ , \tag{3.6}$$

$$Q = -M_2 - \frac{4}{3}\left(b + \frac{1}{4}\right) M^3 \ , \tag{3.7}$$

where,

$$M_2 = -\frac{3}{8\pi} \int \sigma_{lnN} \left(\cos^2\theta - \frac{1}{3}\right) r^4 \sin^2\theta dr d\theta d\phi \ . \tag{3.8}$$

Here, σ_{lnN} is the RHS of Eq. 3.19 of Ref. [130], U is the fluid four-velocity, $E = \Gamma^2(\varepsilon + p) - p$ and $\Gamma = (1 - U^2)^{-1/2}$ and b is defined by Eq. (3.37) of Ref. [135]. The moment of inertia of the rotating star is defined as,

$$I := \left| \frac{J}{\Omega} \right| . \tag{3.9}$$

At lower rotation frequencies, this behaves almost as a linear relation.

3.4 Love number, moment of inertia and quadrupole moment

A static, spherically symmetric star under the influence of a static external quadrupolar tidal field E_{ij}, develops a quadrupole moment Q_{ij}. The tidal deformability λ in the linear order is given by

$$\lambda = -\frac{Qij}{E_{ij}}. \tag{3.10}$$

The $\ell = 2$ dimensionless tidal Love Number (k_2) is related to the tidal deformability as

$$k_2 = \frac{3}{2R^5}\lambda. \tag{3.11}$$

The tidal love number is calculated following the prescription by Hinderer et al. [10,123] in the Regge-Wheeler gauge. A linear, static and even parity $\ell = 2, m = 0$ perturbation leads to the following form of deformed metric,

$$\begin{aligned} ds^2 &= -e^{2\Phi(r)}\left[1 + H(r)Y_{20}(\theta,\varphi)\right]dt^2 \\ &\quad + e^{2\Lambda(r)}\left[1 - H(r)Y_{20}(\theta,\varphi)\right]dr^2 \\ &\quad + r^2\left[1 - K(r)Y_{20}(\theta,\varphi)\right]\left(d\theta^2 + \sin^2\theta d\varphi^2\right), \end{aligned} \tag{3.12}$$

where, $K'(r) = H'(r) + 2H(r)\Phi'(r)$. This leads to a second order differential equation for metric function H

$$\begin{aligned} & H'' + H'\left(\frac{2}{r} + \Phi' - \Lambda'\right) + H\left(-\frac{6e^{2\Lambda}}{r^2} - 2(\Phi')^2\right. \\ & \left. + 2\Phi'' + \frac{3}{r}\Lambda' + \frac{7}{r}\Phi' - 2\Phi'\Lambda' + \frac{f}{r}(\Phi' + \Lambda')\right) = 0. \end{aligned} \tag{3.13}$$

where, $f = d\epsilon/dp$. This equation is solved by integrating outward from the center and using the asymptotic behaviour of $H(r)$, we get the $\ell = 2$ tidal love number,

$$\begin{aligned} k_2 &= \frac{8C^5}{5}(1-2C)^2[2+2C(y-1)-y] \\ &\times\Big\{2C[6-3y+3C(5y-8)] \\ &+4C^3[13-11y+C(3y-2)+2C^2(1+y)] \\ &+3(1-2C)^2[2-y+2C(y-1)]\ln(1-2C)\Big\}^{-1}. \end{aligned} \tag{3.14}$$

Here, we define $y = RH'(R)/H(R)$ and take compactness of the star, $C = M/R$.

The tidal deformability parameter, moment of inertia and quadrupole moment are dependent on the EoS individually. However, it was pointed out that the relation among any two of them in the slow rotation approximation was EoS independent [62]. The following dimensionless quantities are used in this investigation. The dimensionless λ is defined as

$$\bar{\lambda} = \frac{\lambda}{M^5} \tag{3.15}$$

Similarly dimensionless moment of inertia and quadrupole moment are $\bar{I} = \frac{I}{M^3}$ and $\bar{Q} = \frac{Q}{(M^3(J/M^2)^2)}$, respectively. Here Q is compared with the Kerr solution quadrupole moment J^2/M because the dimensionless Q is known as the Kerr factor.

3.5 Results and Discussion

The density dependent parameter set used here is referred to as the DD2 set for nucleon-meson couplings [11, 102]. Hyperon-meson couplings are computed from the SU(6) symmetry relations and hypernuclear data [100, 107]. Λ hyperons, being lightest among all hyperons, might be populated first in dense matter. Therefore, only Λ hyperons are included in this calculation. We consider a potential depth of

-30 MeV for Λ hyperons in normal nuclear matter and estimate the scalar meson coupling. Similarly, kaon-meson couplings are estimated using the quark model, SU(3) relations and kaon atomic data [129]. An attractive potential depth of -120 MeV in normal nuclear matter is adopted for the determination of kaon-scalar meson coupling. Parameters of the quark phase are obtained from Ref. [114, 116]. Using those parameter sets, we calculate various properties of rotating neutron stars as described in sections 3.3-3.4 for four different compositions of matter namely neutron-proton matter (denoted as np), Λ hyperon matter ($np\Lambda$), antikaon condensed matter including Λ hyperons ($np\Lambda K^-$) and hadron-quark matter. Figure 3.1 exhibits

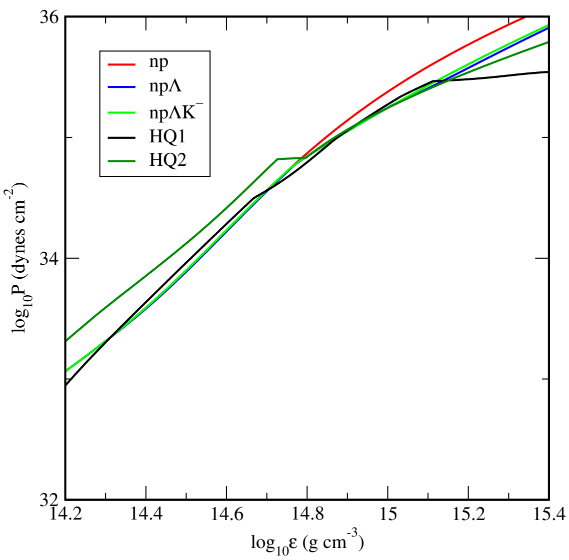

Figure 3.1: Pressure versus energy density is plotted for different compositions of matter [9].

the pressure (P) versus energy density (ε) plot known as the EoS for different compositions of matter. Strange matter components such as Λ hyperons, antikaons in the condensate or quarks make an EoS softer as evident from the figure. Two kinks in both HQ EoSs implies the beginning and end of the hadron-quark mixed phase [114–116]. The HQ1 EoS involving hadron-quark phase transition is the softest EoS among the five EoSs and np matter has the stiffest EoS. We calculate sequences of static neutron stars using those EoSs. The mass-radius relation is plotted in Fig.

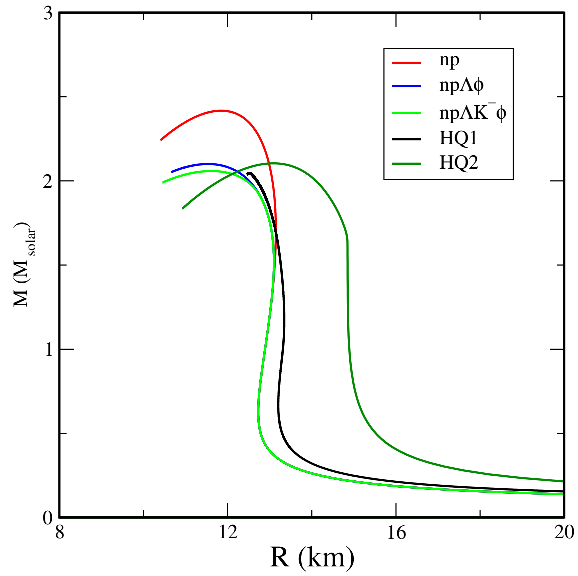

Figure 3.2: Mass versus radius is plotted for equations of state shown in Fig. 1 [9].

3.2. Maximum masses corresponding to np, $np\Lambda$, $np\Lambda K^-$, HQ1 and HQ2 EoS are 2.42, 2.1, 2.06, 2.04 and 2.1 M$_{solar}$, respectively. It shows that all these EoSs are compatible with the 2 M$_{solar}$ constraint.

There is a good chance for the measurement of moment of inertia with the detection of the relativistic pulsar binary PSR J0737-3039 in 2003 Ref. [118]. In particular, the moment of inertia estimation for pulsar A in the double pulsar system might be possible in near future. Masses of both pulsars in the double pulsar system had been accurately measured due to the determination of post Keplerian parameters. The precise measurement of I from observations along with the accurately known mass of pulsar A might lead to better determination of radius [44]. Here we discuss our results on the effects of exotic matter on moment of inertia. Slowly rotating neutron stars with spin frequency 100 Hz are considered in this calculation using LORENE. The behaviour of moment of inertia with neutron star mass is depicted in Fig. 3.3. It is noted that the moment of inertia corresponding to strange matter is lower than that of nuclear matter at higher neutron star masses. As we know the mass (1.337 M$_{solar}$) of pulsar A in PSR J0737-3039, the value of I can be predicted from Fig. 3.3.

Dimensionless moment of inertia ($\bar{I} = \frac{I}{M^3}$) as a function of compactness is shown in Fig. 3.4 for four EoSs. It is found that curves corresponding to np, $np\Lambda$ and $np\Lambda K^-$ merge before the onset of Λ hyperons or antikaon condensate. As soon as strange degrees of freedom set-in in dense neutron star matter, $\bar{I}$ for strange matter EoSs deviate from that of the nuclear matter case at higher compactness. However, it is found that results of $np\Lambda$ and $np\Lambda K^-$ cases show almost a universal behaviour. This may be related to the significant population of Λ hyperons even after the appearance of antikaon condensate. We further investigation the quadrupole moment of rotating

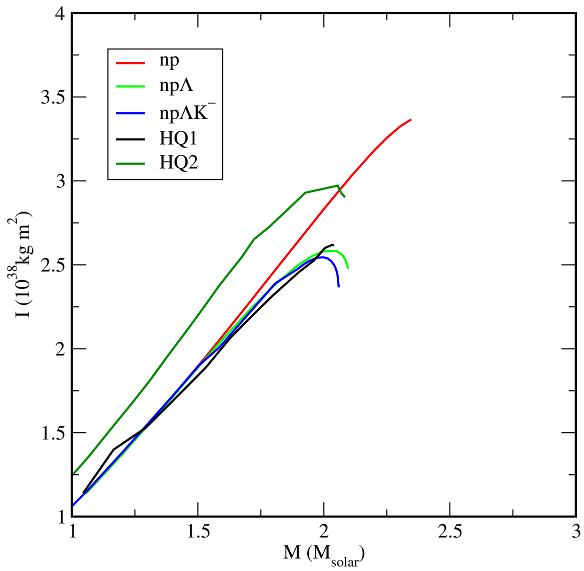

Figure 3.3: Moment of inertia is shown as a function of neutron star mass for different compositions of matter [9].

neutron stars having spin frequency of 100 Hz using LORENE. The behaviour of the quadrupole moment with respect to the Kerr solution is exhibited with neutron star mass in Fig. 3.5. It is found to decrease with mass and approache the Kerr value around maximum neutron star mass. The stiffest EoS corresponding to the nuclear matter case is closest to the Kerr solution. This was already noted by others [73, 136, 137]. The most interesting result is obtained when we plot dimensionless I versus dimensionless Q in Fig. 3.6. All data corresponding to different EoSs used here show no deviations except that of the HQ EoSs. Though I or Q depends on the EoS,

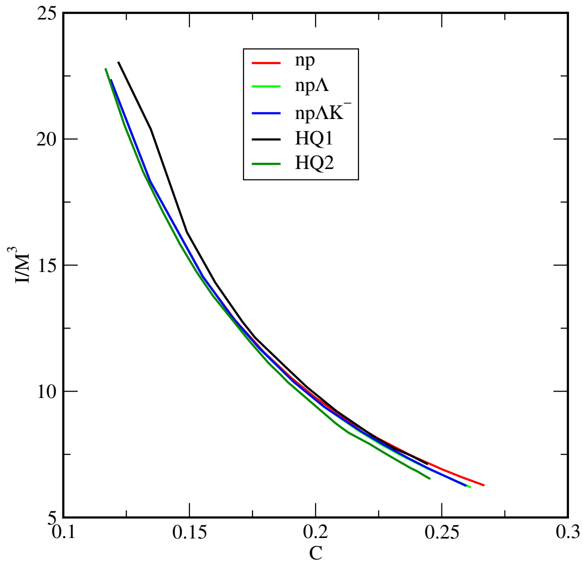

Figure 3.4: Dimensionless moment of inertia ($\bar{I} = I/M^3$) is plotted with compactness [9].

their relationship exhibit universality for np, $np\Lambda$ and $np\Lambda K^-$ EoS. The I-Love-Q universal relation was first predicted by Yagi and Yunes [62]. This holds good for other observables too. When the ratio of critical mass i.e., the maximum mass at the mass-shedding limit and maximum mass for static neutron stars are plotted with normalised angular momentum with respect to maximum angular momentum, it also leads to universal relation [138, 139]. However, the I-Q universality is lost when we look at both HQ EoSs. This may be attributed to a first order hadron-quark phase transition in HQ1 and HQ2.

We further explore the role of first order phase transition on the I-Q universality relation at higher rotational frequencies. It is well known that the rotation induces compositional changes in neutron stars [114]. This significantly impacts the hadron-quark phase transition in rotating neutron stars. As neutron star spins down, its central density increases from smaller values. When the density exceeds the threshold value, a hadron-quark phase transition begins. We study the I-Q relation for 300 and 500 Hz to understand the above effect and the results are shown in Fig. 3.7 and

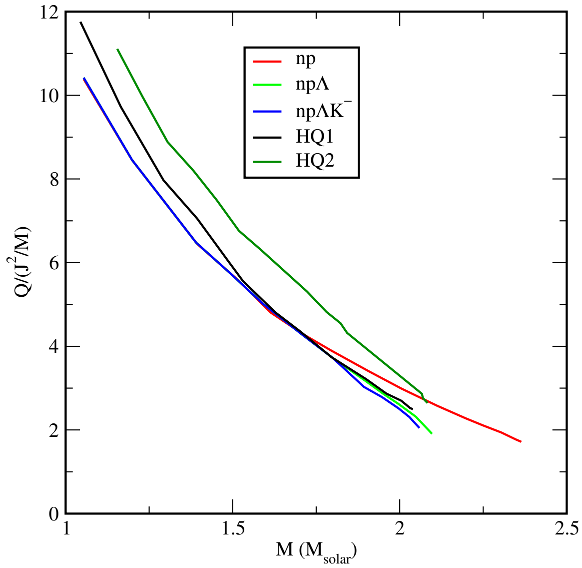

Figure 3.5: Dimensionless quadrupole moment with respect to the Kerr solution is plotted with neutron star mass [9].

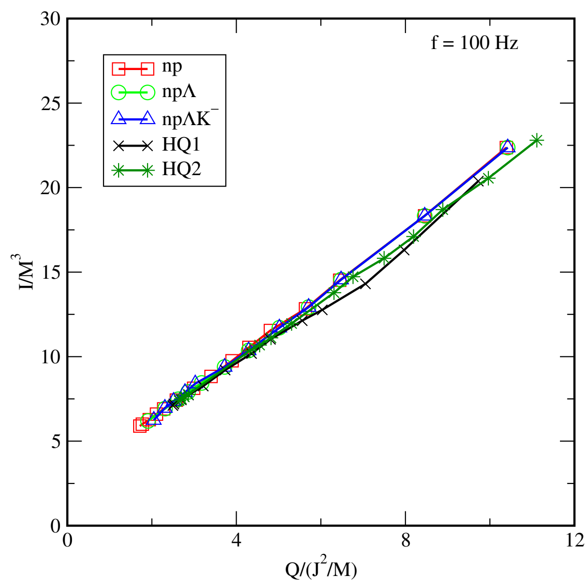

Figure 3.6: Dimensionless moment of inertia is shown as a function of dimensionless quadrupole moment for rotational frequency 100 Hz [9].

Fig. 3.8. For HQ2 EoS, the hadron-quark phase transition disappears at those frequencies and the universality is restored. However, the imprint of the phase transition on the I-Q relation can be observed even at higher rotational frequencies for HQ1 case. The reason behind this is the HQ1 EoS having a much wider mixed

phase compared with that of the HQ2 EoS. Next we investigate the relation between

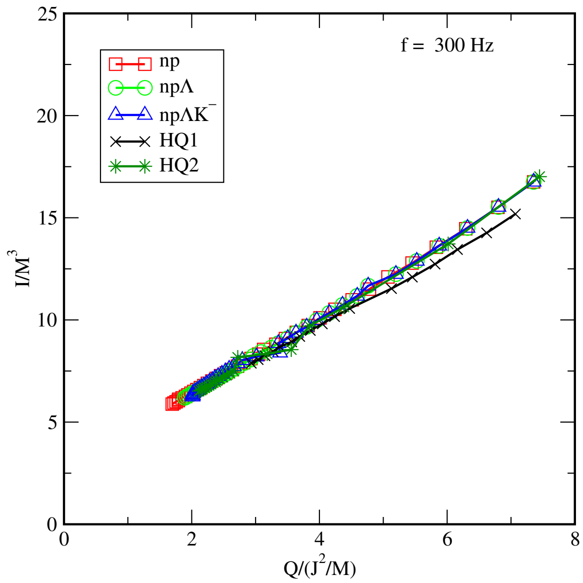

Figure 3.7: Same as Fig. 6 but for rotational frequency 300 Hz [9].

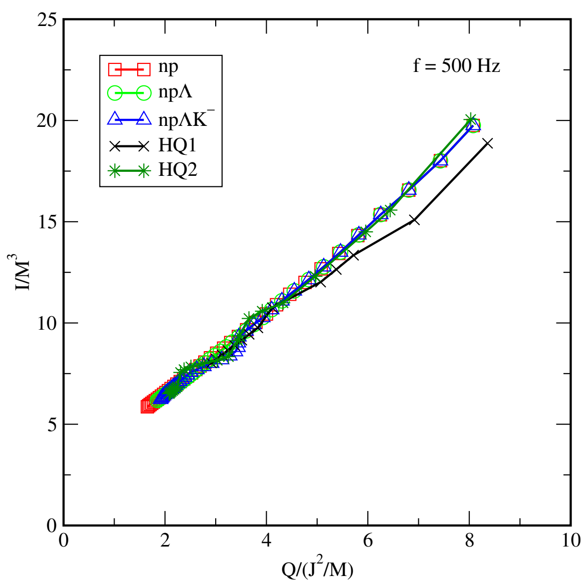

Figure 3.8: Same as Fig. 6 but for rotational frequency 500 Hz [9].

I and Love number for strange matter EoSs adopting slow rotation approximation of Hartle and Thorne [135]. We plot $\ell = 2$ love number (k_2) with compactness ($C = M/R$) in Fig. 3.9 for np, $np\Lambda$, $np\Lambda K^-$ and HQ matter. The love number demonstrates how easy or difficult to deform a neutron star. For each EoS, love number decreases with increasing compactness. More the star is compact, lesser is its love number. Furthermore, this effect is more prominent in softer EoSs i.e. $np\Lambda$, $np\Lambda K^-$ and HQ than that of np matter. The love number approaches zero for black holes corresponding to compactness (M/R) 0.5. Figure 3.10 describes the behaviour of dimensionless moment of inertia with dimensionless tidal deformability parameter $\bar{\lambda}$ as defined in Sec. 3.2 for np, $np\Lambda$, $np\Lambda K^-$ and HQ EoS. Like Fig. 3.6, it is noted that a universal relation exists in $\bar{I}$-$\bar{\lambda}$ for three hadronic EoSs. However, the data of HQ EoSs deviate from the universal relation. It is now obvious that Fig. 3.6 and Fig. 3.10 together produce I-Love-Q relations which do not depend on the compositions and EoS of neutron star matter without a first order phase transition. Neutron star matter below the saturation density is well constrained by nuclear physics experiments in laboratories. All EoSs in this density regime should behave in the same manner and lead to universal relations. However, this is not true at higher densities where many new degrees of freedom are populated in the form of hyperons, antikaon condensate and quarks. We observe significant deviations in EoSs in that density regime. It is then a puzzle to understand what drives the universality when the neutron star compactness increases. This has been attributed to the isodensity contours in neutron stars which are approximately elliptically self similar [69, 124]. It is worth mentioning here this kind of universal relation among I and Q was also found in rotating protoneutron stars [69, 140].

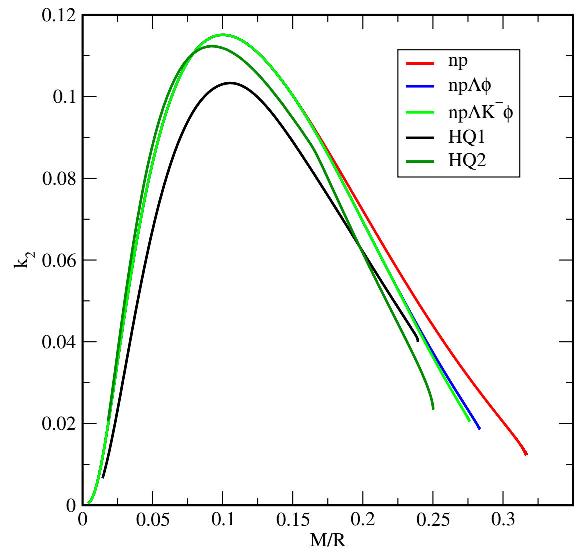

Figure 3.9: Love number is plotted with compactness of neutron star [9].

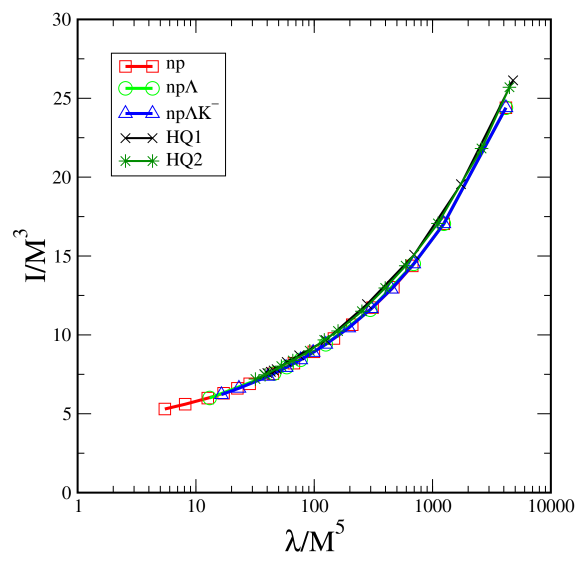

Figure 3.10: Dimensionless moment of inertia is shown as a function of dimensionless deformability parameter ($\bar{\lambda}$) [9].

Chapter 4

Constraining Equation of State with GW170817 observations

4.1 Introduction

The discovery of gravitational waves emitted from the binary neutron star merger event GW170817 and subsequently followed by the detection of its transient counterparts across the electromagnetic (EM) spectrum has heralded a new era in multimessenger astrophysics [58,141]. The observed short Gamma Ray Burst (GRB) 1.7 s after the coalescence time provides clinching evidences for the association of short GRBs with neutron star mergers. This discovery of two colliding neutron stars and its aftermath provided vast amount of information about short Gamma Ray Bursts, binary chirp mass, tidal deformability and dense matter in neutron star interior, speed of gravitational waves, Hubble constant and heavy element synthesis due to r-process in ejected neutron-rich matter. From the gravitational wave data analysis, the binary chirp mass, $\mathcal{M}_{chirp} = (m_1 m_2)^{3/5}/(m_1+m_2)^{1/5}$, in the 90% credible interval is estimated to be $1.188^{+0.004}_{-0.002}$ $M_\odot$ [58]. For low spin prior, the component masses of the binary were found to be in the range 1.17-1.6 $M_\odot$, whereas the total mass of the binary was $2.74^{+0.04}_{-0.01}$ $M_\odot$. The binary mass ratio ($q = m_2/m_1$) was constrained in the range 0.7 - 1.0 for low spin prior. The optical/infrared transient, several hours after GW170817, was consistent with emissions of a Kilonova which was shining through radioactive decays of r-process nuclei synthesised in the neutron-rich ejected matter [142, 143].

The observation of GW170817 revealed many interesting aspects of dense matter in neutron stars and its equation of state (EoS). The fate of the compact remnant formed in the binary neutron star merger might be closely related to the amount of ejected material as estimated from EM signals [144]. A prompt collapse was ruled out by the quantity of blue ejecta observed in optical wavelengths. It was argued that the merger remnant was born as a hypermassive neutron star (HMNS) supported by differential rotation for a short duration of time. This picture of short lived HMNS might be consistent with the large quantity of red ejecta that was observed in the infrared and originating from the accretion torus around the HMNS before its collapse to a black hole. The compact remnant spun down emitting gravitational waves and might have collapsed to a black hole close to the mass-shedding limit of a uniformly rotating neutron star [145]. This conclusion about the merger remnant provided the upper bound on the maximum mass of non-rotating neutron stars and much tighter constraint on the EoS of dense matter [144–147]. The lower bound on the maximum mass of neutron stars is obtained from the galactic pulsar observations.

It was long argued that the tidal effects in the late inspiralling phase of binary neutron stars could be large and detected by gravitational wave detectors [10,122,123]. The tidal deformation of a neutron star could provide crucial information about the dense matter EoS. The effective tidal deformability parameter is expected to be determined from the phase evolution of gravitational wave signals. Indeed this was achieved in GW170817 and GW190425 [58, 119]. The LIGO and VIRGO observations of GW170817 imposed an upper limit on the dimensionless effective tidal deformability $\bar{\Lambda} \leq 800$ in the low spin case at 90% confidence level [58]. A lower limit on $\bar{\Lambda} \geq 400$ was obtained from the observational data of the electromagnetic counterpart of GW170817 combined with numerical relativity simulations [146]. Recently another alternative approach based on radiative transfer simulations of the electromagnetic transient AT2017gfo indicated the lower bound on the tidal deformability to be $\bar{\Lambda} \geq 197$ [148].

Gravitational wave data of GW170817 were reinterpreted by De et al. [149]. The initial analysis of the LIGO/VIRGO collaboration (LVC) differed from that of De et al. in the sense that the same EoS was not adopted for two neutron stars of GW170817 in the former case whereas in the latter case the tidal deformabilities (Λ_1 and Λ_2) and masses of both neutron stars were related through $\Lambda_1/\Lambda_2 \sim q^6$ implying that both neutron stars were described by the same EoS. Later, the LVC analysed the data again using correlations in tidal deformabilities [150]. The correlation among tidal deformabilities led to a 20% reduction in 90% confidence upper bound of the previously estimated effective tidal deformability [149,150]. Tighter bounds on Λ_1/Λ_2 tuned to chirp mass were prescribed in an EoS-independent manner for gravitational waveform analysis [151].

The lower and upper bounds on the tidal deformability parameter provided strong constraints on the dense matter EoS in neutron star interior. Too soft or too stiff EoSs were rejected because of those constraints [146]. The knowledge of tidal deformability from GW170817 was used to constrain the neutron star radius [149, 152–155]. The upper limit of the radius of a 1.4 $M_\odot$ neutron star was shown to be ≤ 13.76 km [152]. In another investigation with one million different EoSs, the radius (R) of a 1.4 $M_\odot$ neutron star was found to be $12.00 \leq R/km \leq 13.45$ [153]. Similar conclusion was drawn about the radius in Ref. [154]. Using the correlation among tidal deformabilities of merger components, radii of both neutron stars were determined to be $8.7 < R/km < 14.1$ at the 90% credible interval [149]. The LVC also calculated the neutron star radii firstly adopting EoS-insensitive relations and secondly the same parameterized EoS for both neutron stars [155]. In the second case, the condition that the EoS was compatible with 1.97 $M_\odot$ neutron stars was taken into account. This resulted in higher radii of neutron stars in the second case than those of the first case [155]. So far we noticed that gravitational wave data from GW170817 as well as its EM counterpart AT2017gfo led to the determination of upper bounds on the mass and radius of non-rotating neutron stars. Besides masses and radii of neutron stars, the measured tidal deformability could put constraints on other properties of merger components of GW170817 such as moment of inertia and quadrupole moment. This motivates us to explore EoS of dense matter and properties of merger components of GW170817 in this work.

4.2 Equations of State of Binary Merger Components

We discuss the computation of tidal deformability, moment of inertia and quadrupole moment in this section. These quantities are EoS dependent [9] as reported in Chapter 3. We adopt different relativistic mean field (RMF) models for the EoS of beta-equilibrated and charge neutral matter. The strong interaction among nucleons from the crust to the core is mediated by the exchange of scalar, vector and isovector mesons in these RMF models. The RMF parameterizations used in this calculations are TM1, TMA, SFHo, SFHx, DD2, DDME2 [84,156] as discussed

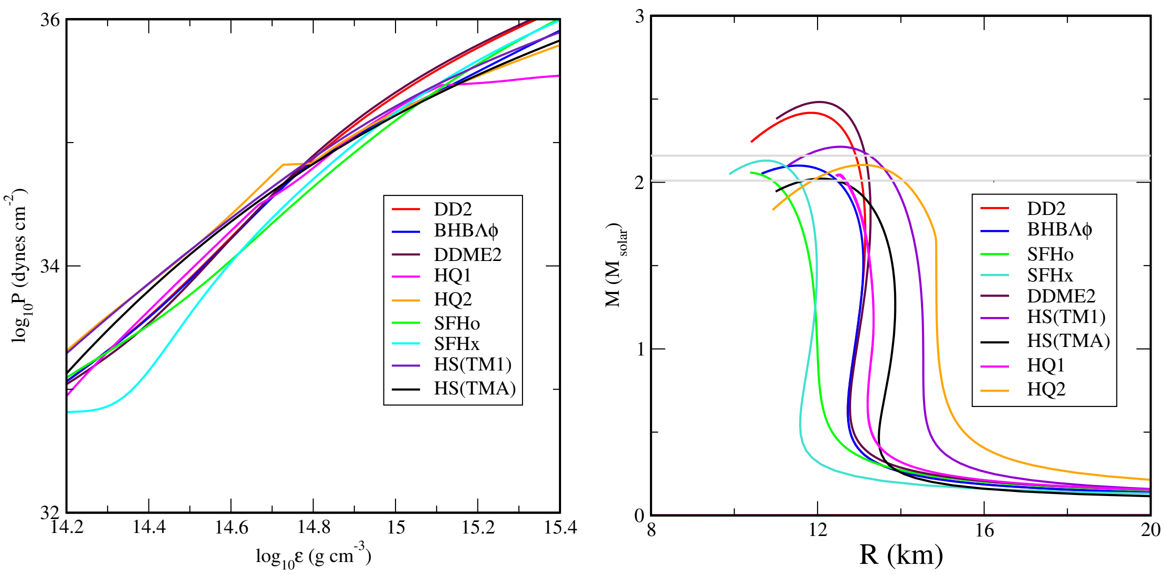

Figure 4.1: Pressure versus energy density is plotted for different compositions (left panel) and mass-radius relation is exhibited for those equations of state (right panel) [13].

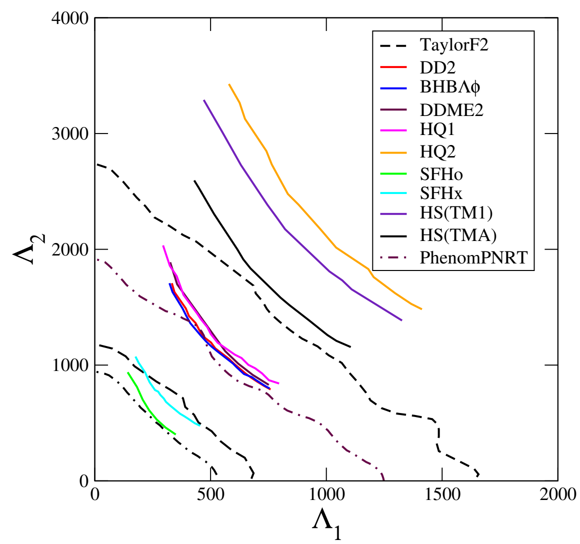

Figure 4.2: Dimensionless tidal deformability parameters Λ_1 and Λ_2 are plotted here for different equations of state [13]. Dashed and dash-dotted lines denote the 50% and 90 % probability contours as obtained from Ref. [58, 150].

in sections 2.4.1, 2.4.2 of Chapter 2. We also consider equations of state (HQ1 and HQ2) involving first-order phase transition from hadronic matter to quark matter as discussed in section 2.4.4 of Chapter 2.

4.3 Results and Discussion

The calculation of Love number and tidal deformability has been discussed in Chapter 3. The dimensionless tidal deformability, dimensionless moment of inertia and dimensionless quadrupole moment are defined as $\Lambda_{1,2} = \frac{\lambda_{1,2}}{m_{1,2}^5}$, $\bar{I}_{1,2} = \frac{I_{1,2}}{m_{1,2}^3}$ and $\bar{Q}_{1,2} = \frac{Q_{1,2}}{(m_{1,2}^3(J_{1,2}/m_{1,2}^2)^2)}$ respectively, where subscripts 1 and 2 correspond to masses of merger components, m_1 and m_2 respectively. Quadrupole moment $Q_{1,2}$ is compared with the Kerr solution quadrupole moment $J_{1,2}^2/m_{1,2}$ and the dimensionless $\bar{Q}_{1,2}$ are known as Kerr factors corresponding to $m_{1,2}$. Moment of inertia and quadrupole moment are calculated by the spectral scheme within the numerical library LORENE [132, 133].

We adopt nuclear EoSs HS(TM1), HS(TMA), HS(SFHo), HS(SFHx), DDME2, HS(DD2), hyperon EoS BHB$\Lambda\phi$ and hadron-quark EoSs HQ1 and HQ2 for the calculation of neutron star properties as shown in the left panel of Figure 4.1. The right panel of Figure 4.1 shows neutron star mass as a function of radius for the above mentioned EoSs. All those EoSs are compatible with 2 $M_\odot$ neutron stars. We could learn valuable lessons about dense matter EoS from the fate of the massive remnant in GW170817. It is inferred that a hypermassive neutron star was born in the binary merger event and later it collapsed to a black hole. In this scenario, different groups estimated the upper bound on the maximum mass of non-rotating neutron stars (M_{max}^{TOV}) to be 2.16 $M_\odot$ [144, 145, 147, 157]. On the other hand, the lower limit on the neutron star maximum mass 2.01±0.04 $M_\odot$ was obtained from the observations of galactic neutron stars. Both bounds on the neutron star maximum mass i.e. $2.01 \pm 0.04 \leq M_{TOV}/M_\odot \leq 2.16 \pm 0.03$, imposed strong constraints on the EoS of dense matter. All EoSs except DD2, DDME2 and HS(TM1) satisfy these constraints on M_{max}^{TOV} as demonstrated by two horizontal lines in the right panel of Fig. 4.1.

Tidal deformability Λ_2 is plotted with Λ_1 in Fig. 4.2 for all those EoSs considered here. Dimensionless tidal deformabilities of both merger components are calculated using the same EoS. It also shows the 50% and 90% credible intervals (dashed and dash-dotted lines) for the low spin case obtained using waveform models of TaylorF2 and PhenomPNRT [58, 150]. As the tidal deformability is directly proportional to R^5, the compactness increases from top right corner to bottom left corner of Fig. 4.2. The SFHo EoS represents neutron stars with maximum compactness among all EoSs. The HQ2 EoS on the top right corner implies the least compact neutron stars and lies far outside the 90% credible interval. It is noted that HS(DD2) and BHB$\Lambda\phi$ EoSs which were allowed by TaylorF2 model, are now marginally compatible with the 90% contour of PhenomPNRT. The other EoSs which fall well inside 50% and 90% confidence intervals of PhenomPNRT are validated.

It has been noted that the tidal deformability parameter could probe the dense matter EoS. This can be further understood from Figs. 4.1 and 4.2. The upper limit on neutron star maximum mass is compatible with HQ2 and HS(TMA) along with several other EoSs as evident from Fig. 4.1. However, HQ2 and HS(TMA) EoSs are ruled out by the 90% confidence contour in Fig. 4.2. This demonstrates that the low density parts of HQ2 and HS(TMA) EoSs are not well constrained and lead to larger radii ($>$ 14 km) for merger components. Besides this, the nuclear matter EoS in hadron-quark phase transition in HQ2 is described by the NL3 EoS which is very stiff. On the other hand, the neutron star maximum mass is estimated by the overall EoS which becomes softer due to the phase transition to quark matter.

A correlation among tidal deformabilities and mass ratio of neutron stars was reported by different groups [149–151]. When both neutron stars are described by the same EoS, it is found that tidal deformabilities follow the relation $\Lambda_1/\Lambda_2 \sim q^6$ [149, 151]. Furthermore, analytical lower and upper bounds on Λ_1/Λ_2 tuned to chirp

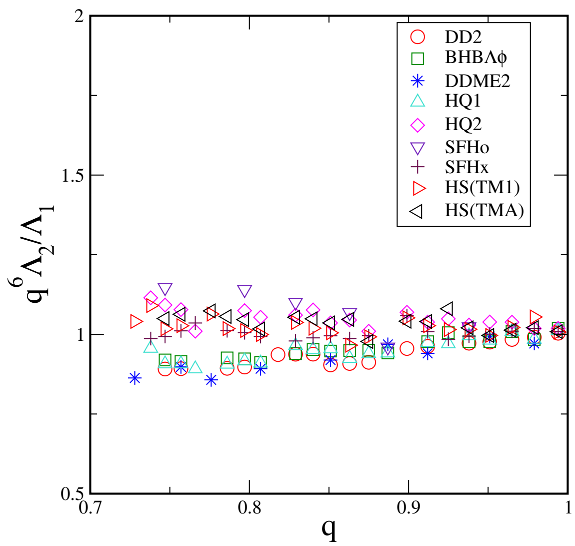

Figure 4.3: The quantity $q^6\Lambda_2/\Lambda_1$ is shown as a function of mass ratio (q) for chirp mass 1.188 $M_\odot$ and different equations of state [13].

mass were estimated studying large number of piecewise polytropic EoSs with and without strong first order hadron-quark phase transitions [151]. We investigate this correlation among tidal deformabilities and mass ratio for EoSs considered in Figs. 4.1 and 4.2. Figure 4.3 shows $q^6\Lambda_2/\Lambda_1$ as a function of mass ratio q. It is noted that this correlation holds good for values of mass ratio $q \geq 0.9$ for most EoSs adopted in this work. However, it is observed that the quantity $q^6\Lambda_2/\Lambda_1$ deviates from the value of unity for smaller values of q.

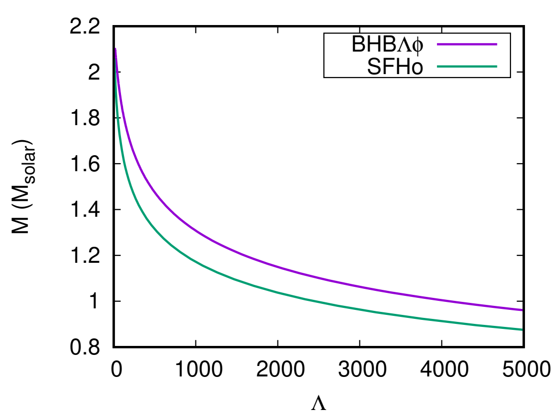

Figure 4.4: Mass of neutron star is plotted as a function of tidal deformability for BHB$\Lambda\phi$ and SFHo equations of state [13].

Neutron star mass is plotted as a function of tidal deformability for BHB$\Lambda\phi$ and SFHo EoSs in Fig. 4.4. The tidal deformability decreases as the neutron star becomes more massive. This also results in higher compactness. Consequently, more compact neutron stars will be less deformed. The tidal deformability for a 1.4 $M_\odot$ neutron star is 697 and 334 in case of BHB$\Lambda\phi$ and SFHo EoSs, respectively.

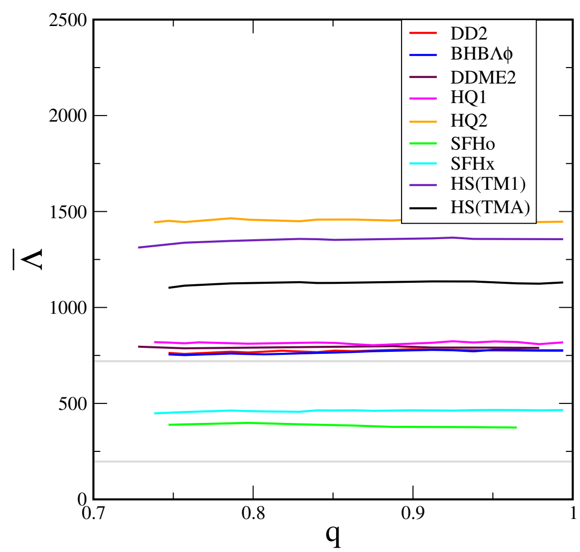

Figure 4.5: Tidal parameter $\bar{\Lambda}$ is plotted against mass ratio q for a fixed chirp mass $\mathcal{M}_{chirp}$ = 1.188 M_{solar}. Observational upper and lower limits (grey lines) are shown here [13].

LIGO and Virgo observations extracted the tidal contribution from the inspiral phase. The parameter ($\bar{\Lambda}$) that enters into the phase of the gravitational wave signal is a mass-weighted linear combination of individual dimensionless tidal deformabilities as [158]

$$\bar{\Lambda} = \frac{16}{13}\frac{(m_1 + 12m_2)m_1^4\Lambda_1 + (m_2 + 12m_1)m_2^4\Lambda_2}{(m_1 + m_2)^5} \tag{4.1}$$

which is considered to be $\lesssim$ 720 at 90% confidence level for low spin prior [150]. Also an additional constraint placed on $\bar{\Lambda} \geq 197$ is based on EM observations of GW170817 [148]. So the allowed window for $\bar{\Lambda}$ is now $197 \leq \bar{\Lambda} \leq 720$.

Mass weighted average tidal deformability parameter $\bar{\Lambda}$ is plotted against the ratio (q) of masses of merger components for a fixed chirp mass $\mathcal{M}_{chirp}$ = 1.188 M$_\odot$ in case of low spin scenario in Fig. 4.5. Here results are shown for all EoSs as marked in the figure. Upper and lower boundaries on $\bar{\Lambda}$ that were obtained from the gravitational wave and EM observations, respectively, are also shown in Fig. 4.5. It is found that results corresponding to all EoSs satisfy the lower boundary. However, this can not be said about several EoSs with respect to the upper boundary. It is evident from Fig. 4.5 that HS(DD2) and BHB$\Lambda\phi$ EoSs are marginally outside the upper boundary whereas HS(TM1), HS(TMA), HQ1 and HQ2 EoSs are conclusively ruled out by the GW data. It is worth mentioning here that the estimates of both boundaries are strongly model dependent [146, 148, 150]. It is also noted from Fig. 4.5 that $\bar{\Lambda}$ is independent of q. This is also demonstrated analytically by Zhao and Lattimer [151].

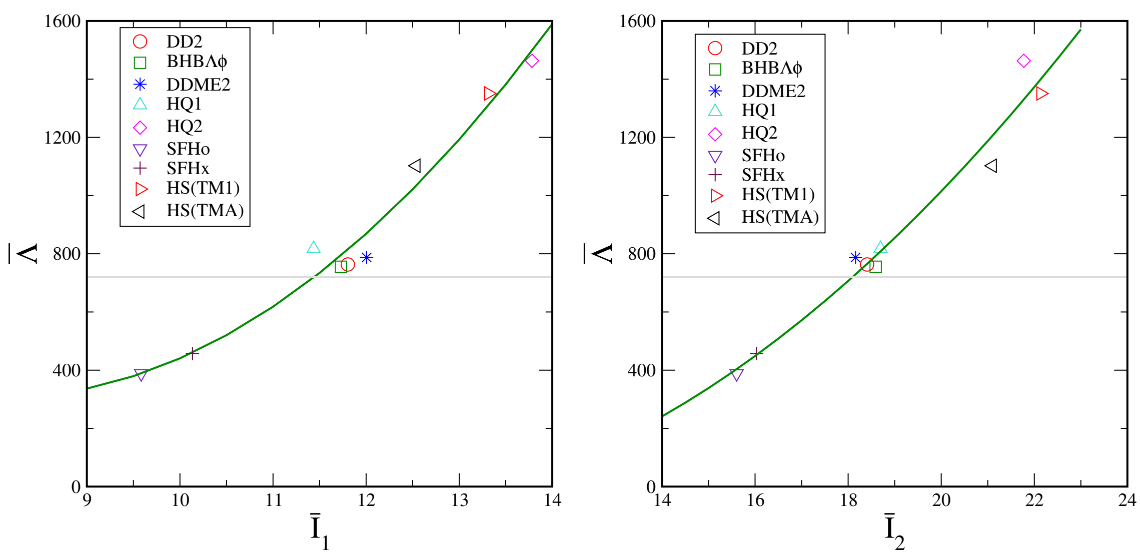

Figure 4.6: Mass weighted average tidal deformability parameter $\bar{\Lambda}$ is plotted against dimensionless moment of inertia of the heavier component of the neutron star binary having mass 1.58 M$_\odot$ (left panel) and and for the lighter component of the neutron star binary having mass 1.18 M$_\odot$ (right panel) [13].

We calculate gross properties such as moment of inertia and quadrupole moment of slowly rotating neutron stars with spin frequency 100 Hz in this calculation using LORENE [132, 133]. Figure 4.6 shows the relations between the parameter $\bar{\Lambda}$ versus dimensionless moments of inertia of merger components $\bar{I}_1$ (left panel) and $\bar{I}_2$ (right panel), respectively. These results are obtained for masses of merger components (m_1 =1.58, m_2 =1.18) $M_\odot$ as obtained from the chirp mass. The upper bound on $\bar{\Lambda}$ at 90% confidence level as obtained from gravitational wave data of GW170817 is also included on the plot. The intersections of the curves with the upper bound of $\bar{\Lambda}$ give upper limits on the values of moments of inertia of two merger components. The values of I_1 and I_2 so obtained are $\sim 2.0 \times 10^{45}$ g/cm^2 and $\sim 1.2 \times 10^{45}$ g/cm^2, respectively. These values of moments of inertia are consistent with the theoretically predicted values of Ref. [159].

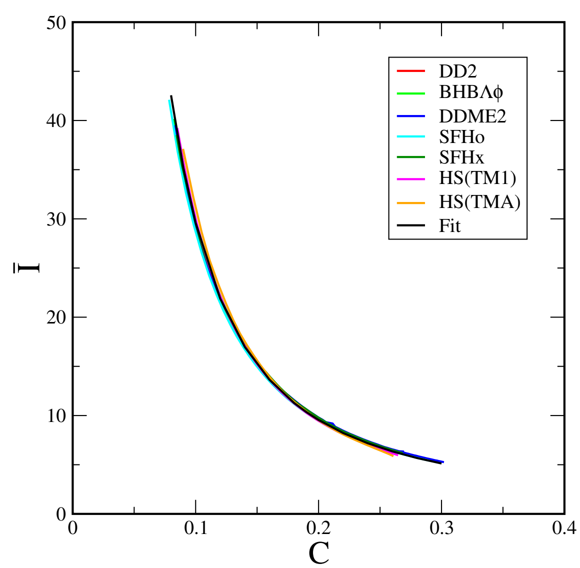

Figure 4.7: Dimensionless moment of inertia is plotted with compactness of neutron star for different hadronic equations of state [13].

As we know the moment of inertia and mass of each component, it is possible to estimate the radius of the corresponding component. This is done using the universal relation between dimensionless moment of inertia and compactness of neutron star [138]. This universal relation is shown in Fig. 4.7 for equations of state considered here except HQ EoSs in Fig. 4.1. The universal relation is fitted with the functional form as given by Eq. (20) of Ref. [138]. It is evident that the upper limit on the tidal deformability constrains radii of merger components to be ~ 13 km which are independent of component masses [154]. It is worth mentioning here that HQ EoSs violate the universality [9].

We do the similar investigation for quadrupole moments (Q_1, Q_2) of merger components in GW170817. Figure 4.8 exhibits the behaviour of mass weighted average tidal deformability parameter with dimensionless quadrupole moments $\bar{Q}_1$ (left panel) and $\bar{Q}_2$ (right panel), respectively. The upper limit on $\bar{\Lambda}$ from gravitational wave observation of GW170817 is also shown in both figures by horizontal lines. The values of upper bounds on quadrupole moments are found to be in the range 0.29 - 0.30 $\times 10^{43}$ g cm^2. Unlike the cases of moments of inertia in Fig. 4.6, the estimated value of upper bound on Q_1 is less than that of Q_2 because the latter merger component is less compact and it is easy to deform the star.

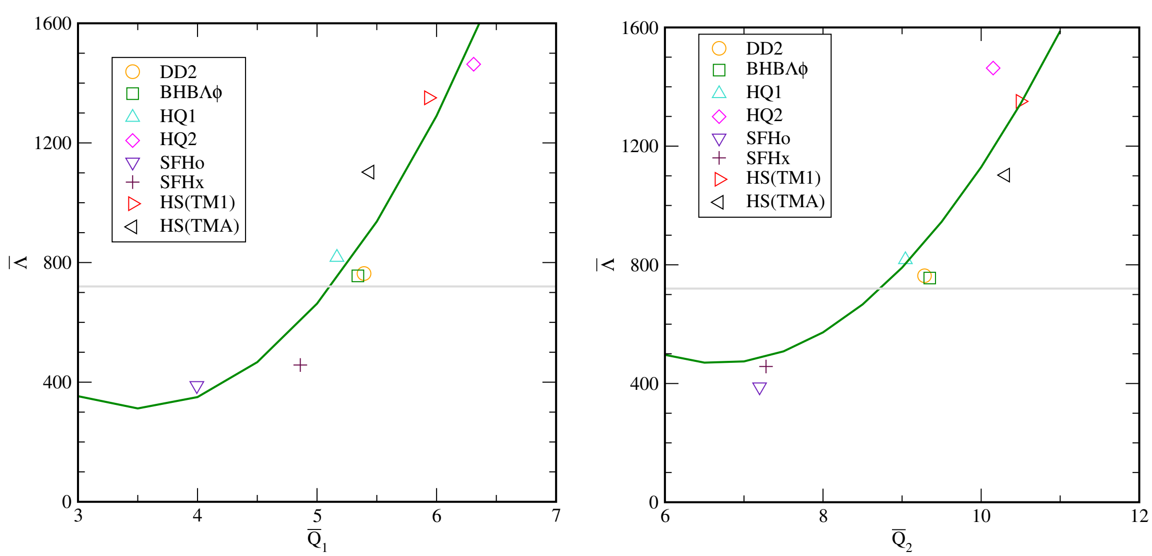

Figure 4.8: Mass weighted average tidal deformability parameter ($\bar{\Lambda}$) is plotted against dimensionless quadrupole moment of the heavier component (left panel) and lighter component (right panel) [13].

Chapter 5

Cooling of Dark-Matter Admixed Neutron Stars

5.1 Introduction

Neutron stars are excellent celestial laboratories for investigating the supradense nuclear matter which is otherwise inaccessible to terrestrial laboratories. The density inside neutron stars is several times the nuclear saturation density, hence exotic particles like hyperons [1,2], pion or kaon condensate [3,4], quarks [5] are believed to be present inside the core. Dark matter (DM) particles [6–8] may also be captured and accumulated inside neutron stars. Exotic particles soften the equation of state (EoS) and reduce the tidal deformability of the neutron star [9]. Exact nature of the matter is a challenging task and yet to be known. Any model suggested should not only describe the superdense matter but also reproduce the properties of matter observed at saturation density [160,161]. Recently, the unprecedented joint detection of neutron star merger GW170817 by Advanced LIGO and Virgo observatories has put stronger constraints on the equation of state by constraining tidal deformability of NSs [58,141]. Using Shapiro delay measurements, a very massive neutron star PSR J0740+6620 with mass $2.14^{+0.10}_{-0.09}$ [42] has been found. This can constrain the equation of state significantly.

Nowadays there are various cosmological and astrophysical indications for the existence of dark matter in the Universe like large-scale structures of the Universe, rotation curves of spiral galaxies, anisotropies of cosmic microwave background radiation (CMBR), gravitational lensing etc. The detection of dark matter is attempted following three different ways i.e. direct detection, indirect detection and collider searches (LHC). However, till now no experimental signature of dark matter has been discovered. Direct detection experiments usually provide us upper bounds on the dark matter-nucleon elastic scattering cross-sections for various DM masses. In the literature, several theoretical particle models of dark matter are proposed to indirectly detect the dark matter and to explain the existence of few unsolved phenomenological evidences such as gamma ray excesses observed by Fermi-LAT gamma ray telescope [162,163], positron excesses measured by PAMELA [164], AMS-02 [165], DAMPE [166] experiments etc. Till now many particle candidates of dark matter are proposed like Weakly Interacting Massive Particles (WIMPs) [167–170], Axions [171,172], Feebly interacting Massive Particles (FIMPs) [173,174], Fuzzy dark matter [175,176], neutralino [167], Kaluza Klein dark matter [177] etc. In this work, our proposed particle candidate of dark matter is WIMP. In the early Universe, WIMPs are produced thermally and initially they are at thermal equilibrium but when the temperature drops below the WIMPs mass they are decoupled at a particular temperature ($\sim \frac{M_\chi}{20}$) called freeze-out temperature. After decoupling, WIMP would possibly be a relic particle and may constitute a particle candidate of cold dark matter (CDM). WIMPs can cluster with stars gravitationally and also form a background density in the universe.

Several studies have indicated that neutron stars being highly compact objects can capture more dark matter particles during the formation stage in the supernova explosion as compared to the non-compact objects [178]. Recently, it is shown that the admixture of DM inside NSs softens the equation of state and hence tidal deformability is reduced [179]. It has been proven in Ref. [180] that the DM capture could be highly improved if it happens in binary pulsars. Since the DM present inside DM admixed NSs can possibly change the global properties of neutron stars, this opens another indirect window to study DM apart from other numerous ways. The structures of DM admixed NSs have been studied recently. It is shown that mass and radius of NSs can be remarkably affected by mirror DM [181]. It has been shown that fermionic DM could soften the equation of state and hence reduce the maximum mass supported by the NS [179]. This effect is sensitive to the mass of DM particle and the self-interaction within the dark matter. Since the normal matter and DM are believed to interact gravitationally, presence of DM can hardly influence the distribution of particles inside NS but can significantly modify the structure as well as EoS of NS.

Cooling of neutron stars has been well studied by several authors [29, 182–185]. Some study has been done on the effect of DM on cooling of NSs [186]- [188]. It has been found that the heating due to dark matter annihilation can affect the temperature of the stars older than 10^7 years and consequently flattening out the temperature at 10^4 K for the neutron stars [187, 189]. Moreover, recently it has been found that slowdown in the pulsar rotation can drive the NS matter out of beta equilibrium and the resultant imbalance in chemical potentials can induce late-time heating, named as rotochemical heating which can heat a NS up to 10^6 K for $t = 10^6 - 10^7$ years [188]. In Ref. [186], the authors have studied the cooling of DM admixed NS with dark matter mass ranging from 0.1 GeV to 1.3 GeV. In the present work, we have considered low as well as high dark matter masses (up to 500

GeV) and also varied the dark matter Fermi momenta for the cooling calculations. For these calculations, we have considered dark matter admixed density-dependent (DD2) EoS [11,102] and the results are compared with the observational data. Also, our work is different from the above mentioned works [187, 188] because we don't consider heating due to WIMP annihilation owing to the very small annihilation cross-section. We consider indirect effect on cooling of NS stars due to change in the neutron star structure in presence of dark matter. With the introduction of dark matter, cooling properties can change significantly as compared to the normal NSs mainly because of changes in neutrino emissivity, neutrino luminosity and heat capacity. For given mass, neutron emissivity will be different due to significant change in stellar structures and consequently, neutrino luminosity will also be different. Heat capacity related to EoS will be different for normal NSs and DM admixed NSs because of softening of the EoS in latter case. Thus, normal NSs can be distinguished from DM admixed NSs using astronomical observation data related to surface temperature and age of pulsars. We have considered cooling data of Geminga, PSR B0656+14 and PSR B1055-52 [190] in our work. It is sufficient to carry out fits to selected objects rather than carrying a global fit to the population of all thermally radiating neutron stars. As representatives for late time-cooling, a group of above mentioned three NSs is chosen forming a class of nearby objects that allows spectral fits to their X-ray emission [190–193] (and references therein). We have studied NS cooling of both normal NSs using DD2 EoS [11,102] and Akmal-Pandharipande-Ravenhall (APR) EoS [194] and DM admixed NSs using DD2 EoS modified with DM sector. It is important to mention here although DD2 is marginally allowed by the tidal deformability constraint obtained from the the analysis of GW170817 with PhenomPNRT model [13], DM admixed DD2 will be softened and might be considerably allowed by the GW170817 constraints. Earlier DM admixed NSs were studied by some groups [6–8] where they adopted σ-ω-ρ model but our approach differs from theirs in the sense that meson-nucleon couplings are density-dependent in our model which gives rise to an extra term called the rearrangement term [101, 102] in the nucleon chemical potential.

This Chapter is organised as follows. In section 5.2, we describe DM modified baryonic EoS model. We constrain DM-Higgs coupling parameter from the direct detection experiments as discussed in section 5.3. In section 5.4, we discuss the cooling mechanism of neutron star. Finally, the results and calculations are presented in section 5.5.

5.2 Effect of Dark Matter on Equation of State

A uniformly distributed fermionic dark matter, WIMP, is considered inside the neutron star. Dark matter interacts with Higgs field h with coupling strength y. DM-Higgs coupling y is explicitly discussed in Section 5.3. Three different WIMP masses ($M_\chi = 50$ GeV, 200 GeV, 500 GeV) are considered in our calculations. Higgs field h interacts with the nucleons via effective Yukawa coupling fM_n/v, where f denotes the nucleon-Higgs form factor and is estimated to be approximately 0.35 [195] and $v = 246.22$ GeV denotes Higgs vacuum expectation value (VEV). In the Higgs potential, terms higher than quadratic are dropped because they are negligible in the mean field approximation (MFA). Hence the dark sector and its interaction with nucleons and Higgs field is described by the Lagrangian density

$$\mathcal{L}_{DM} = \bar{\chi}(i\gamma_\mu\partial^\mu - M_\chi + yh)\chi + \frac{1}{2}\partial_\mu h\partial^\mu h - \frac{1}{2}M_h^2 h^2 + f\frac{M_n}{v}\bar{\psi}h\psi. \tag{5.1}$$

Here we consider the assumptions that the average dark matter number density inside the neutron star is 10^3 times smaller than the saturated nuclear matter number density [6–8, 196] and the Fermi momentum of dark matter is constant [6–8] throughout the neutron star. With these assumptions, the fractional mass of dark matter inside the neutron star for $M_\chi = 200$ GeV can be expressed as

$$\frac{M_\chi}{M_{NS}} \approx \frac{1}{6}.$$

Given $n_0 = 0.149065 fm^{-3}$, dark matter number density is $n_{DM} \sim 10^{-3} n_0 \sim 0.15 \times 10^{-3} fm^{-3}$. Number density of dark matter is related to Fermi momentum via $n_{DM} = \frac{(k_F^{DM})^3}{3\pi^2}$ which gives $k_F^{DM} \sim 0.033$ GeV. We vary k_F^{DM} in our calculations from 0.01 GeV to 0.06 GeV and dark matter densities n_{DM} will also vary accordingly. Equations of motion for nucleon doublet

$$\psi = \begin{bmatrix} \psi_p \\ \psi_n \end{bmatrix},$$

scalar meson (σ), vector meson (ω^μ) and isovector meson ($\boldsymbol{\rho^\mu}$), DM particle (χ) and Higgs boson h can be derived from Eq. (2.17) of section 2.4.1 (considering only nucleons and excluding ϕ meson terms) and Eq. (5.1) as

$$[\gamma^\mu(i\partial_\mu - \Sigma_B) - (M_n - g_{\sigma B}\sigma - \frac{fM_n}{v}h)]\psi_B = 0,$$

$$\begin{aligned}
\partial_\mu\partial^\mu\sigma + m_\sigma^2\sigma &= g_{\sigma B}\bar{\psi}_B\psi_B, \\
\partial_\mu\omega^{\mu\nu} + m_\omega^2\omega^\nu &= g_{\omega B}\bar{\psi}_B\gamma^\nu\psi_B, \\
\partial_\mu\boldsymbol{\rho}^{\ \mu\nu} + m_\rho^2\boldsymbol{\rho}^{\ \nu} &= g_{\rho B}\bar{\psi}_B\gamma^\nu\boldsymbol{\tau_B}\ \psi_B, \\
(i\gamma_\mu\partial^\mu - M_\chi + yh)\chi &= 0, \\
\partial_\mu h\partial^\mu h + M_h^2 h^2 &= y\bar{\chi}\chi + f\frac{M_n}{v}\bar{\psi}_B\psi_B, \qquad (5.2)
\end{aligned}$$

where masses of DM particle and Higgs particle are denoted by M_χ and $M_h =$

125.09 GeV, respectively. $\Sigma_B = \Sigma_B^0 + \Sigma_B^r$ is the vector self energy in which the first term contains the usual non-vanishing components of vector mesons i.e. $\Sigma_B^0 = g_{\omega B}\omega_0 + g_{\rho B}\tau_{3B}\rho_{\mathbf{03}}$ and the second term is called the rearrangement term i.e. $\Sigma_B^r = \sum_B[-g'_{\sigma B}\sigma n_B^s + g'_{\omega B}\omega_0 n_B + g'_{\rho B}\tau_{3B}\rho_{\mathbf{03}} n_B]$ which appears because of the density-dependence of meson-nucleon couplings [101]. Here $g'_{\alpha B} = \frac{\partial g_{\alpha B}}{\partial n_B}$ where $\alpha = \sigma, \omega, \rho$ and τ_{3B} is the isospin projection of n, p. Due to the density dependence of nucleon-meson couplings, chemical potential of nucleons takes the form

$$\mu_B = \sqrt{k_B^2 + M_n^{*2}} + \Sigma_B^0 + \Sigma_B^r.$$

In the mean-field approximation (MFA), fields are replaced by their expectation values and above equations are simplified as

$$\begin{aligned}
\sigma &= \frac{1}{m_\sigma^2}(g_{\sigma B}\langle\bar{\psi}_B\psi_B\rangle), \\
\omega_0 &= \frac{g_{\omega B}}{m_\omega^2}\langle\psi_B^\dagger\psi_B\rangle = \frac{g_{\omega B}}{m_\omega^2}(n_p + n_n), \\
h_0 &= \frac{y\langle\bar{\chi}\chi\rangle + f\frac{M_n}{v}\langle\bar{\psi}_B\psi_B\rangle}{M_h^2}, \\
\rho_{03} = \frac{g_{\rho B}}{m_\rho^2}\langle\psi_B^\dagger\tau_{3B}\psi_B\rangle &= \frac{g_{\rho B}}{m_\rho^2}(n_p - n_n), \\
(i\gamma^\mu\partial_\mu - \Sigma_B - M_n^*)\psi_B &= 0, \\
(i\gamma^\mu\partial_\mu - M_\chi^*)\chi &= 0.
\end{aligned} \tag{5.3}$$

The effective masses of nucleons and dark matter are respectively given as

$$\begin{aligned}
M_n^* &= M_n - g_{\sigma B}\sigma - \frac{fM_n}{v}h_0, \\
M_\chi^* &= M_\chi - yh_0.
\end{aligned} \tag{5.4}$$

The baryon density (n_B), scalar density (n_s) and dark matter density (n_s^{DM})

are

$$\begin{aligned}
n = \langle \psi^\dagger \psi \rangle &= \frac{\gamma}{(2\pi)^3} \int_0^{k_F} d^3k, \\
n_s = \langle \bar{\psi} \psi \rangle &= \frac{\gamma}{(2\pi)^3} \int_0^{k_F} \frac{M_n^*}{\sqrt{k^2 + M_n^{*2}}} d^3k, \\
n_s^{DM} = \langle \bar{\chi} \chi \rangle &= \frac{\gamma}{(2\pi)^3} \int_0^{k_F^{DM}} \frac{M_\chi^*}{\sqrt{k^2 + M_\chi^{*2}}} d^3k,
\end{aligned} \tag{5.5}$$

where k_F and k_F^{DM} are the Fermi momenta for nucleonic matter and dark matter respectively and $\gamma = 2$ is the spin degeneracy factor of nucleons. The masses of σ, ω and ρ mesons are 546.212459, 783.0 and 763.0 MeV, respectively and meson-nucleon couplings at the saturation density n_0 are given in Table 2.1 [83,102]. In order to get the density dependent profile for M_n^* and M_χ^*, Eqs. (5.3) and (5.5) should be solved self consistently. The energy and pressure i.e. EoS is provided by expectation values of energy-momentum tensor in the static case as $\epsilon = \langle T^{00} \rangle$ and $P = \frac{1}{3} \langle T^{ii} \rangle$.

The total energy density and pressure for the combined Lagrangian $\mathcal{L}_B + \mathcal{L}_{DM}$ are obtained as

$$\begin{aligned}
\epsilon = g_{\omega B}\omega_0(n_p + n_n) + g_{\rho B}\rho_{03}(n_p - n_n) + \frac{1}{\pi^2}\int_0^{k_F^p} dk k^2 \sqrt{k^2 + M_n^{*2}} \\
+ \frac{1}{\pi^2}\int_0^{k_F^n} dk k^2 \sqrt{k^2 + M_n^{*2}} + \frac{1}{\pi^2}\int_0^{k_F^{DM}} dk k^2 \sqrt{k^2 + M_\chi^{*2}} \\
+ \frac{1}{2}m_\sigma^2\sigma^2 - \frac{1}{2}m_\omega^2\omega_0^2 - \frac{1}{2}m_\rho^2\rho_{03}^2 + \frac{1}{2}M_h^2 h_0^2,
\end{aligned} \tag{5.6}$$

$$\begin{aligned}
P = \frac{1}{3\pi^2}\int_0^{k_F^p} dk \frac{k^4}{\sqrt{k^2 + M_n^{*2}}} + \frac{1}{3\pi^2}\int_0^{k_F^n} dk \frac{k^4}{\sqrt{k^2 + M_n^{*2}}} \\
+ \frac{1}{3\pi^2}\int_0^{k_F^{DM}} dk \frac{k^4}{\sqrt{k^2 + M_\chi^{*2}}} \\
- \frac{1}{2}m_\sigma^2\sigma^2 + \frac{1}{2}m_\omega^2\omega_0^2 + \frac{1}{2}m_\rho^2\rho_{03}^2 - \frac{1}{2}M_h^2 h_0^2,
\end{aligned} \tag{5.7}$$

where n_n and n_p are the neutron and proton number densities and k_F^n and k_F^p are the corresponding Fermi momenta of neutron and proton respectively. The nuclear matter inside the neutron star will be charge neutral and β-equilibrated. The conditions of charge neutrality and β-equilibrium are given as

$$n_p = n_e + n_\mu, \tag{5.8}$$

and

$$\begin{aligned} \mu_n &= \mu_p + \mu_e, \\ \mu_e &= \mu_\mu, \end{aligned} \tag{5.9}$$

respectively. Here, the chemical potentials μ_e and μ_μ are given as

$$\begin{aligned} \mu_e &= \sqrt{k_e^2 + m_e^2}, \\ \mu_\mu &= \sqrt{k_\mu^2 + m_\mu^2}, \end{aligned} \tag{5.10}$$

whereas the nucleon chemical potentials contain the rearrangement term also because of density-dependence of couplings as mentioned earlier. The particle fractions of neutron, proton, electron and muon will be determined by the self consistent solution of Eqs. (5.8) and (5.9) for a given baryon density. The energy density and pressure due to the non-interacting leptons are given as

$$\epsilon_l = \frac{1}{\pi^2}\int_0^{k_F^l} dk k^2 \sqrt{k^2 + m_l^2}, \tag{5.11}$$

$$P_l = \frac{1}{3\pi^2}\int_0^{k_F^l} dk \frac{k^4}{\sqrt{k^2 + m_l^2}}. \tag{5.12}$$

So the total energy density and pressure of the charge neutral β-equilibrated neutron star matter are

$$\epsilon_{NM} = \epsilon_l + \epsilon, \tag{5.13}$$

$$P_{NM} = P_l + P. \tag{5.14}$$

In Figure 5.1, we present EoSs for different DM masses and Fermi momenta along with APR and DD2 EoSs. It is evident that for a fixed DM-Higgs coupling y and fixed DM mass, EoS becomes softer for higher values of DM Fermi momentum and is the softest for $k_F^{DM} = 0.06$ GeV for lower to moderate values of density and APR is the stiffest for higher values of density. Moreover, it is inferred from the comparison of three panels of Figure 5.1 that for fixed values of y and k_F^{DM}, higher values of DM masses leads to softer EoS. It is important to mention here that for the higher DM mass $M_\chi = 500$GeV, the EoS corresponding to $k_F^{DM} = 0.06$ becomes softest among all the cases of DM masses. This sudden softening of EoS for $k_F^{DM} = 0.06$ at $M_\chi = 500$GeV might be due to dominance of dark matter over baryonic matter at such extreme parameters of DM. Nevertheless all the neutron star configurations for the dark matter densities considered in this work are stable and will not undergo black hole formation [196]. For all the EoSs considered in our work, we solve numerically Tolman-Oppenheimer-Volkoff (TOV) [197] equations of hydrostatic equilibrium to generate the mass-radius and pressure-radius profiles as shown in Figures 5.2-5.3. In Figure 5.2, the mass-radius profile is plotted for NS masses $1M_\odot$, $1.4M_\odot$ and $2M_\odot$. These plots can be explained the same way as in case of Figure 5.1. Here also the mass-radius profile for $k_F^{DM} = 0.06$ at $M_\chi = 500$GeV follows a trend contrary to other combinations of k_F^{DM} and M_χ. In this case the majority of mass contribution is from DM and hence leading to smaller radius than other cases due to enhanced gravitational contraction. Figure 5.3 shows the pressure-radius profile for different NS masses where it is evident that for fixed DM mass and NS mass, higher values of k_F^{DM} leads to lower pressure except for the case of $M_\chi = 500$ and $M_{NS} = 2M_\odot$ where $k_F^{DM} = 0.06$ GeV leads to higher pressure in the inner region of the star. This is because the star becomes more centrally condensed at very high DM mass.

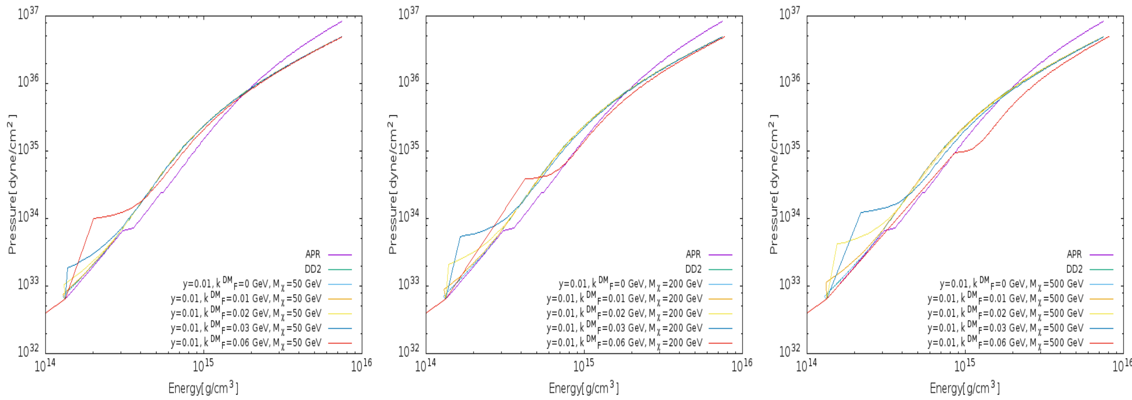

Figure 5.1: Pressure versus energy plots for $M_\chi = 50$ GeV (Left panel), $M_\chi = 200$ GeV (middle panel), $M_\chi = 500$ GeV (right panel) with varying DM Fermi momenta in each panel [14].

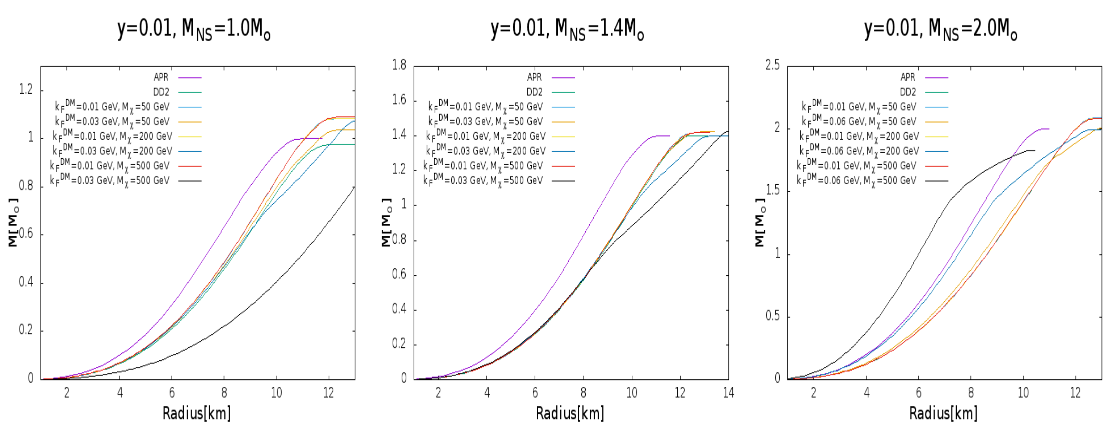

Figure 5.2: Enclosed mass versus radius plots for $M_{NS} = 1.0M_\odot$ (Left panel), $M_{NS} = 1.4M_\odot$ (middle panel), $M_{NS} = 2.0M_\odot$ (right panel) with varying DM mass and Fermi momentum in each panel [14].

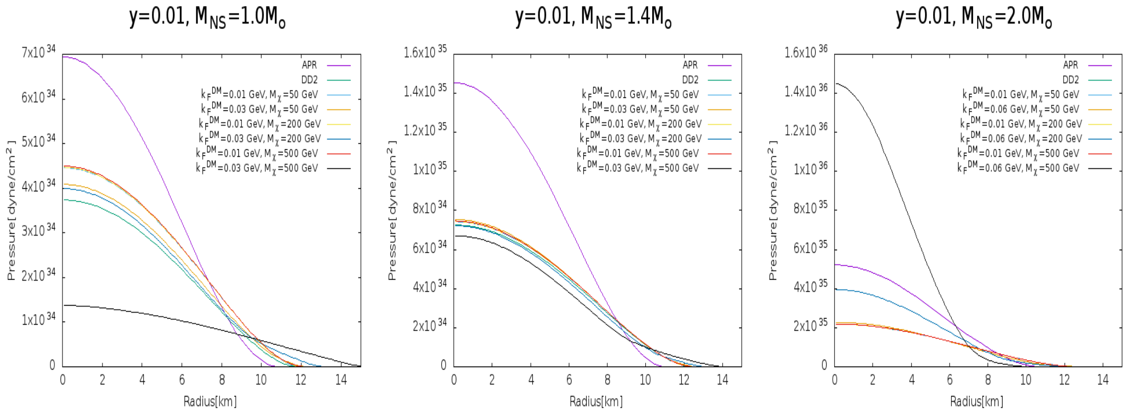

Figure 5.3: Pressure versus radius plots for $M_{NS} = 1.0M_{\odot}$ (Left panel), $M_{NS} = 1.4M_{\odot}$ (middle panel), $M_{NS} = 2.0M_{\odot}$ (right panel) with varying DM mass and Fermi momentum in each panel [14].

5.3 Direct Detection

Dark matter direct detection experiments do not show any signatures of collision events as of now. These experiments provide us an upper bound on the elastic scattering cross-section as a function of dark matter mass. In the present scenario, there can be an elastic collision between the fermionic dark matter, WIMP, and the detector nucleus at the quark level by the Higgs exchange. Therefore, the effective Lagrangian contains the scalar operator $\bar{\chi}\chi\bar{q}q$ and can be written as

$$\mathcal{L}_{\text{eff}} = \alpha_q \bar{\chi}\chi\bar{q}q, \tag{5.15}$$

where q represent the valence quarks and $\alpha_q = y(\frac{m_q}{v})\left(\frac{1}{m_h^2}\right)$. This scalar operator contributes to the spin independent (SI) scattering cross-section for the fermionic dark matter candidate and can be given by the expression as

$$(\sigma_{\rm SI}) = \frac{y^2 f^2 M_n^2}{4\pi} \frac{m_r^2}{v^2 M_h^4}, \tag{5.16}$$

where $m_r = \frac{M_n M_\chi}{M_n + M_\chi}$ is the reduced mass. We calculate the SI scattering cross-section using Eq. (5.16) and then constrain the parameter "y" using the direct detection experiments in such a way that the calculated scattering cross-section for different dark matter masses are below the experimental bounds. In the present scenario, we use XENON-1T [198], PandaX-II [199], LUX [200] and DarkSide-50 [201] experimental bounds for constraining the parameter "y". We have checked that by varying the value of the parameter "y" in the cooling calculations, no significant differences are found and hence, we accordingly fixed "y" to be 0.01 and calculate the corresponding scattering cross-section for three chosen DM masses as tabulated in Table 5.1.

m_χ in GeV	y	$\sigma_{\rm SI}$ cm^2
50	0.01	1.4115×10^{-47}
200	0.01	1.4514×10^{-47}
500	0.01	1.4596×10^{-47}

Table 5.1: Calculated values of spin independent DM-nucleon scattering cross-section for three chosen DM masses at fixed DM-Higgs coupling y.

5.4 Cooling Mechanism of Neutron Stars

It is well known that the surface temperature of a neutron star decreases with time which is the direct indication of cooling. In order to calculate the thermal evolution of the neutron star, one needs to solve the the energy balance equation for the neutron star which can be expressed as [202]

$$\frac{dE_{\rm th}}{dt} = C_v \frac{dT}{dt} = -L_\nu(T) - L_\gamma(T_e) + H(T) \tag{5.17}$$

where $E_{\rm th}$ represents the thermal energy content of the star, T and T_e are the internal and effective temperatures of the star, respectively, C_v is the heat capacity of the core and H is the source term which includes different "heating mechanisms" important in the later stage of neutron star evolution. In Eq. (5.17), L_ν and L_γ denote the neutrino and photon luminosities, respectively. $H(T)$ is considered here to be zero. The photon luminosity is calculated using the Stefan-Boltzmann law [203] as

$$L_\gamma = S\, T^{2+4\alpha} = 4\pi\, \sigma\, R^2\, T_e^4 \ . \tag{5.18}$$

This relation is obtained using $T_e \propto T^{0.5+\alpha}$ $(\alpha \ll 1)$, where R is the radius of the star and σ denotes the Stefan-Boltzmann constant. The NSCool code [204] is utilised in the present work for calculating the neutrino and photon luminosities. Several neutrino emitting processes contribute in the cooling of neutron stars [193, 202, 205]. Direct Urca processes and modified Urca processes are the two main neutrino emitting processes for the cooling. The direct Urca processes are

$$n \rightarrow p + e^- + \overline{\nu}_e,$$

$$p + e^- \rightarrow n + \nu_e.$$

These are possible in neutron stars only if the proton fraction crosses a critical threshold. The two processes are fast and the luminosity varies with the temperature as $L_\nu^{fast} \propto T_9^6$ where $T_9 = (T/10^9)K$.

The modified Urca process will become more dominant provided the proton fraction is below the threshold. The modified processes are

$$n + n \rightarrow n + p + e^- + \overline{\nu}_e,$$

$$n + p + e^- \rightarrow n + n + \nu_e,$$

$$p + n \rightarrow p + p + e^- + \overline{\nu}_e$$

$$\text{and } p + p + e^- \rightarrow p + n + \nu_e.$$

These are slow processes and luminosity varies with the temperature as $L_\nu^{slow} \propto T_9^8$.

The Cooper pairing of nucleons is the other set of neutrino emitting processes as given by

$$n + n \rightarrow [nn] + \nu + \overline{\nu},$$

$$p + p \rightarrow [pp] + \nu + \overline{\nu}.$$

These are medium processes where luminosity varies with temperature as $L_\nu^{medium} \propto T_9^7$.

There are several other neutrino emitting processes involved in the cooling as follows

$e^- + e^+ \rightarrow \nu + \overline{\nu}$ (electron-positron pair annihilation),

$e^- \rightarrow e^- + \nu + \overline{\nu}$ (electron synchrotron),

$\gamma + e^- \rightarrow e^- + \nu + \overline{\nu}$ (photoneutrino emission),

$e^- + Z \rightarrow e^- + Z + \nu + \overline{\nu}$ (electron-nucleus bremsstrahlung),

$n + n \rightarrow n + n + \nu + \overline{\nu}$ (neutron-neutron bremsstrahlung) and

$n + Z \rightarrow n + Z + \nu + \overline{\nu}$ (neutron-nucleus bremsstrahlung).

5.5 Calculations and Results

We utilised the NSCool Numerical code for studying cooling of NSs adopting different EoSs like APR, DD2 and DM admixed DD2. We considered different neutron star masses namely 1.0 $M_\odot$, 1.4 $M_\odot$ and 2.0 $M_\odot$ for the calculations. In case of DM admixed DD2, we explored the effect of variation of DM mass (50 GeV, 200 GeV and 500 GeV) and DM Fermi momentum k_F^{DM} (0 GeV, 0.01 GeV, 0.02 GeV, 0.03 GeV and 0.06 GeV) on the cooling of NSs. It is important to mention here that $k_F^{DM} = 0$ GeV means dark matter density is zero but the effective mass of nucleons will be affected due to non-zero Higgs-nucleon Yukawa coupling (Eq. (5.1)). For demonstrating DM-effect on neutron star cooling we plot the variations of luminosity with time (Figures 5.4-5.6) and effective temperature with time (Figures 5.7-5.9). As seen in all these plots, shortly after birth, NS cooling becomes dominated by neutrino emitting processes as mentioned earlier. When the internal temperature has sufficiently dropped in nearly about $10^4 - 10^5$ year then the cooling is dominated by photon emission from the NSs surface. In Figures 5.4-5.6, luminosity versus time are plotted for different NS masses and for every NS mass, different EoSs are considered. For lower NS masses, the cooling with DD2 EoS is the fastest and with APR EoS it is the slowest. Moreover, for fixed DM mass, the cooling is faster for higher values of DM Fermi momentum. But in heavier NSs, the cooling with APR EoS becomes the fastest which might be due to appearance of extra neutrino emitting channels and variation due to k_F^{DM} is the same as previously. For both the medium mass as well as heavier DM admixed NSs all chosen DM Fermi momenta are considerably consistent with cooling data of pulsars namely Geminga and PSR B0656+14 but for lower mass NS all DM Fermi momenta barely agree with the observations (Geminga, PSR B0656+14). The effect of k_F^{DM} on the cooling of heavier NSs becomes more and more prominent at higher values of DM mass as is evident from the right most panels of Figures 5.5 and 5.6. Figures 5.7-5.9 are effective temperature versus time profiles and these can be explained in the same way as Figures 5.4-5.6. In Figures 5.10-5.11 for luminosity versus time, DM Fermi momentum is fixed and DM mass is varied for both heavier and lighter NSs. These figures clearly show that the cooling is faster for higher values of DM mass and in this case also cooling for heavier NSs is fastest with APR EoS. Figures 5.12-5.13 are effective temperature versus time plots for lighter and heavier NSs where k_F^{DM} is fixed and DM mass is varied. These Figures can be explained in the same way as Figures 5.10-5.11. Figure 5.14 (left panel) for luminosity versus time profile can be explained in the same way as Figures 5.10-5.11 and Figure 5.14 (right panel) for effective temperature versus time profile can be explained in the same way as Figures 5.12-5.13. In this case (Figures 5.10-5.13), the effect on the cooling due to varying DM masses becomes more evident for lower mass NSs except for the case of $k_F^{DM} = 0.06$ GeV where variation due to DM mass is prominent even for heavier mass NS (Figure 5.14) which is due to very high DM Fermi momentum. Moreover, it can be observed from Figures 5.10-5.14 that all chosen DM masses agree well with the observations (Geminga, PSR B0656+14) in case of medium and heavier NSs but only lower DM mass agrees with observations (Geminga, PSR B0656+14) in case of lighter NSs. These observed pulsars might contain dark matter with lower to moderate masses and lower Fermi momentum. Furthermore, as seen from left most panels of Figures 5.10-5.13, it is evident that if small mass and super cold NSs are found in future astronomical cooling observations we can say that heavy WIMPS may actually exist inside NSs.

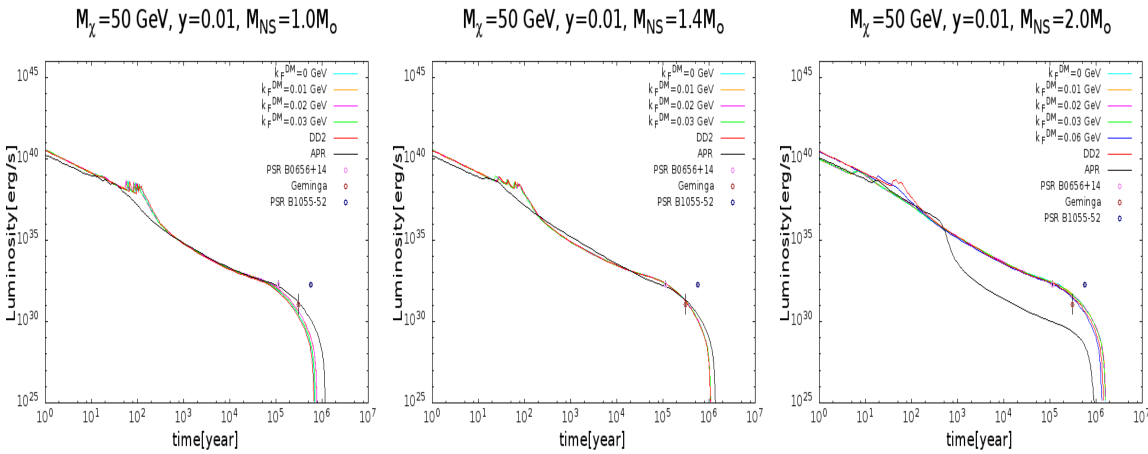

Figure 5.4: Variation of luminosity with time for three differently chosen NS masses $M_{NS} = 1.0M_{\odot}$ (Left panel), $M_{NS} = 1.4M_{\odot}$ (middle panel), $M_{NS} = 2.0M_{\odot}$ (right panel) with varying k_F^{DM} and fixed $M_{\chi} = 50$ GeV in each panel. The theoretical calculations are compared with the astronomical cooling data of three observed pulsars namely Geminga, PSR B0656+14 and PSR B1055-52 shown by dots with error bars from left to right [14].

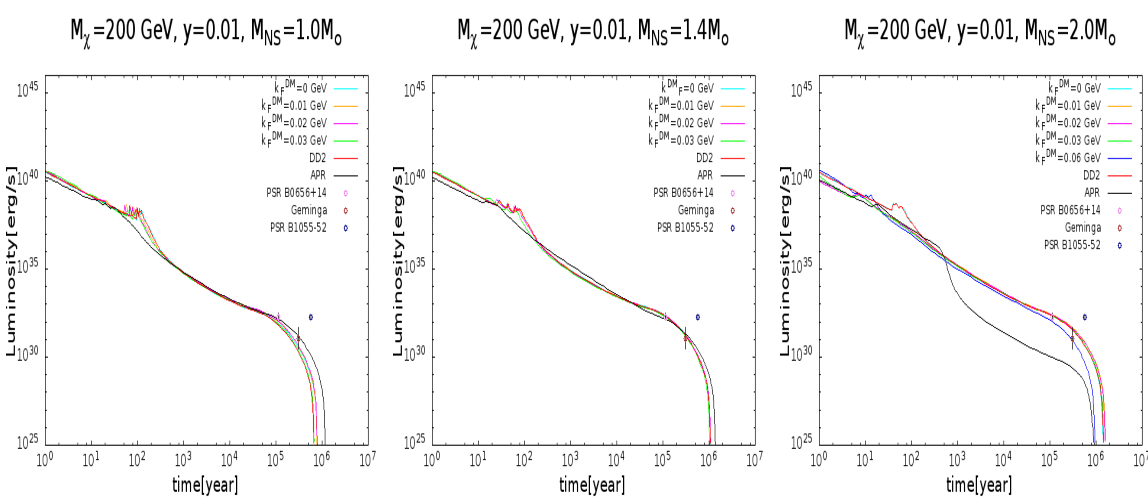

Figure 5.5: Same as in Figure 5.4 but for $M_{\chi} = 200$ GeV [14].

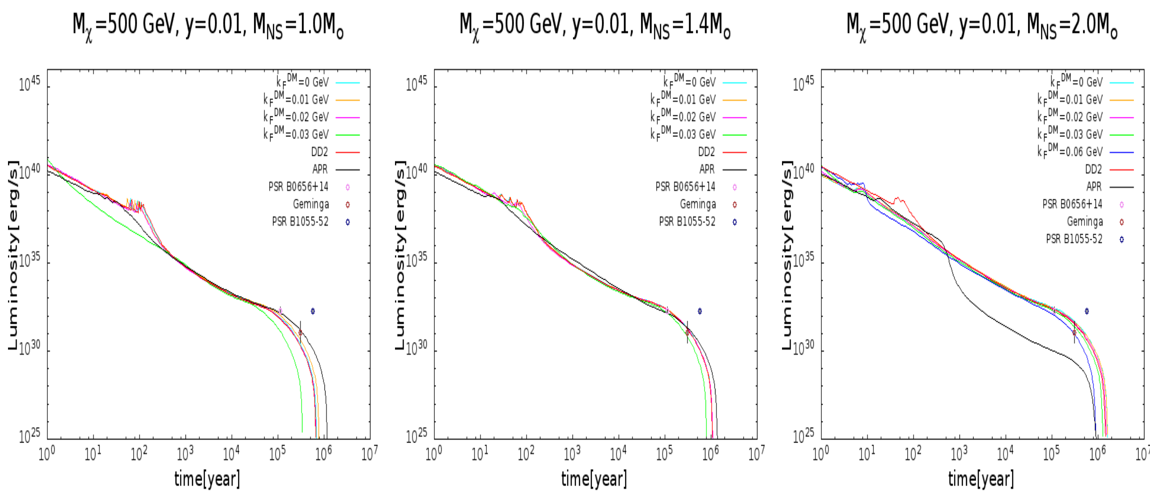

Figure 5.6: Same as in Figure 5.4 but for $M_\chi = 500$ GeV [14].

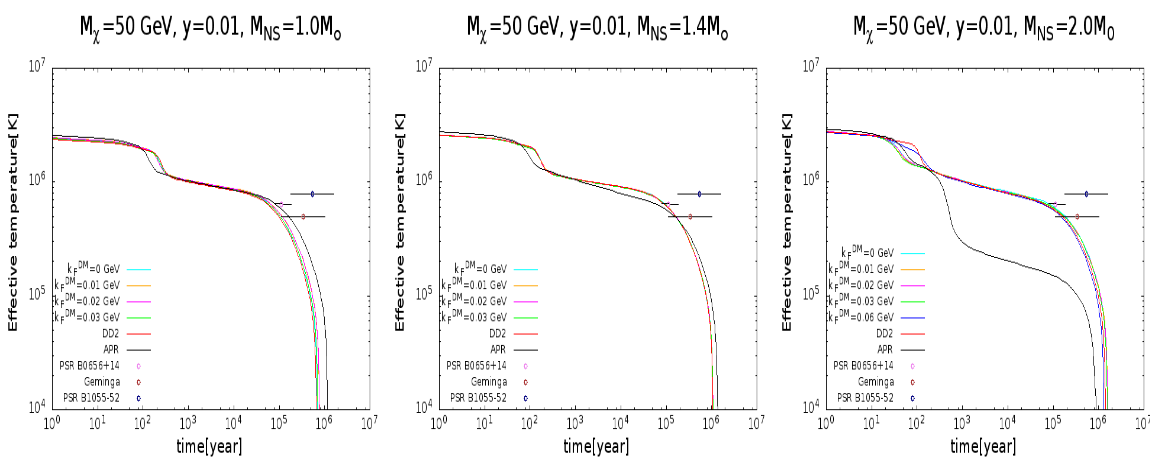

Figure 5.7: Variation of effective temperature with time for three differently chosen NS masses $M_{NS} = 1.0M_\odot$ (Left panel), $M_{NS} = 1.4M_\odot$ (middle panel), $M_{NS} = 2.0M_\odot$ (right panel) with varying k_F^{DM} and fixed $M_\chi = 50$ GeV in each panel. The theoretical calculations are compared with the astronomical cooling data of three observed pulsars namely Geminga, PSR B0656+14 and PSR B1055-52 shown by dots with error bars from left to right [14].

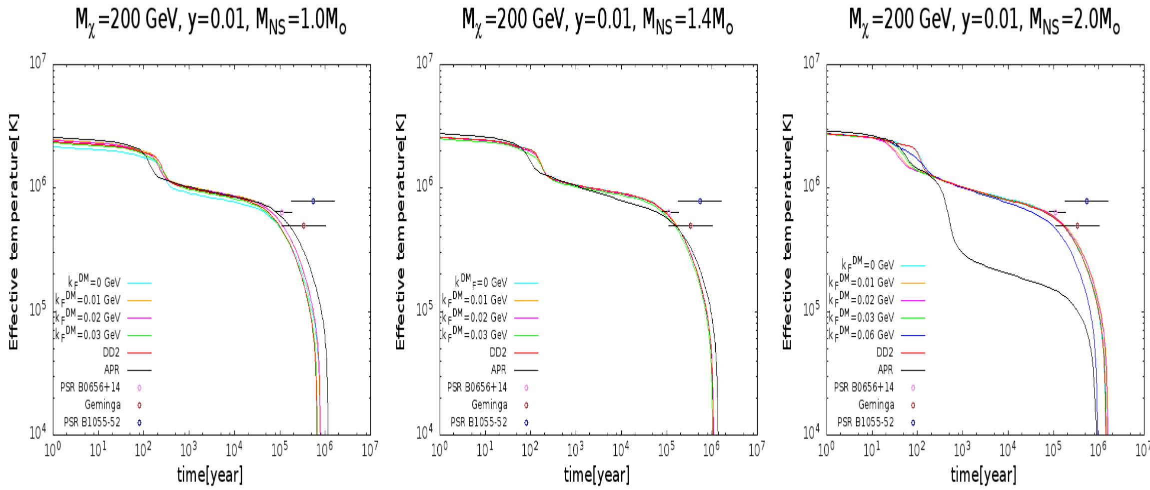

Figure 5.8: Same as in Figure 5.7 but for $M_\chi = 200$ GeV [14]

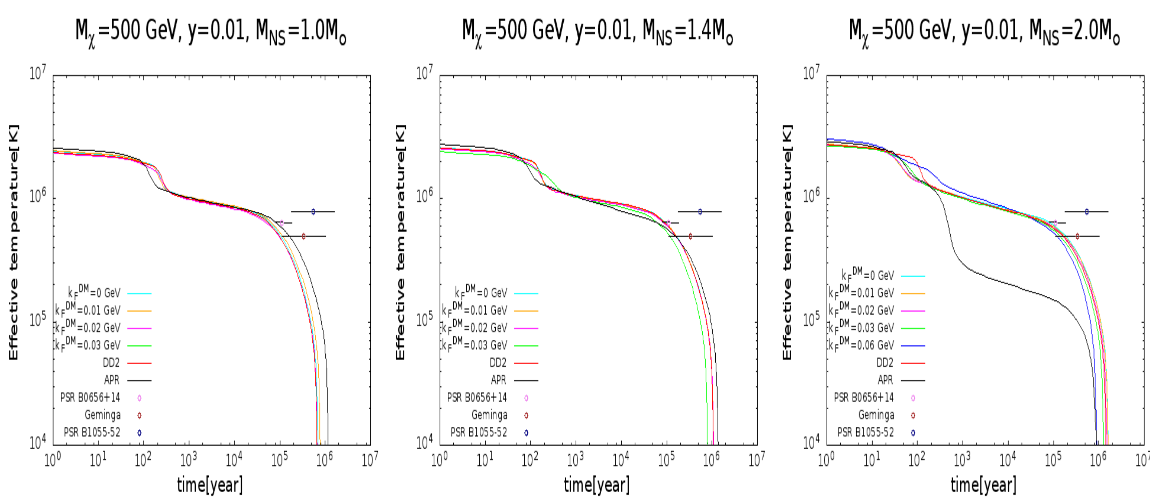

Figure 5.9: Same as in Figure 5.7 but for $M_\chi = 500$ GeV [14]

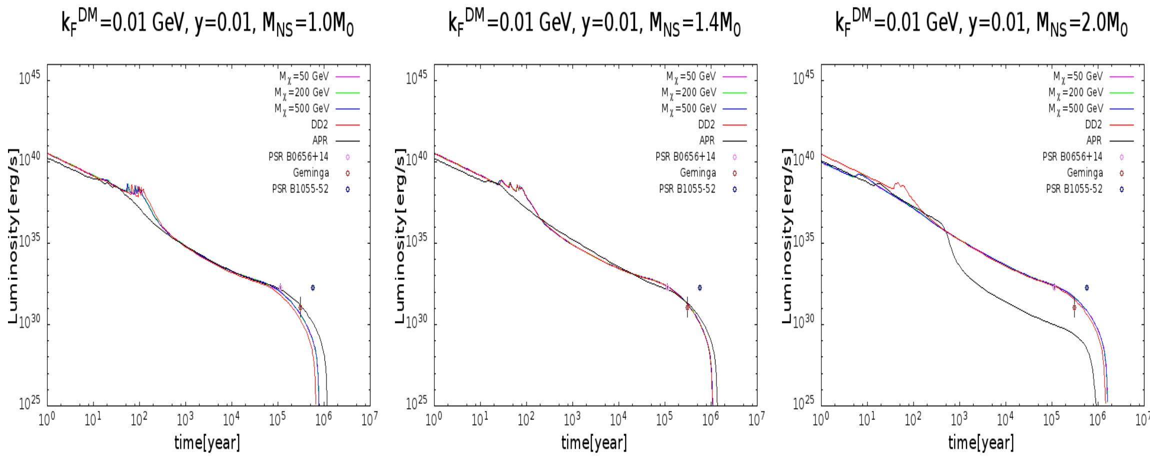

Figure 5.10: Variation of luminosity with time for three differently chosen NS masses $M_{NS} = 1.0M_\odot$ (Left panel), $M_{NS} = 1.4M_\odot$ (middle panel), $M_{NS} = 2.0M_\odot$ (right panel) with varying M_χ and fixed $k_F^{DM} = 0.01$ GeV in each panel. The theoretical calculations are compared with the astronomical cooling data of three observed pulsars namely Geminga, PSR B0656+14 and PSR B1055-52 shown by dots with error bars from left to right [14].

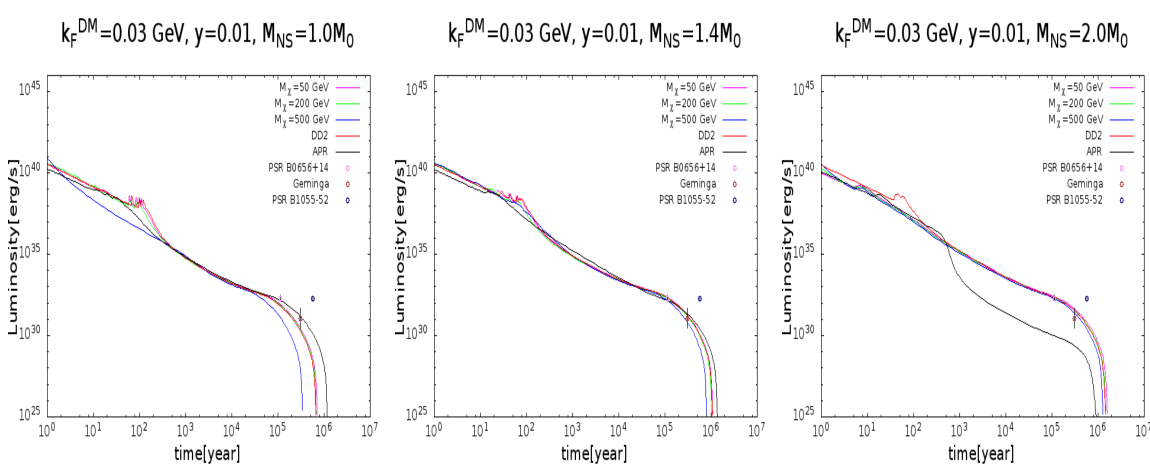

Figure 5.11: Same as in Figure 5.10 but for $k_F^{DM} = 0.03$ GeV [14]

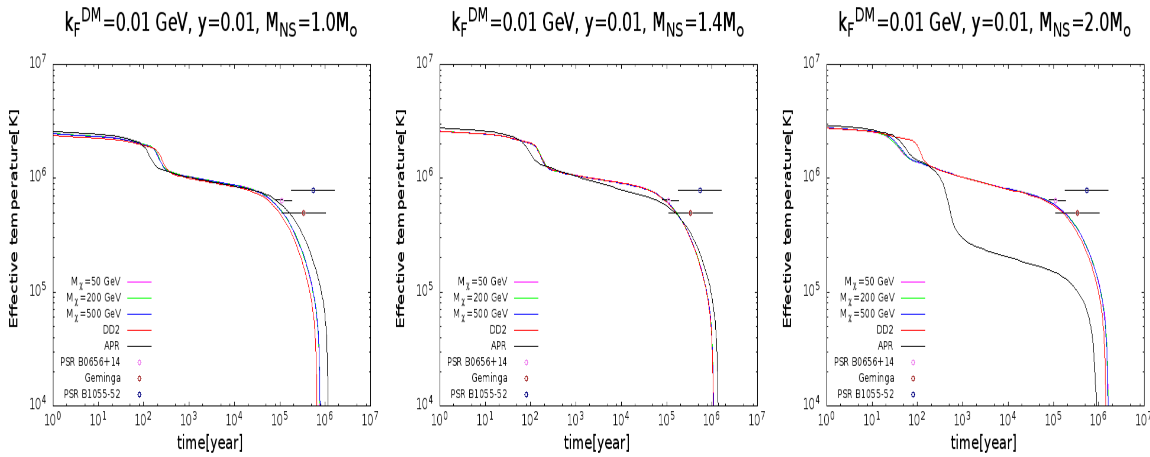

Figure 5.12: Variation of effective temperature with time for chosen three different NS masses $M_{NS} = 1.0M_\odot$ (Left panel), $M_{NS} = 1.4M_\odot$ (middle panel), $M_{NS} = 2.0M_\odot$ (right panel) with varying M_χ and fixed $k_F^{DM} = 0.01$ GeV in each panel. The theoretical calculations are compared with the astronomical cooling data of three observed pulsars namely Geminga, PSR B0656+14 and PSR B1055-52 shown by dots with error bars from left to right [14].

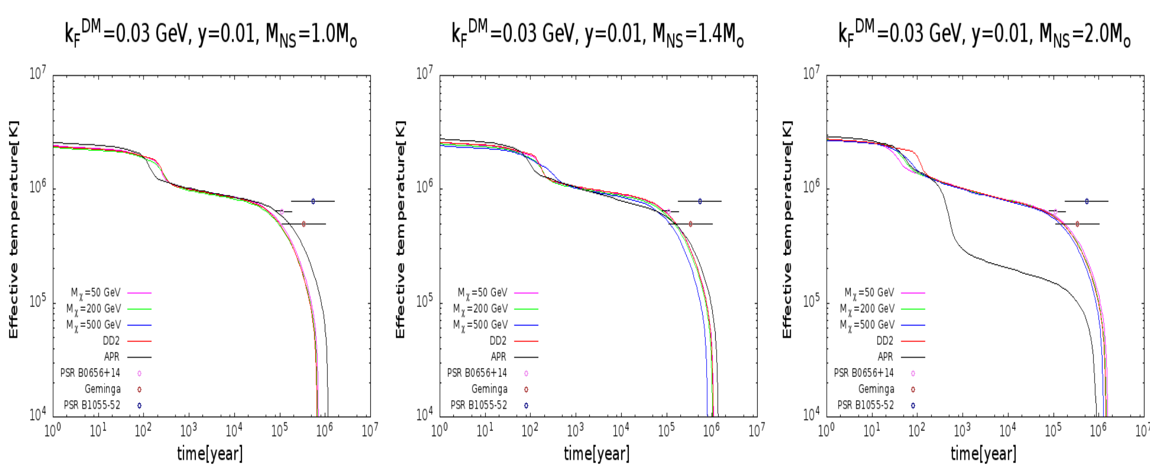

Figure 5.13: Same as in Figure 5.12 but for$k_F^{DM} = 0.03$ GeV [14]

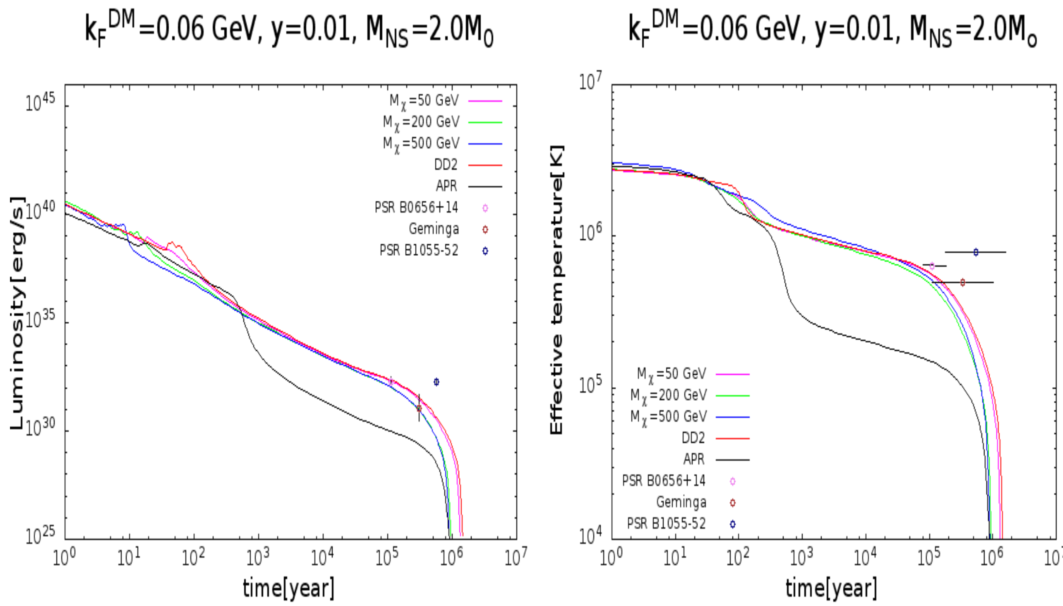

Figure 5.14: Left panel is for luminosity versus time and right panel is for effective temperature versus time with varying M_χ and fixed $k_F^{DM} = 0.06$ GeV in both panels. The theoretical calculations are compared with the astronomical cooling data of three observed pulsars namely PSR Geminga, B0656+14 and PSR B1055-52 shown by dots with error bars from left to right [14].

Chapter 6

Conclusions

We have studied the properties of rotating neutron stars using the LORENE as well as Hartle-Thorne prescription of slowly rotating neutron stars. We adopted different EoSs involving nucleons, hyperons, Bose-Einstein condensate of antikaons within the framework of RMF models with and without density dependent meson-baryon couplings. Quarks are described by the effective bag model including quark interaction and non-local extension of Nambu-Jona-Lasinio model (NJL) model. The behaviour of moment of inertia, quadrupole moment and their dimensionless counter parts with gravitational mass and compactness of neutron stars have been investigated in details. Furthermore, we have studied the Love number for different EoSs. We have found that all those quantities are dependent on EoSs. It is also noted that the tidal Love number approaches a smaller value for large compactness. Similarly, the quadrupole moment of a rotating neutron star moves closer towards the Kerr value of a black hole for maximum mass neutron stars.

We have further investigated the relations among dimensionless moment of inertia, quadrupole moment and tidal deformability parameter. The universal I-

Q and I-Love number relations are observed in our calculation for EoSs including nucleons, hyperons and antikaon condensate as predicted by Yagi and Yunes [12, 62]. However, we have shown for the first time that the universal relations are violated for HQ EoSs undergoing a first order phase transition [9].

We have investigated the constraints on EoS of neutron star matter and properties of merger components of GW170817. We have exploited a large number of EoSs involving nucleons, hyperons, and quarks in this study. We have computed mass-radius relation, tidal deformabilities, moment of inertia and quadrupole moment of the merger components using the same EoS for both binary components. It is found that 50% and 90% credible intervals for the mass weighted average tidal deformability parameter $\bar{\Lambda}$ obtained from gravitational wave analysis of GW170817 allow soft to moderately stiff EoSs. BHB$\Lambda\phi$ EoS might be allowed by 90% credible interval whereas too stiff EoS like HS(TM1), HS(TMA) and HQ2 are ruled out. It is also observed that tidal deformabilities and mass ratio of merger components satisfy $\Lambda_1/\Lambda_2 \sim q^6$ as predicted by other groups [149, 151]. Next, we have obtained upper bounds on moments of inertia and quadrupole moments of slowly rotating neutron stars using the upper limit on the effective tidal deformability parameter $\bar{\Lambda}$ of GW170817. It has been possible to estimate radii of two merger components $\sim$ 13 km as masses and moments of inertia of two merger components are known [13].

We have constructed dark-matter admixed DD2 equation of state and investigated the effect of dark matter mass and Fermi momentum on EoS of neutron stars. Dark matter direct detection experiments namely XENON-1T, PandaX-II, LUX and DarkSide-50 are used to constrain the dark matter-Higgs coupling. The cooling of normal NSs has been investigated considering APR and DD2 EoSs whileas the cooling of DM admixed neutron stars has been explored considering dark-matter modified DD2 EoS with varying dark matter mass and Fermi momentum for the fixed

DM-Higgs coupling. We have performed our analysis with three neutron star masses one each from the lighter (1.0 $M_{\odot}$), medium (1.4 $M_{\odot}$) and heavier (2.0 $M_{\odot}$) NSs. We have demonstrated our results by choosing three different DM masses namely 50 GeV, 200 GeV and 500 GeV and different Fermi momenta k_F^{DM} namely 0.01 GeV, 0.02 GeV, 0.03 GeV and 0.06 GeV. The variations of luminosity and temperature of the above mentioned neutron star masses with time have been investigated and compared with the astronomical cooling data of three observed pulsars namely PSR B0656+14, Geminga and PSR B1055-52. It is found that the cooling with APR EoS agrees well with the pulsar data for lighter and medium mass NSs whereas that of DD2 EoS agrees well for medium and heavier mass NSs and marginally for low mass NSs. For the DM modified DD2 EoS, it is found that the results with all chosen DM Fermi momenta agree well with the observational data in case of medium and heavier NSs, but for lower mass NS the results with different DM Fermi momenta barely agree with the observations. Furthermore, it is found that our findings for all chosen DM masses agree well with the observations in case of medium and heavier NSs but only the results with lower DM mass agrees well with observations in case of lighter NSs. The cooling becomes slightly faster as compared to normal NSs when DM masses and Fermi momenta are increased. It is inferred from the cooling calculations that if lower mass super cold NSs are observed in future that may support existence of heavier WIMP inside neutron stars [14].

Bibliography

[1] "Neutron Stars Are Giant Hypernuclei?," N. K. Glendenning, Astrophys. J., **1985**, 293, 470 .

[2] N.K. Glendenning, Compact Stars, Nuclear Physics, Particle Physics and General Relativity(New York, Springer, 1997).

[3] See Mesons in Nuclei, vol. 3, M. Rho, D. Wilkinson, Eds. (North-Holland, Amsterdam, 1979).

[4] "Strange Goings on in Dense Nucleonic Matter," D. B. Kaplan and A. E. Nelson, Phys. Lett. B, **1986**, 175, 57.

[5] "Superdense Matter: Neutrons Or Asymptotically Free Quarks?," J. C. Collins and M. J. Perry, Phys. Rev. Lett., **1975**, 34, 1353.

[6] "Dark matter effect on realistic equation of state in neutron stars," G. Panotopoulos and I. Lopes, Phys. Rev. D, **2017**, 96, no. 8, 083004.

[7] "Confronting nuclear equation of state in the presence of dark matter using GW170817 observation in relativistic mean field theory approach," A. Das, T. Malik and A. C. Nayak, Phys. Rev. D, **2019**, 99, no. 4, 043016.

[8] "GW170817 constraints on the properties of a neutron star in the presence of WIMP dark matter," A. Quddus, G. Panotopoulos, B. Kumar, S. Ahmad and S. K. Patra, arXiv:1902.00929 [nucl-th].

[9] "Moment of inertia, quadrupole moment, Love number of neutron star and their relations with strange matter equations of state," D. Bandyopadhyay, S. A. Bhat, P. Char and D. Chatterjee, Eur. Phys. J. A, **2018**, 54, no. 26.

[10] "Tidal Love numbers of neutron stars," T. Hinderer, Astrophys. J., **2008**, 677, 1216.

[11] "New Hyperon Equations of State for Supernovae and Neutron Stars in Density-dependent Hadron Field Theory," S. Banik, M. Hempel and D. Bandyopadhyay, Astrophys. J. Suppl., **2014**, 214, no. 2, 22.

[12] "Dense matter in strong gravitational field of neutron star," S. A. Bhat and D. Bandyopadhyay, J. Astrophys. Astron., **2018**, 39, no. 1, 18.

[13] "Neutron star equation of state and GW170817," S. A. Bhat and D. Bandyopadhyay, J. Phys. G, **2019**, **46**, no. 1, 014003.

[14] "Cooling of Dark-Matter Admixed Neutron Stars with density-dependent Equation of State," S. A. Bhat and A. Paul, arXiv:1905.12483 [hep-ph].

[15] "Equation of state of hypernuclear matter: impact of hyperon–scalar-meson couplings," G. Colucci and A. Sedrakian, Phys. Rev. C, **2013**, 87, 055806.

[16] "Massive Neutron Stars with a Color Superconducting Quark Matter Core," T. Tanimoto, W. Bentz and I. C. CloÃńt, arXiv:1903.06851 [nucl-th].

[17] "Color superconducting quark matter in neutron stars," H. Heiselberg, hep-ph/9912419.

[18] "Lev Landau and the concept of neutron stars," D. G. Yakovlev, P. Haensel, G. Baym and C. J. Pethick, Phys. Usp., **2013**, 56, 289.

[19] "Possible Existence of a Neutron," J. Chadwick, Nature, **1932**, 129, 312.

[20] "On the theory of stars," Landau L. D., Phys. Z. Sowjetunion, **1932**, 1, 285.

[21] "Remarks on Super-Novae and Cosmic Rays," Baade W, Zwicky F. Phys. Rev., **1934**, 45, 138, Phys. Rev.,**1934**, 46, 76.

[22] "On Super-Novae," Baade W, Zwicky F. *Proc. National Acad. Sci.*, **1934**, 20, 254-259.

[23] "Observation of a rapidly pulsating radio source," A. Hewish, S. J. Bell, J. D. H. Pilkington, P. F. Scott and R. A. Collins, Nature, **1968**, 217, 709.

[24] " How a Supernova Explodes," H. A. Bethe and G. E. Brown Scientific American, **1985**, 252, 60-68.

[25] "Revival of a stalled supernova shock by neutrino heating," H. A. Bethe and J. R. Wilson, Astrophys. J., **1985**, 295, 14.

[26] "The birth of neutron stars," A. Burrows and J. M. Lattimer, Astrophys. J., **1986**, 307, 178.

[27] Image taken from https://en.wikipedia.org/wiki/

[28] "Cooling of Compact Stars with Color Superconducting Phase in Quark Hadron Mixed Phase," T. Noda, M. A. Hashimoto, N. Yasutake, T. Maruyama, T. Tatsumi and M. Fujimoto, Astrophys. J., **2013**, 765, 1.

[29] "Neutron star cooling," D. G. Yakovlev and C. J. Pethick, Ann. Rev. Astron. Astrophys., **2004**, 42, 169-210.

[30] Geppert U.R. (2016) Thermal Evolution of Neutron Stars. In: Alsabti A., Murdin P. (eds) Handbook of Supernovae. Springer, Cham

[31] "Direct Observation of the Cooling of the Cassiopeia A Neutron Star," C. O. Heinke and W. C. G. Ho, Astrophys. J., **2010**, 719, L167.

[32] "Rapid Cooling of the Neutron Star in Cassiopeia A Triggered by Neutron Superfluidity in Dense Matter," D. Page, M. Prakash, J. M. Lattimer and A. W. Steiner, Phys. Rev. Lett., **2011**, 106, 081101.

[33] "Cooling of the Cassiopeia A neutron star and the effect of diffusive nuclear burning," W. C. G. Ho, M. J. P. Wijngaarden, P. Chang, C. O. Heinke, D. Page, M. Beznogov and D. J. Patnaude, AIP Conf. Proc., **2019**, 2127, no. 1, 020007.

[34] "A Neutron Star with a Carbon Atmosphere in the Cassiopeia A Supernova Remnant," W. C. G. Ho and C. O. Heinke, Nature, **2009**, 462, 71.

[35] "Mesoscopic pinning forces in neutron star crusts," S. Seveso, P. M. Pizzochero, F. Grill and B. Haskell, Mon. Not. R. Astron. Soc., **2016**, 455, 3952.

[36] "Superfluidity in the Interiors of Neutron Stars," J. A. Sauls, NATO ASI Series C, **1989**, 262, 457-490.

[37] "The Structure and Evolution of Neutron Stars," R. Tamagaki and S. Tsurata, (Addison-Wesley, Redwood City, Calif., 1992).

[38] "Crystalline structure of the mixed confined - deconfined phase in neutron stars," N. K. Glendenning and S. Pei, Phys. Rev. C **52**, 2250 (1995).

[39] Courtesy Dany Page, National Autonomous University of Mexico (UNAM).

[40] "Shapiro Delay Measurement of A Two Solar Mass Neutron Star," P. Demorest, T. Pennucci, S. Ransom, M. Roberts and J. Hessels, Nature, **2010**, 467, 1081.

[41] "A Massive Pulsar in a Compact Relativistic Binary," J. Antoniadis, P. C. C. Freire, N. Wex, T. M. Tauris, R. S.Lynch, et al., Science, **2013**, **340**, 448.

[42] "Relativistic Shapiro delay measurements of an extremely massive millisecond pulsar," H. T. Cromartie *et al.*, Nat. Astron., **2019**, 4, no. 1, 72-76.

[43] "A Double - pulsar system - A Rare laboratory for relativistic gravity and plasma physics," A. G. Lyne *et al.*, Science, **2004**, **303**, 1153.

[44] "Constraining the equation of state with moment of inertia measurements," J. M. Lattimer and B. F. Schutz, Astrophys. J., **2005**, 629, 979.

[45] "Constraining the Mass and Radius of Neutron Stars in Globular Clusters," A. W. Steiner, C. O. Heinke, S. Bogdanov, C. Li, W. C. G. Ho, A. Bahramian and S. Han, Mon. Not. Roy. Astron. Soc., **2018**, 476, no. 1, 421.

[46] "Bayesian parameter constraints for neutron star masses and radii using X-ray timing observations of accretion-powered millisecond pulsars," T. Salmi, J. Nättilä and J. Poutanen, Astron. Astrophys., **2018**, 618, A161.

[47] "Neutron star mass and radius measurements from atmospheric model fits to X-ray burst cooling tail spectra," J. Nättilä, M. C. Miller, A. W. Steiner, J. J. E. Kajava, V. F. Suleimanov and J. Poutanen, Astron. Astrophys., **2017**, 608, A31.

[48] "Observational Constraints on Neutron Star Masses and Radii," M. C. Miller and F. K. Lamb, Eur. Phys. J. A, **2016**, 52, no. 3, 63.

[49] "Determining Neutron Star Properties by Fitting Oblate-star Waveform Models to X-ray Burst Oscillations," M. C. Miller and F. K. Lamb, Astrophys. J., **2015**, 808, no. 1, 31.

[50] "Soft x-rays from polar caps of the millisecond pulsar j0437-4715," V. E. Zavlin and G. G. Pavlov, Astron. Astrophys., **1998**, 329, 583.

[51] "The Nearest Millisecond Pulsar Revisited with XMM-Newton: Improved Mass-Radius Constraints for PSR J0437-4715," S. Bogdanov, Astrophys. J., **2013**, 762, 96.

[52] "PSR J0030+0451 Mass and Radius from NICER Data and Implications for the Properties of Neutron Star Matter," M. C. Miller *et al.*, Astrophys. J. Lett., **2019**, 887, L24.

[53] "A NICER View of PSR J0030+0451: Millisecond Pulsar Parameter Estimation," T. E. Riley *et al.*, Astrophys. J. Lett., **2019**, 887, L21.

[54] "A gravitational and electromagnetic analogy," Heaviside O., Electromagnetic Theory, **1893**, 1, 455-466 Appendix B .

[55] "A Brief History of Gravitational Waves," J. L. Cervantes-Cota, S. Galindo-Uribarri and G. F. Smoot, Universe, **2016**, 2, no. 3, 22.

[56] "Measurements of general relativistic effects in the binary pulsar PSR 1913+16," J. H. Taylor, L. A. Fowler and P. M. McCulloch, Nature, **1979**, 277, 437.

[57] "Observation of Gravitational Waves from a Binary Black Hole Merger," B. P. Abbott *et al.* [LIGO Scientific and Virgo Collaborations], Phys. Rev. Lett., **2016**, 116, no. 6, 061102.

[58] "GW170817: Observation of Gravitational Waves from a Binary Neutron Star Inspiral," B. P. Abbott *et al.* [LIGO Scientific and Virgo Collaborations], Phys. Rev. Lett., **2017**, 119, no. 16, 161101.

[59] "A new test of general relativity: Gravitational radiation and the binary pulsar PSR 1913+16," J. H. Taylor and J. M. Weisberg, Astrophys. J., **1982**, 253, 908.

[60] K. Thorne, Three Hundred Years of Gravitation, edited by S. W. Hawking and W. Israel (Cambridge University Press,Cambridge, U.K., 1987), pp. 330-448.

[61] "Properties of the binary neutron star merger GW170817," B. P. Abbott *et al.* [LIGO Scientific and Virgo Collaborations], Phys. Rev. X, **2019**, 9, no. 1, 011001.

[62] "I-Love-Q," K. Yagi and N. Yunes, Science, **2013**, 341, 365.

[63] "On the universality of I-Love-Q relations in magnetized neutron stars," B. Haskell, R. Ciolfi, F. Pannarale and L. Rezzolla, Mon. Not. Roy. Astron. Soc., **2014**, 438, no. 1, L71.

[64] "Breakdown of I-Love-Q universality in rapidly rotating relativistic stars," D. D. Doneva, S. S. Yazadjiev, N. Stergioulas and K. D. Kokkotas, Astrophys. J., **2013**, 781, L6.

[65] "Effectively universal behavior of rotating neutron stars in general relativity makes them even simpler than their Newtonian counterparts," G. Pappas and T. A. Apostolatos, Phys. Rev. Lett., **2014**, 112, 121101.

[66] "Testing universal relations of neutron stars with a nonlinear matter-gravity coupling theory," Y. H. Sham, L. M. Lin and P. T. Leung, Astrophys. J., **2014**, 781, 66.

[67] "Slowly rotating neutron stars in scalar-tensor theories," P. Pani and E. Berti, Phys. Rev. D, **2014**, 90, no. 2, 024025.

[68] "Implications from GW170817 and I-Love-Q relations for relativistic hybrid stars," V. Paschalidis, K. Yagi, D. Alvarez-Castillo, D. B. Blaschke and A. Sedrakian, Phys. Rev. D, **2018**, 97, no. 8, 084038.

[69] "Rotating protoneutron stars: Spin evolution, maximum mass, and I-Love-Q relations," G. Martinon, A. Maselli, L. Gualtieri and V. Ferrari, Phys. Rev. D, **2014**, 90, no. 6, 064026.

[70] "I-Love-Q anisotropically: Universal relations for compact stars with scalar pressure anisotropy," K. Yagi and N. Yunes, Phys. Rev. D, **2015**, 91, no. 12, 123008.

[71] "I-Love-Q relations for gravastars and the approach to the black-hole limit," P. Pani, Phys. Rev. D, **2015**, 92, no. 12, 124030.

[72] "Tidal deformability and I-Love-Q relations for gravastars with polytropic thin shells," N. Uchikata, S. Yoshida and P. Pani, Phys. Rev. D, **2016**, 94, no. 6, 064015.

[73] "I-Love-Q Relations in Neutron Stars and their Applications to Astrophysics, Gravitational Waves and Fundamental Physics," K. Yagi and N. Yunes, Phys. Rev. D, **2013**, 88, no. 2, 023009.

[74] "Why I-Love-Q: Explaining why universality emerges in compact objects," K. Yagi, L. C. Stein, G. Pappas, N. Yunes and T. A. Apostolatos, Phys. Rev. D, **2014**, **90**, no. 6, 063010.

[75] "Unveiling the universality of I-Love-Q relations," Y. H. Sham, T. K. Chan, L. M. Lin and P. T. Leung, Astrophys. J., **2015 798**, no. 2, 121.

[76] "Universality and stationarity of the I-Love relation for self-bound stars," T. K. Chan, A. P. O. Chan and P. T. Leung, Phys. Rev. D, **2016**, 93, no. 2, 024033.

[77] "Matching post-Newtonian and numerical relativity waveforms: systematic errors and a new phenomenological model for non-precessing black hole binaries," L. Santamaria *et al.*, Phys. Rev. D, **2010**, 82, 064016.

[78] "Gravitational waves from inspiraling compact binaries: The Quadrupole moment term," E. Poisson, Phys. Rev. D, **1998**, 57, 5287.

[79] "Reconstructing the neutron-star equation of state with gravitational-wave detectors from a realistic population of inspiralling binary neutron stars," B. D. Lackey and L. Wade, Phys. Rev. D, **2015**, 91, no. 4, 043002.

[80] "The Ground state of matter at high densities: Equation of state and stellar models," G. Baym, C. Pethick and P. Sutherland, Astrophys. J., **1971**, 170, 299.

[81] "Neutron star matter at subnuclear densities," J. W. Negele and D. Vautherin, Nucl. Phys. A, **1973**, 207, 298.

[82] "Statistical Model for a Complete Supernova Equation of State," M. Hempel and J. Schaffner-Bielich, Nucl. Phys. A, **2010**, 837, 210.

[83] "Relativistic model for nuclear matter and atomic nuclei with momentum-dependent self-energies," S. Typel, Phys. Rev. C, **2005**, 71, 064301.

[84] "New relativistic mean-field interaction with density-dependent meson-nucleon couplings," G. A. Lalazissis, T. Niksic, D. Vretenar and P. Ring, Phys. Rev. C, **2005**, 71, 024312.

[85] "A New parametrization for the Lagrangian density of relativistic mean field theory," G. A. Lalazissis, J. Konig and P. Ring, Phys. Rev. C, **1997**, 55, 540.

[86] "The Equation of State from Observed Masses and Radii of Neutron Stars," A. W. Steiner, J. M. Lattimer and E. F. Brown, Astrophys. J. **2010**, 722, 33.

[87] "Core-collapse supernova equations of state based on neutron star observations," A. W. Steiner, M. Hempel and T. Fischer, Astrophys. J. **2013**, 774, 17.

[88] "Relativistic mean field theory for unstable nuclei with nonlinear sigma and omega terms," Y. Sugahara and H. Toki, Nucl. Phys. A, **1994**, 579, 557.

[89] "Relativistic many body approach for unstable nuclei and supernova," H. Toki, D. Hirata, Y. Sugahara, K. Sumiyoshi and I. Tanihata, Nucl. Phys. A, **1995**,

588, no. 1, c357.

[90] “The Ame2003 atomic mass evaluation (II). Tables, graphs and references,” G. Audi, A. H. Wapstra and C. Thibault, Nucl. Phys. A, **2002**, 729, 337.

[91] “Nuclear ground state masses and deformations,” P. Moller, J. R. Nix, W. D. Myers and W. J. Swiatecki, Atom. Data Nucl. Data Tabl., **1995**, 59, 185.

[92] “Equation of state of nucleon matter and neutron star crust,” A. Akmal, V. R. Pandharipande, and D. G. Ravenhall, Phys. Rev. C, **1998**, 58, 1804.

[93] “The Landau-Migdal parameters, g-prime(N N) and g-prime(N Delta) and pion condensations,” T. Suzuki, H. Sakai and T. Tatsumi, nucl-th/9901097.

[94] “Physics of Neutron Star Interiors,” D. Blashke, N. K. Glendenning and A. Sedrakian (Eds.), LNP, **2001**, 578, 127-174.

[95] “Properties of highly excited nuclei,” P. Bonche, S. Levit and D. Vautherin, Nucl. Phys. A, **1984**, 427, 278.

[96] “Statistical properties and stability of hot nuclei,” P. Bonche, S. Levit and D. Vautherin, Nucl. Phys. A, **1985**, 436, 265.

[97] “Semi-classical calculations of hot nuclei,” E. Suraud, Nucl. Phys. A **462**, 109 (1987).

[98] “Explosion - Evaporation Model For Fragment Production In Medium-energy Nuclear Collisions,” G. I. Fai and J. Randrup, Nucl. Phys. A, **1982**, 381, 557.

[99] “The Relativistic Nuclear Many Body Problem,” B. D. Serot and J. D. Walecka, Adv. Nucl. Phys., **1986**, 16, 1.

[100] "Hyperon rich matter in neutron stars," J. Schaffner and I. N. Mishustin, Phys. Rev. C, **1996**, 53, 1416.

[101] "Density dependent hadron field theory for neutron stars with anti-kaon condensates," S. Banik and D. Bandyopadhyay, Phys. Rev. C, **2002**, 66, 065801.

[102] "Composition and thermodynamics of nuclear matter with light clusters," S. Typel, G. Ropke, T. Klahn, D. Blaschke and H. H. Wolter, Phys. Rev. C, **2010**, 81, 015803.

[103] "Multiply strange nuclear systems," J. Schaffner, C. B. Dover, A. Gal, C. Greiner, D. J. Millener and H. Stoecker, Annals Phys. **1994**, 235, 35.

[104] "Relativistic mean field calculations with density dependent meson nucleon coupling," S. Typel and H. H. Wolter, Nucl. Phys. A, **1999**, 656, 331.

[105] "Nuclear Systems With Strangeness," R. E. Chrien and C. B. Dover, Ann. Rev. Nucl. Part. Sci., **1989**, 39, 113.

[106] "Hyperon Nucleus Potentials," C. B. Dover and A. Gal, Prog. Part. Nucl. Phys., **1985**, 12, 171.

[107] "Hyperons and massive neutron stars: the role of hyperon potentials," S. Weissenborn, D. Chatterjee and J. Schaffner-Bielich, Nucl. Phys. A, **2012**, 881, 62.

[108] "Latest results for the antikaon-nucleon optical potential," V. K. Magas, J. Yamagata-Sekihara, S. Hirenzaki, E. Oset and A. Ramos, Few Body Syst., **2011**, 50, 343.

[109] "New Equations of State in Simulations of Core-Collapse Supernovae," M. Hempel, T. Fischer, J. Schaffner-Bielich and M. Liebendorfer, Astrophys. J. **2012**, 748, 70.

[110] "A Third family of superdense stars in the presence of anti-kaon condensates," S. Banik and D. Bandyopadhyay, Phys. Rev. C, **2001**, 64, 055805.

[111] "Anti-kaon condensation and the metastability of protoneutron stars," S. Banik and D. Bandyopadhyay, Phys. Rev. C, **2002**, 63, 035802.

[112] "Anti-Kaon condensation in neutron stars," S. Pal, D. Bandyopadhyay and W. Greiner, Nucl. Phys. A, **2000**, 674, 553.

[113] "First order kaon condensate," N. K. Glendenning and J. Schaffner-Bielich, Phys. Rev. C, **1999**, 60, 025803.

[114] "Quark Deconfinement in Rotating Neutron Stars," R. D. Mellinger, F. Weber, W. Spinella, G. A. Contrera and M. G. Orsaria, Universe, **2017**, 3, no. 1, 5.

[115] We use the hadron-quark (HQ) EoS table of Fridolin Weber (private communication).

[116] "Phase transition in compact stars due to a violent shock," I. Mishustin, R. Mallick, R. Nandi and L. Satarov, Phys. Rev. C, **2015**, 91, 055806.

[117] "Quark-hybrid matter in the cores of massive neutron stars," M. Orsaria, H. Rodrigues, F. Weber and G. A. Contrera, Phys. Rev. D, **2013**, 87, no. 2, 023001.

[118] “An Increased estimate of the merger rate of double neutron stars from observations of a highly relativistic system,” M. Burgay *et al.*, Nature, **2003**, 426, 531.

[119] “GW190425: Observation of a Compact Binary Coalescence with Total Mass $\sim 3.4 M_{\odot}$,” B. P. Abbott *et al.* [LIGO Scientific and Virgo Collaborations], arXiv:2001.01761 [astro-ph.HE].

[120] http://www.gw.iucaa.in/ligo-india/

[121] “Probing Extreme-Density Matter with Gravitational Wave Observations of Binary Neutron Star Merger Remnants,” D. Radice, S. Bernuzzi, W. Del Pozzo, L. F. Roberts and C. D. Ott, Astrophys. J., **2017**, 842, no. 2, L10.

[122] “Constraining neutron star tidal Love numbers with gravitational wave detectors,” E. E. Flanagan and T. Hinderer, Phys. Rev. D, **2008**, 77, 021502.

[123] “Tidal deformability of neutron stars with realistic equations of state and their gravitational wave signatures in binary inspiral,” T. Hinderer, B. D. Lackey, R. N. Lang and J. S. Read, Phys. Rev. D, **2010**, 81, 123016.

[124] “Approximate Universal Relations for Neutron Stars and Quark Stars,” K. Yagi and N. Yunes, Phys. Rept., **2017**, 681, 1.

[125] “The Hyperon Composition Of Neutron Stars,” N. K. Glendenning, Phys. Lett., **1982**, 114B, 392.

[126] “Do hyperons exist in the interior of neutron stars?,” D. Chatterjee and I. Vidaña, Eur. Phys. J. A, **2016**, 52, no. 2, 29.

[127] "Strangeness in hadronic stellar matter," R. Knorren, M. Prakash and P. J. Ellis, Phys. Rev. C, **1995**, 52, 3470.

[128] "Strange Matter," E. Farhi and R. L. Jaffe, Phys. Rev. D, **1984**, 30, 2379.

[129] "Massive Neutron Stars with Antikaon Condensates in a Density Dependent Hadron Field Theory," P. Char and S. Banik, Phys. Rev. C, **2014**, 90, no. 1, 015801.

[130] "Axisymmetric rotating relativistic bodies: A new numerical approach for 'exact' solutions," S. Bonazzola, E. Gourgoulhon, M. Salgado and J. A. Marck, Astron. Astrophys., **1993**, 278, 421.

[131] "High precision rotating neutron star models. I. Analysis of neutron star properties," M. Salgado, S. Bonazzola, E. Gourgoulhon, and P. Haensel, Astron. Astrophys., **1994**, 291, 155-170.

[132] "LORENE spectral methods differential equation solver," E. Gourgoulhon, P. Grandclément, J.-A. Marck, J. Novak and K. Taniguchi, Astrophysics Source Code Library **ascl:1608.018**, (2016).

[133] http://www.lorene.obspm.fr/

[134] "Revising the multipole moments of numerical spacetimes, and its consequences," G. Pappas and T. A. Apostolatos, Phys. Rev. Lett., **2012**, 108, 231104.

[135] J. L. Friedman and N. Stergioulas, *Rotating Relativistic Stars*, Cambridge University Press, 2013

[136] "Fast Rotating Neutron Stars with Realistic Nuclear Matter Equation of State," F. Cipolletta, C. Cherubini, S. Filippi, J. A. Rueda and R. Ruffini, Phys. Rev. D, **2015**, 92, no. 2, 023007.

[137] "Quadrupole moments of rotating neutron stars and strange stars," M. Urbanec, J. C. Miller and Z. Stuchlik, Mon. Not. Roy. Astron. Soc., **2013**, 433, 1903.

[138] "Maximum mass, moment of inertia and compactness of relativistic stars," C. Breu and L. Rezzolla, Mon. Not. Roy. Astron. Soc., **2016**, 459, no. 1, 646.

[139] "Critical mass, moment of inertia and universal relations of rapidly rotating neutron stars with exotic matter," S. S. Lenka, P. Char and S. Banik, Int. J. Mod. Phys. D, **2017**, 26, no. 11, 1750127.

[140] "New temperature dependent hyperonic equation of state: Application to rotating neutron star models and I-Q relations," M. Marques, M. Oertel, M. Hempel and J. Novak, Phys. Rev. C, **2017**, 96, no. 4, 045806.

[141] "Gravitational Waves and Gamma-rays from a Binary Neutron Star Merger: GW170817 and GRB 170817A," B. P. Abbott *et al.* [LIGO Scientific and Virgo and Fermi-GBM and INTEGRAL Collaborations], Astrophys. J., **2017**, 848, no. 2, L13.

[142] "Electromagnetic Counterparts of Compact Object Mergers Powered by the Radioactive Decay of R-process Nuclei," B. D. Metzger *et al.*, Mon. Not. Roy. Astron. Soc., **2010**, 406, 2650.

[143] "Electromagnetic Counterparts of Compact Object Mergers Powered by the Radioactive Decay of R-process Nuclei," B. D. Metzger *et al.*, Mon. Not. Roy. Astron. Soc., **2010**, 406, 2650.

[144] "Constraining the Maximum Mass of Neutron Stars From Multi-Messenger Observations of GW170817," B. Margalit and B. D. Metzger, Astrophys. J., **2017**, 850, no. 2, L19.

[145] "Using gravitational-wave observations and quasi-universal relations to constrain the maximum mass of neutron stars," L. Rezzolla, E. R. Most and L. R. Weih, Astrophys. J., **2018**, 852, no. 2, L25.

[146] "GW170817: Joint Constraint on the Neutron Star Equation of State from Multimessenger Observations," D. Radice, A. Perego, F. Zappa and S. Bernuzzi, Astrophys. J., **2018**, 852, no. 2, L29.

[147] "GW170817, General Relativistic Magnetohydrodynamic Simulations, and the Neutron Star Maximum Mass," M. Ruiz, S. L. Shapiro and A. Tsokaros, Phys. Rev. D, **2018**, **97**, no. 2, 021501.

[148] "Constraints on the neutron star equation of state from AT2017gfo using radiative transfer simulations," M. W. Coughlin *et al.*, Mon. Not. Roy. Astron. Soc., **2018**, 480, no. 3, 3871.

[149] "Tidal Deformabilities and Radii of Neutron Stars from the Observation of GW170817," S. De, D. Finstad, J. M. Lattimer, D. A. Brown, E. Berger and C. M. Biwer, Phys. Rev. Lett., **2018**, 121, no. 9, 091102. Erratum: [Phys. Rev. Lett., **2018**, 121, no. 25, 259902.]

[150] "Properties of the binary neutron star merger GW170817," B. P. Abbott *et al.* [LIGO Scientific and Virgo Collaborations], Phys. Rev. X, **2019**, 9, no. 1, 011001.

[151] "Tidal Deformabilities and Neutron Star Mergers," T. Zhao and J. M. Lattimer, Phys. Rev. D, **2018**, 98, no. 6, 063020.

[152] "Neutron Skins and Neutron Stars in the Multimessenger Era," F. J. Fattoyev, J. Piekarewicz and C. J. Horowitz, Phys. Rev. Lett., **2018**, 120, no. 17, 172702.

[153] "New constraints on radii and tidal deformabilities of neutron stars from GW170817," E. R. Most, L. R. Weih, L. Rezzolla and J. Schaffner-Bielich, Phys. Rev. Lett., **2018**, 120, no. 26, 261103.

[154] "Tidal deformability from GW170817 as a direct probe of the neutron star radius," C. Raithel, F. Özel and D. Psaltis, Astrophys. J., **2018**, 857, no. 2, L23.

[155] "GW170817: Measurements of neutron star radii and equation of state," B. P. Abbott *et al.* [LIGO Scientific and Virgo Collaborations], Phys. Rev. Lett., **2018**, 121, no. 16, 161101.

[156] "Equations of state for supernovae and compact stars," M. Oertel, M. Hempel, T. Klähn and S. Typel, Rev. Mod. Phys., **2017**, 89, no. 1, 015007.

[157] "Dense Matter in Neutron Star: Lessons from GW170817," S. Banik and D. Bandyopadhyay, arXiv:1712.09760 [astro-ph.HE].

[158] "Systematic parameter errors in inspiraling neutron star binaries," M. Favata, Phys. Rev. Lett., **2014**, 112, 101101.

[159] "Millisecond radio pulsars with known masses: parameter values and equation of state models," S. Bhattacharyya, I. Bombaci, D. Bandyopadhyay, A. V. Thampan and D. Logoteta, New Astron., **2017**, 54, 61.

[160] "A Theory of highly condensed matter," J. D. Walecka, Annals Phys., **1974**, 83, 491.

[161] "Recent progress in quantum hadrodynamics," B. D. Serot and J. D. Walecka, Int. J. Mod. Phys. E, **1997**, 6, 515.

[162] "A Tentative Gamma-Ray Line from Dark Matter Annihilation at the Fermi Large Area Telescope," C. Weniger, JCAP, **2012**, 1208, 007.

[163] "Fermi LAT Search for Internal Bremsstrahlung Signatures from Dark Matter Annihilation," T. Bringmann, X. Huang, A. Ibarra, S. Vogl and C. Weniger, JCAP, **2012**, 1207, 054.

[164] "An anomalous positron abundance in cosmic rays with energies 1.5-100 GeV," O. Adriani *et al.* [PAMELA Collaboration], Nature, **2009**, 458, 607.

[165] " Electron and Positron Fluxes in Primary Cosmic Rays Measured with the Alpha Magnetic Spectrometer on the International Space Station," M. Aguilar et al. [AMS collaboration], Phys. Rev. Lett., **2014**, 113, 121102.

[166] "Direct detection of a break in the teraelectronvolt cosmic-ray spectrum of electrons and positrons," G. Ambrosi *et al.* [DAMPE Collaboration], Nature, **2017**, 552, 63.

[167] "Supersymmetric dark matter," G. Jungman, M. Kamionkowski and K. Griest, Phys. Rept., **1996**, 267, 195.

[168] "Possible explanation of indirect gamma ray signatures from hidden sector fermionic dark matter," A. Dutta Banik, D. Majumdar and A. Biswas, Eur. Phys. J. C, **2016**, 76, 346.

[169] "Nonthermal two component dark matter model for Fermi-LAT γ-ray excess and 3.55 keV X-ray line," A. Biswas, D. Majumdar and P. Roy, JHEP, **2015**,

1504, 065.

[170] “Two Component Dark Matter : A Possible Explanation of 130 GeV γ-Ray Line from the Galactic Centre,” A. Biswas, D. Majumdar, A. Sil and P. Bhattacharjee, JCAP, **2013**, 1312, 049.

[171] “The Strong CP problem and axions,” R. D. Peccei, Lect. Notes Phys., **2008**, 741, 3.

[172] “A New Light Boson?,” S. Weinberg, Phys. Rev. Lett., **1978**, 40, 223.

[173] “The Singlet Scalar as FIMP Dark Matter,” C. E. Yaguna, JHEP, **2011**, 1108, 060.

[174] “FIMP realization of the scotogenic model,” E. Molinaro, C. E. Yaguna and O. Zapata, JCAP, **2014**, 1407, 015.

[175] “Implications of a prereionization 21-cm absorption signal for fuzzy dark matter,” A. Lidz and L. Hui, Phys. Rev. D, **2018**, 98, 023011.

[176] “First constraints on Fuzzy Dark Matter from the dynamics of stellar streams in the Milky Way,” N. C. Amorisco and A. Loeb, arXiv:1808.00464 [astro-ph.GA].

[177] “X-ray Radiation from the Annihilation of Dark Matter at the Galactic Center,” L. Bergstrom, M. Fairbairn and L. Pieri, Phys. Rev. D, **2006**, 74, 123515.

[178] “Dark Matter-induced Collapse of Neutron Stars: A Possible Link Between Fast Radio Bursts and the Missing Pulsar Problem,” J. Fuller and C. Ott, Mon. Not. Roy. Astron. Soc., **2015**, 450, L71.

[179] "Confronting nuclear equation of state in the presence of dark matter using GW170817 observation in relativistic mean field theory approach," A. Das, T. Malik and A. C. Nayak, Phys. Rev. D, **2019**, 99, 043016.

[180] "Enhancement of dark matter capture by neutron stars in binary systems," L. Brayeur and P. Tinyakov, Phys. Rev. Lett., **2012**, 109, 061301.

[181] "Effects of mirror dark matter on neutron stars," F. Sandin and P. Ciarcelluti, Astropart. Phys., **2009**, 32, 278.

[182] "Neutrino Emission from Cooper Pairs and Minimal Cooling of Neutron Stars," D. Page, J. M. Lattimer, M. Prakash and A. W. Steiner, Astrophys. J., **2009**, 707, 1131.

[183] "Minimal cooling of neutron stars: A New paradigm," D. Page, J. M. Lattimer, M. Prakash and A. W. Steiner, Astrophys. J. Suppl., **2004**, 155, 623.

[184] "Magnetic neutron star cooling and microphysics," A. Y. Potekhin and G. Chabrier, Astron. Astrophys., **2018**, 609, A74.

[185] "Neutron stars - cooling and transport," A. Y. Potekhin, J. A. Pons and D. Page, Space Sci. Rev., **2015**, 191, no. 1-4, 239.

[186] "Neutrino Emission and Cooling of Dark-Matter-Admixed Neutron Stars," Wen-Bo Ding and Zi Yu and Yan Xu and Chun-Jian Liu and Tmurbagan Bao, Chinese Phys. Lett., **2019**, 36, 049701.

[187] "WIMP Annihilation and Cooling of Neutron Stars," C. Kouvaris, Phys. Rev. D, **2008**, 77, 023006.

[188] "Dark Matter Heating vs. Rotochemical Heating in Old Neutron Stars," K. Hamaguchi, N. Nagata and K. Yanagi, Phys. Lett. B, **2019**, 795, 484.

[189] "Reheating neutron stars with the annihilation of self-interacting dark matter," C. S. Chen and Y. H. Lin, JHEP, **2018**, 1808, 069.

[190] "On the polar caps of the 3 Musketeers," A. De Luca, P. A. Caraveo, S. Mereghetti, M. Negroni and G. F. Bignami, Astrophys. J., **2005**, 623, 1051.

[191] "Axion cooling of neutron stars," A. Sedrakian, Phys. Rev. D, **2016**, 93, no. 6, 065044.

[192] "Axion mass limits from cooling neutron stars," H. Umeda, N. Iwamoto, S. Tsuruta, L. Qin and K. Nomoto, astro-ph/9806337.

[193] "Neutron star cooling via axion emission by nucleon-nucleon axion bremsstrahlung," A. Paul, D. Majumdar and K. Prasad Modak, Pramana, **2019**, 92, 44.

[194] "The Equation of state of nucleon matter and neutron star structure," A. Akmal, V. R. Pandharipande and D. G. Ravenhall, Phys. Rev. C, **1998**, 58, 1804.

[195] "Update on scalar singlet dark matter," J. M. Cline, K. Kainulainen, P. Scott and C. Weniger, Phys. Rev. D 88, 055025 (2013), Erratum: Phys. Rev. D, **2015**, 92, 039906.

[196] "Gravitational effects of condensate dark matter on compact stellar objects," X. Li, F. Wang and K. S. Cheng, JCAP, **2012**, 10, 031.

[197] "On Massive neutron cores," J. R. Oppenheimer and G. M. Volkoff, Phys. Rev., **1939**, 55, 374.

[198] "Physics reach of the XENON1T dark matter experiment," E. Aprile *et al.* [XENON Collaboration], JCAP, **2016**, 1604, 027.

[199] "Dark Matter Results from First 98.7 Days of Data from the PandaX-II Experiment," A. Tan *et al.* [PandaX-II Collaboration], Phys. Rev. Lett., **2016**, 117, 121303.

[200] "Results from a search for dark matter in the complete LUX exposure," D. S. Akerib *et al.* [LUX Collaboration], Phys. Rev. Lett., **2017**, 118, 021303.

[201] "Current status of the dark matter experiment DarkSide-50," L. Marini *et al.* [DarkSide Collaboration], Nuovo Cim. C, **2016**, 39, 247.

[202] "The Cooling of compact stars," D. Page, U. Geppert and F. Weber, Nucl. Phys. A, **2006**, 777, 497.

[203] Dany Page, Cooling of Neutron Stars, Lecture 2, http://www.astroscu.unam.mx/neutrones/NSCool/.

[204] We use the file Crust-EOS-Cat-HZD-NV.dat for the equation of state input, http://www.astroscu.unam.mx/neutrones/NSCool/.

[205] "Neutrino emission from neutron stars," D. G. Yakovlev, A. D. Kaminker, O. Y. Gnedin and P. Haensel, Phys. Rept., **2001** , 354, 1.